SHALLOW SEA TIDAL FRICTION

and SEDIMENT TRANSPORT

by:

J.F. Venn

Submitted, in November 1989, to the

Council for National Academic Awards,

in partial fulfilment of the

requirements for the degree of

Doctor of Philosophy.

Faculty of:

Computing, Management Science,

Mathematics and Statistics.

CITY OF LONDON POLYTECHNIC

ACKNOWLEDGEMENTS

The original idea for the investigation of the flow over a Southern Bight sand bank is due to my supervisor Dr. B. D'Olier. His support for, and active participation in, the experimental programme was much appreciated.

I should also like to thank Dr. M. G. Smith, my second supervisor, for his encouragement and support.

My thanks also to Professor R. S. Scorer for the emphasis upon secondary vorticity effects in his course on partly turbulent flow, for the use of hydrodynamics laboratory facilities and for guidance in laboratory experimentation and techniques.

My thanks to the many other people who contributed to the work, a few of whom I should like to single out for special mention.

Capt John Merriman and the crew of the 'Sir John Cass', for their help with the early field work.
The NERC crews and RVS Barry, for expert guidance: particularly Phil Taylor for the 1980 data.
Dr. A. G. Davies and Dr. R. Soulsby for discussion, criticism and help with the formulation of the main investigation.
Gordon Burton and Alan Aldridge for work on the U100 rig.
Owen Saxton at H.R.E.M. at the University of Cambridge for the digitising of the Seasat image.
Geoff Reason for help with equipment in the hydrodynamics laboratory at Imperial College.
Dr. N. Kenyon for the generous loan of a slide of the Seasat image of the Southern bight.
Colleagues in D.A.M.T.P. at the University of Cambridge, and in the Department of Electronic and Electrical Engineering at the University of Birmingham, for patience, help and support.

ABSTRACT

The dissertation addresses one aspect of the hydrodynamic and bottom topography interactions within a shallow sea. We investigate causes for the suprising lack of overall motion of the linear sand ridges that lie within the energetic wind—wave and tidal regime of the Southern Bight.

There are many problems associated with the accurate estimation of ocean fluid velocity. However, it was found that this was the only significant parameter that could be collected and analysed with the accuracy required for a scientific investigation. No detailed measurements were taken of the sea—bed features or of the suspended and bed—load sediment concentrations.

The particular linear sand ridge investigated was the South Falls bank. The tidal flow was measured using current meter rigs on and off the bank. Analytical and numerical modelling of the hydrodynamic equations was compared with these current meter values for the fluid velocity field. It was found that a simple two—dimensional model that agreed well with observations of fluid velocity implies that, locally the tidal friction is insensitive to change of depth.

A Seasat synthetic aperture radar image of the Southern Bight showed grey—scale variation strongly related to the bottom topography, with increased brightness on the western flank of the sandbanks and sand waves of the region. A tidal surface velocity field was generated, for the time of the image, by reference to the measured velocities over the bank. It was estimated that the wave—current interaction, due to radiation stress effects, would have produced changes in the surface roughness over the bank that relate well to the image brightness variation.

The flow over a rough strip of the sea—bed within a constant depth region or a core of relict beach material are each sufficient for bank generation. The relation of the present flow regime over South Falls bank to that of the flow over a rough strip suggests that the cross—sectional area of the central portion of the bank is stable. The South Falls cross—section shape may be a result of wave blocking rather than a westward sediment transport. Secondary flow acts to give a frictional bottom flow everywhere within the Southern Bight. This must change at the bank and may integrate to helical vortices.

NOMENCLATURE

containing: Roman notation

Greek notation

Abbreviations

Acronyms

Mathematical symbols

Chapters and sections are listed on the CONTENTS page.

Chapter numerals are Roman .... I.

Section numerals are Arabic .... N.2.

Equation and figure numbering (and table lettering) restart with the begining of each new chapter.

FIGURES ARE PLACED NEAR TO THE APPROPRIATE REFERRING TEXT.

Subsection numerals are Arabic .... N.n.1.

Equation numerals are bracketed .... N.n.(1)

Equation subdivisions lower-case labelled N.n.(1)a,b

Figure numerals are prefixed fig........ fig.N.n.1

Figure subdivisions lower-case labelled fig.N.n.1a,b

Tables are upper-case labelled .... table N.n.A,B

References are bracketed and include author name and date.

The scheme for the symbols detailed below follows the usage in POND(1978)

Roman notation

a .... Wave amplitude,
Rossby radius of deformation

$\hat{A}$ .... Kinematic eddy viscosity

$A_x A_y A_z$. Kinematic eddy viscosity
in the x, y, z directions.

B .... Roughness function

c .... Wave phase velocity

c_s .. .. .. (shallow)

c_d .. .. .. (deep)

c_g .. .. .. (group)

c_x .. .. .., positive direction

d .... Pseudo-bathymetric depth

d' .... transformed d

D_E .... Ekman layer depth

$E_x E_y E_z$. Ekman number in coordinate direction

E .... Energy, wave energy = a^2

f .... planetary vorticity
horizontal Coriolis parameter = $2\Omega \sin\phi$

f( ) ..... Function of ( )

F .... Force, Friction force, Magnus force

F_r .... Froude number

g .... Acceleration due to
gravity = 9.80 m/s/s

G .... Grey-scale brightness, Intensity

$G(\theta)$... Wave directional variation

Roman notation continued...

h, H ..... height of sea surface at LAT above the sea bed

k .... wave number, roughness, relative friction

K .... coeff. of virtual internal friction

$\ell_x\ \ell_y\ \ell_z$. lengthscale in coordinate direction

L .... wavelength of water surface wave

N .... Brunt–Vaisala frequency

p .... modified pressure = P/ρ

P .... pressure

R_e .... Reynolds number

R_i .... Richardson number

R_o .... Rossby number

$S(\omega)$.... spreading parameter, even integer

s .... space or time coordinate

t .... time

$u, v, w,$. velocity components in x, y, z directions

V .... velocity vector $(u^2 + v^2 + w^2)^{1/2}$

x, y, z... orthogonal directions

$X\ Y$ .... surface slope in x, y directions

Z .... water height above sea bed $= h - z$

Z_o .... height above sea bed of zero water velocity vector

Greek notation

α .... alpha, angle of tide to bank crest line

β .... beta = $\partial f / \partial \phi$, variation of coriolis parameter with latitude

δ .... delta, viscous sub-layer depth

Δ .... Delta, an increment, or measured sea-bed roughness

ε .... epsilon, $G(\theta)$ minimum value

ζ .... zeta, relative vorticity

η .... eta, vertical displacement of the sea surface above LAT

θ .... theta, angle from wind direction

κ .... kappa, von Karmans constant

λ .... lambda, wavelength of radio wave

μ .... mu, dynamic molecular viscosity

ν .... nu, kinematic molecular viscosity

ξ, γ, ζ xi, gamma, zeta : relative vorticity components about x, y, z axes

ρ ...... rho, density of sea water

τ .... tau, frictional stress

ϕ .... phi, Geographic latitude, scalar velocity potential

Φ .... Phi, geopotential

ψ .... psi, stream function

Ψ .... Psi, planetary vorticity vertical Coriolis parameter = $2\Omega \cos \phi$

ω .... omega, frequency

Ω .... Omega, angular speed of rotation of the earth

Abbreviations

const .... Constant
D .... Dimension
2–D .... Two–Dimensional
3–D .... Three–Dimensional

h .... hour
kg .... kilogram
km .... kilometre

Lat .... Latitude
Long .... Longitude

max .... maximum
min .... minimum
m .... metre
m/s .... metres/second
refs .... references
s .... second
sect .... section
subs .... subsection
yr .... year

Acronyms

BP ....Before Present, historical time.
HRS ....Hydralics Research Station, Wallingford.
IOS ....Institute of Oceanographic Sciences.
LAT .... Lowest astronomical tide
LHS0 ....Longuet–Higgins and Stewart,1960 see refs
LHS1 ....Longuet–Higgins and Stewart,1961 see refs
NERC ....Natural Environment Research Council.
RVS ....Research Vessel Services, NERC–IOS base for oceanographic experiment support, Barry Docks
ETT ....Equivalent tidal time (to SST)
SST ....Seasat overpass time, for fig.IV.6.1

Mathematical symbols

$=$ .... equal to

$\simeq$ .... approximately equal to

$\sim$ .... of the order of

$O(\quad)$ .... of order at most $(\quad)$

$>$ .... greater than

$\gg$ .... much greater than

$<$ .... less than

$\ll$ .... much less than

$|\quad|$ .... absolute value of

$\overline{}$ .... overbar, average operator

$\bullet$ .... scalar product

$\times$ .... vector product

∇ .... gradient operator

$\nabla\bullet$ .... divergence operator

∇^2 .... Laplacian operator

$\dfrac{d(\quad)}{ds}$ .... derivative of $(\quad)$ wrt s

$\dfrac{\partial(\quad)}{\partial s}$ .... partial derivative of $(\quad)$ wrt s

$\dfrac{d(\quad)}{dt}$ .... instantaneous substantive derivative of $(\quad)$ wrt time

$\dfrac{D(\quad)}{Dt}$ .... meaned substantive derivative of $(\quad)$ wrt time

$\dfrac{\partial(\ ,\ )}{\partial(x,y)}$ ..... Jacobian

Many computer programs have been written in Algol, Basic, Fortran and Simula for all aspects of the work. Most of them are of scientific rather than computational interest. Accordingly, they are described in the text, where this is relevant, and no source listings are bound with this volume.

ILLUSTRATIONS

CONTENTS

I INTRODUCTION

This dissertation addresses one aspect of the general problem of estimating interactions between the bottom topography and the hydrodynamics of shallow seas. The submerged continental margins contain a quantity of loose particulate matter that has accumulated as sedimentary bedforms which are often modified by the water flow that they locally distort. However, within this highly mobile hydraulic regime some bedforms are suprisingly stable. It has been suggested by Jelgersma(1979) that some linear sand ridges have not changed in size or position since 6000 BP. The unexpected longevity and positional stability of these bedforms is the subject under investigation.

Within this chapter we first give a summary of the content and contribution of this dissertation. We then cover some basic material in order to formulate the problem of estimating the hydrodynamics of a linear sand ridge and then review the history of the problem.

Chapter II covers the preliminary investigations into field work techniques and research methods to be used.

Chapter III contains the work on tidal flow over a sand ridge. The measured flow is compared with a modelled velocity field generated from the hydrodynamic equations.

Chapter IV contains the investigation into the relationship between the bank and the gravity waves that impinge upon it.

The last chapter has discussion, a summary and conclusions.

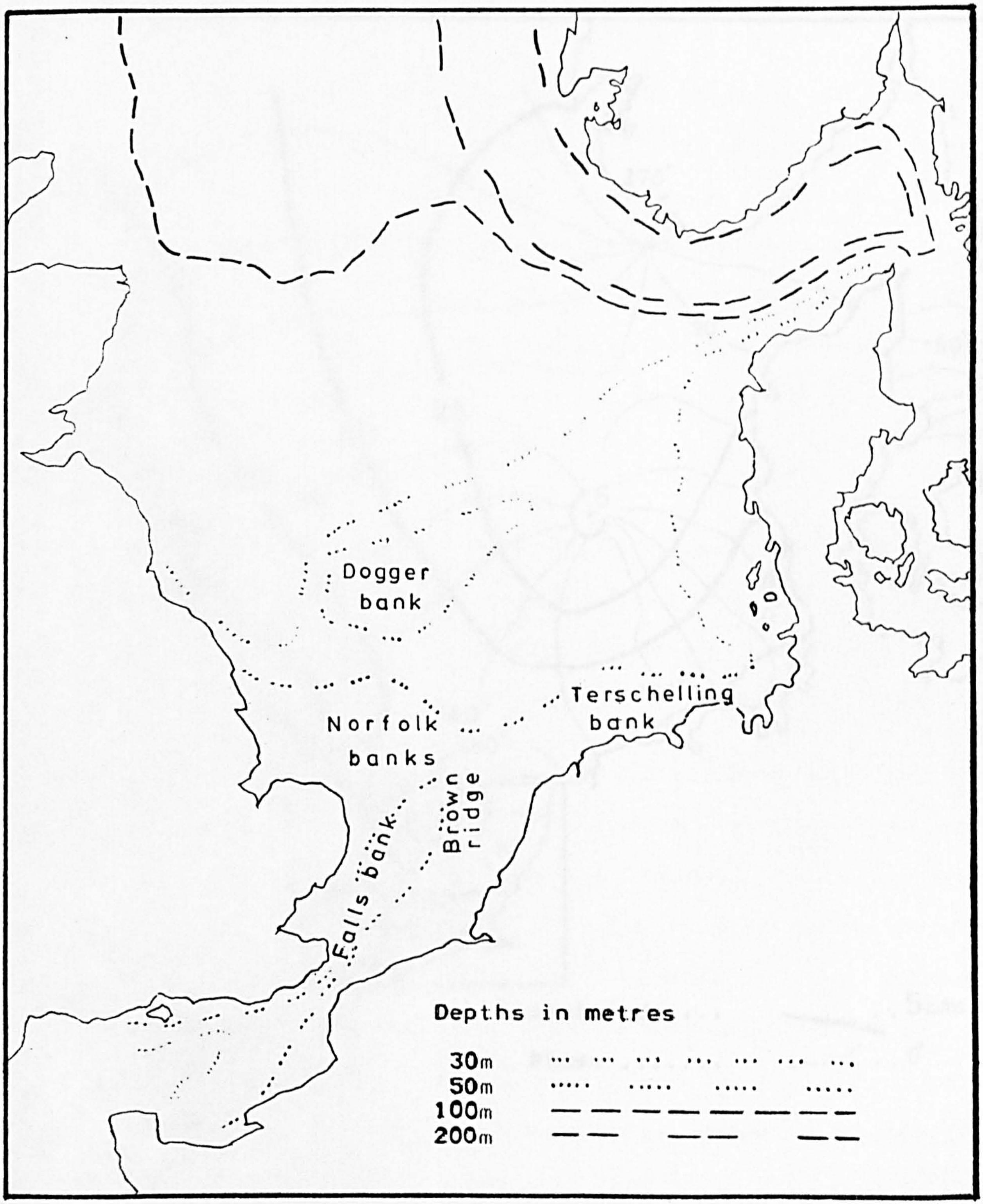

Fig.I.1a North Sea .... Topography

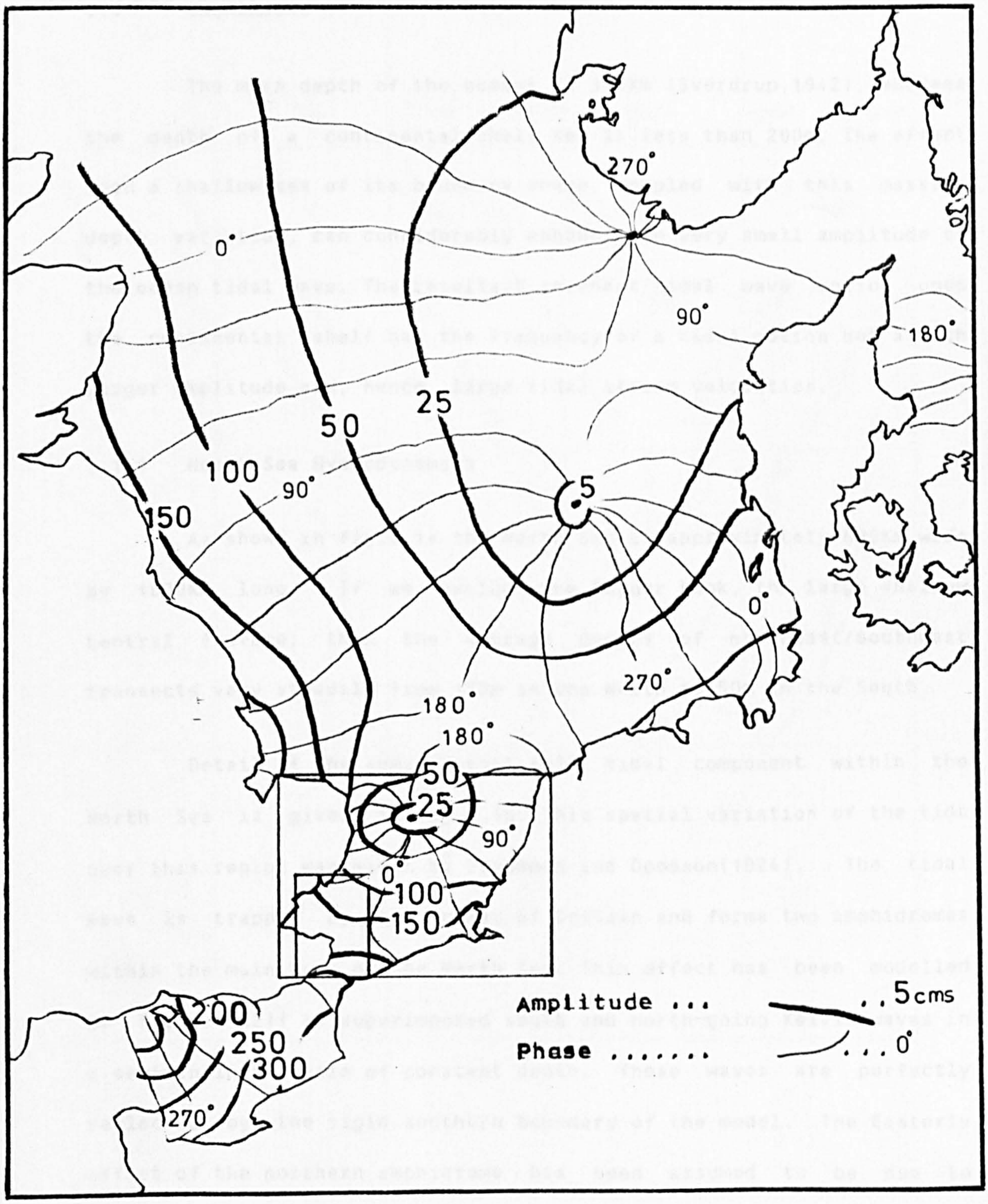

Fig.I.1b North Sea .... M2 — Tide

I.1 BACKGROUND

The mean depth of the oceans is 3.8Km (Sverdrup,1942), whereas the depth of a continental shelf sea is less than 200m. The effect upon a shallow sea of its boundary shape, coupled with this massive depth variation, can considerably enhance the very small amplitude of the ocean tidal wave. The resultant resonant tidal wave motion upon the continental shelf has the frequency of a tidal motion but a much larger amplitude and, hence, large tidal stream velocities.

I.1.1 North Sea Hydrodynamics

As shown in fig.I.1a the North Sea is approximately 600Km wide by 1000Km long. If we exclude the Dogger bank, the large shallow central feature, then the average depths of northeast/southwest transects vary steadily from 150m in the North to 50m in the South.

Detail of the semi-diurnal (M2) tidal component within the North Sea is given in fig.I.1b. This spatial variation of the tide over this region was given by Proudman and Doodson(1924). The tidal wave is trapped by the coast of Britain and forms two amphidromes within the main body of the North Sea. This effect has been modelled by Taylor(1921) as superimposed south and north-going Kelvin waves in a semi-infinite basin of constant depth. These waves are perfectly reflected by the rigid southern boundary of the model. The Easterly offset of the northern amphidrome has been assumed to be due to friction effects (Defant,1960). However, an alternate explanation was given by Brown(1978) who modelled the amphidromic offset as an effect of the energy flow through an oscillating southern boundary.

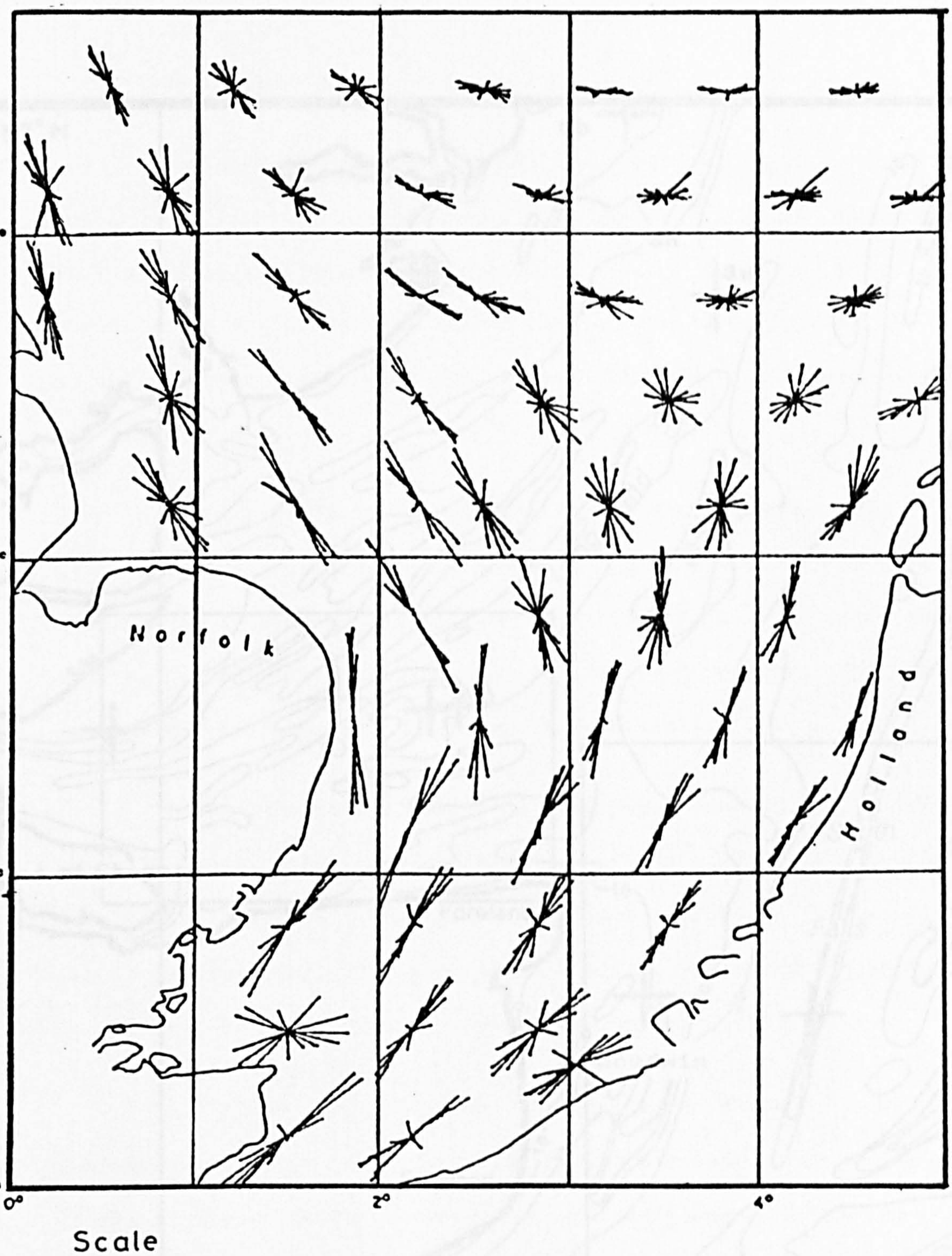

(after Deutsches Hydrographisches Institut 1956)

Fig.I.2 Southern Bight .... Tidal Ellipses

Direction and strength of the average tidal currents at the surface during one tidal cycle.

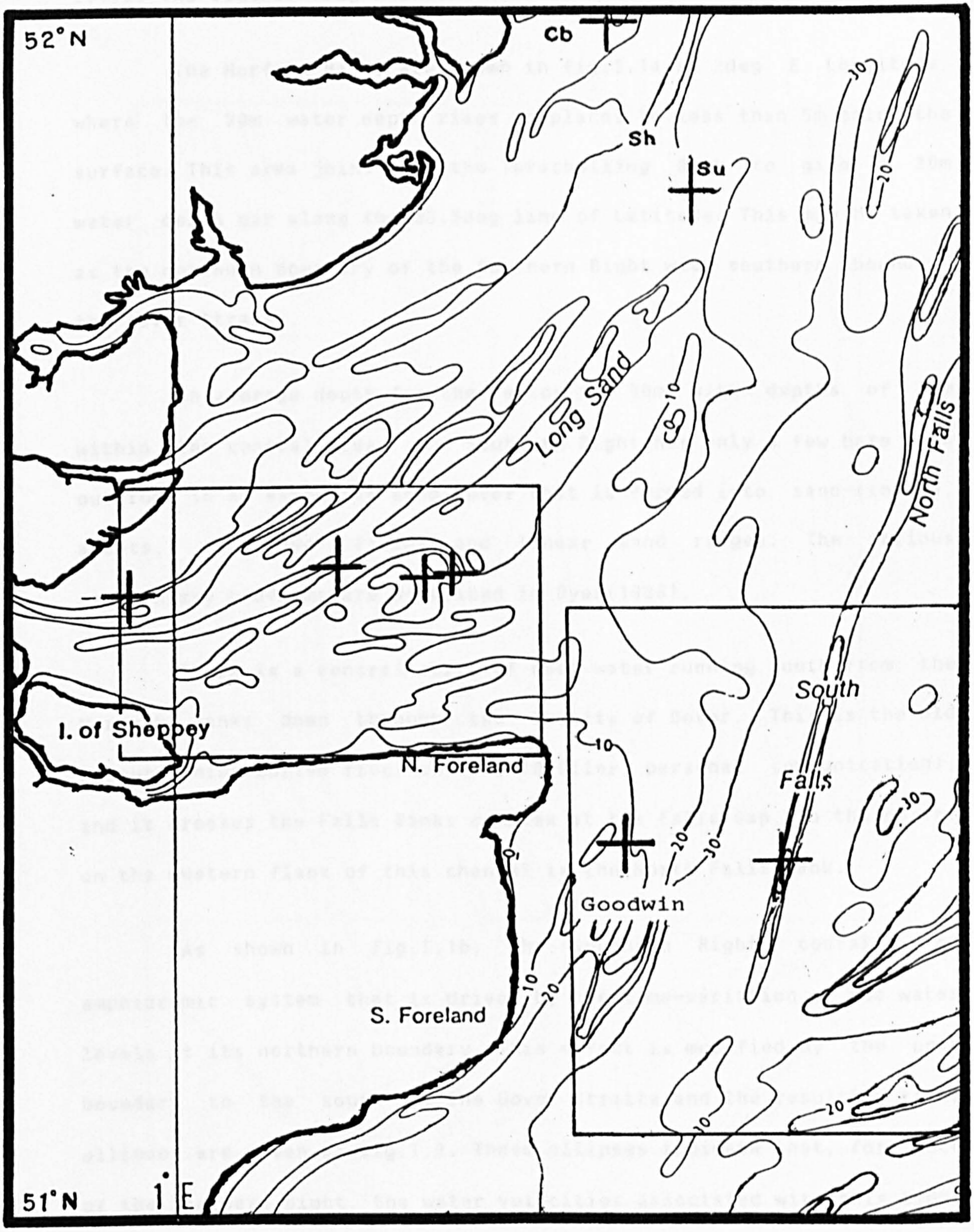

Fig.I.3 Southern Bight .... Field work region

I.1.2. The Southern Bight of the North Sea

The Norfolk Banks are shown in fig.I.1a at 2deg E Longitude, where the 30m water depth rises in places to less than 5m below the surface. This area joins with the Terschelling Bank to give a 30m water depth bar along the 53.5deg line of Latitude. This may be taken as the northern boundary of the Southern Bight with southern boundary the Dover Straits.

An average depth for the region is 30m with depths of 40m within the central area. The Southern Bight has only a few bare rock outcrops in an extensive sand cover that is formed into sand-ribbons, sheets, sand-wave fields and linear sand ridges. The various sedimentary bedforms are described in Dyer(1986).

There is a central strip of deep water running south from the Norfolk Banks down through the Straits of Dover. This is the old Lobourg/Rhine buried river channel (D'Olier, personal communication), and it crosses the Falls Banks complex at the Falls Gap. To the north, on the western flank of this channel is the North Falls Bank.

As shown in fig.I.1b, the Southern Bight contains an amphidromic system that is driven by the time-variation of the water levels at its northern boundary. This effect is modified by the open boundary to the south at the Dover Straits and the resulting tidal ellipses are given as fig.I.2. These ellipses indicate that, for much of the Southern Bight, the water velocities associated with this tidal frequency wave are rectilinear in nature, giving a reversing flow which resembles that of a narrow estuary.

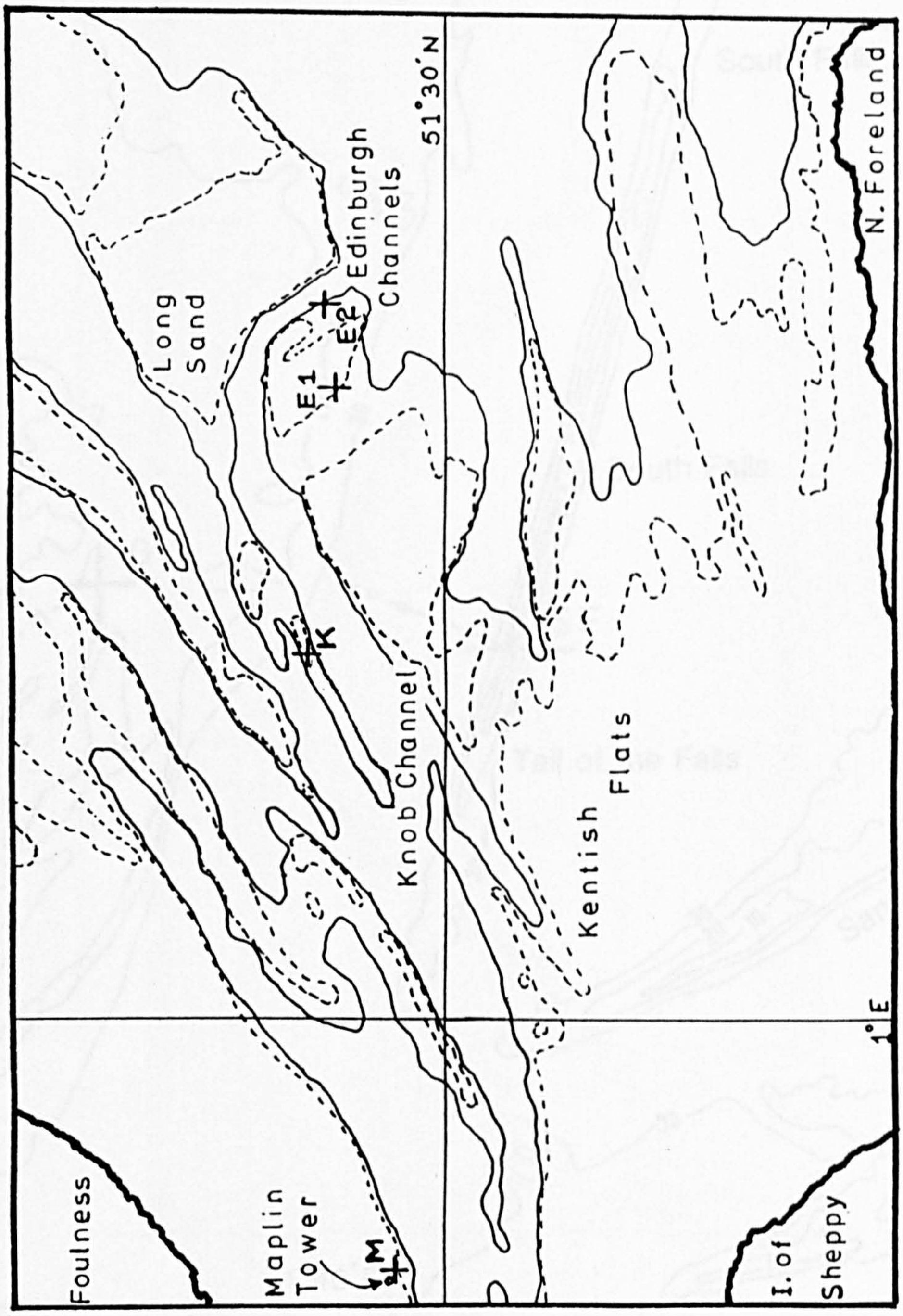

Fig.I.4 Thames Estuary .... Field work region

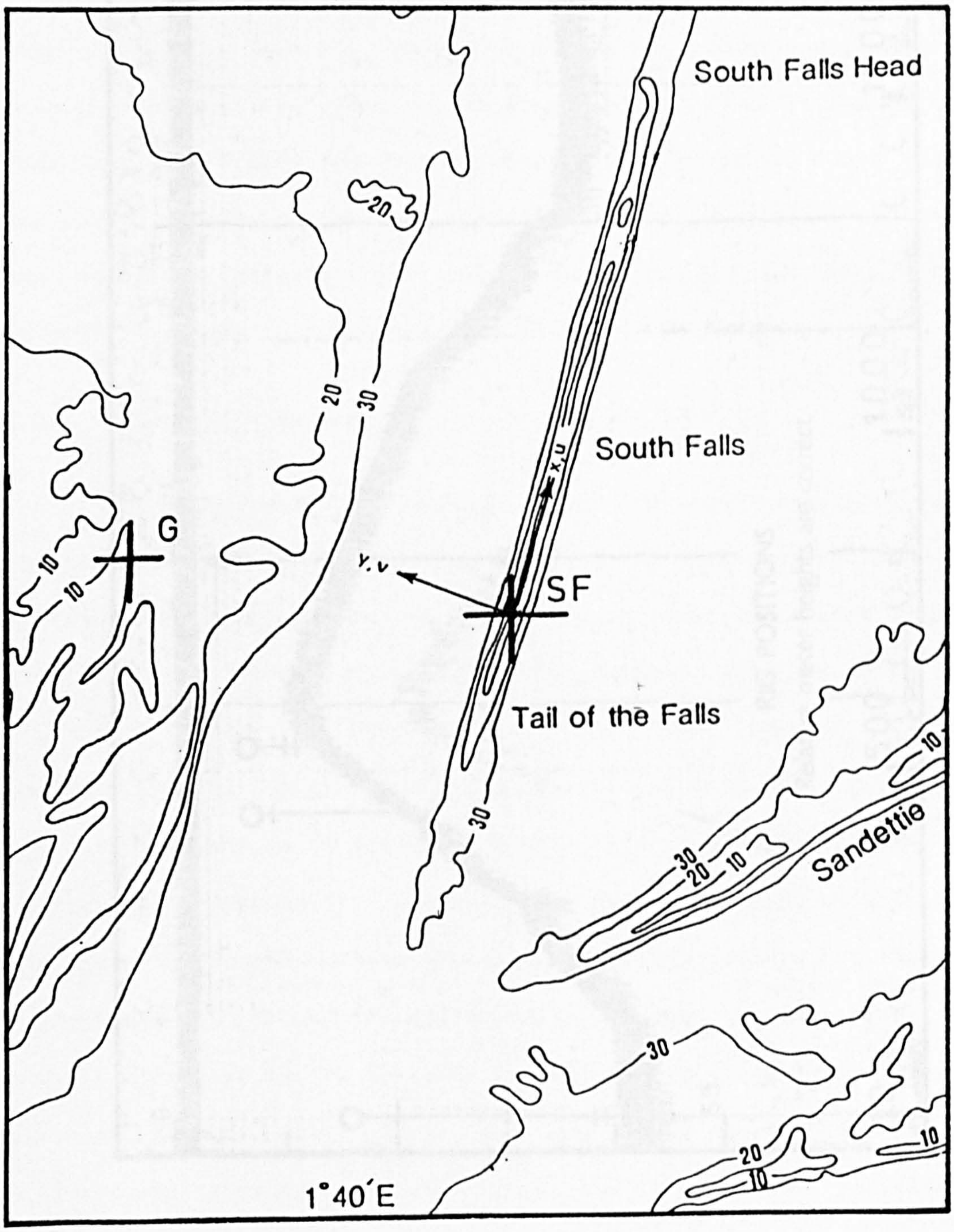

Fig.I.5 South Falls .... Topography

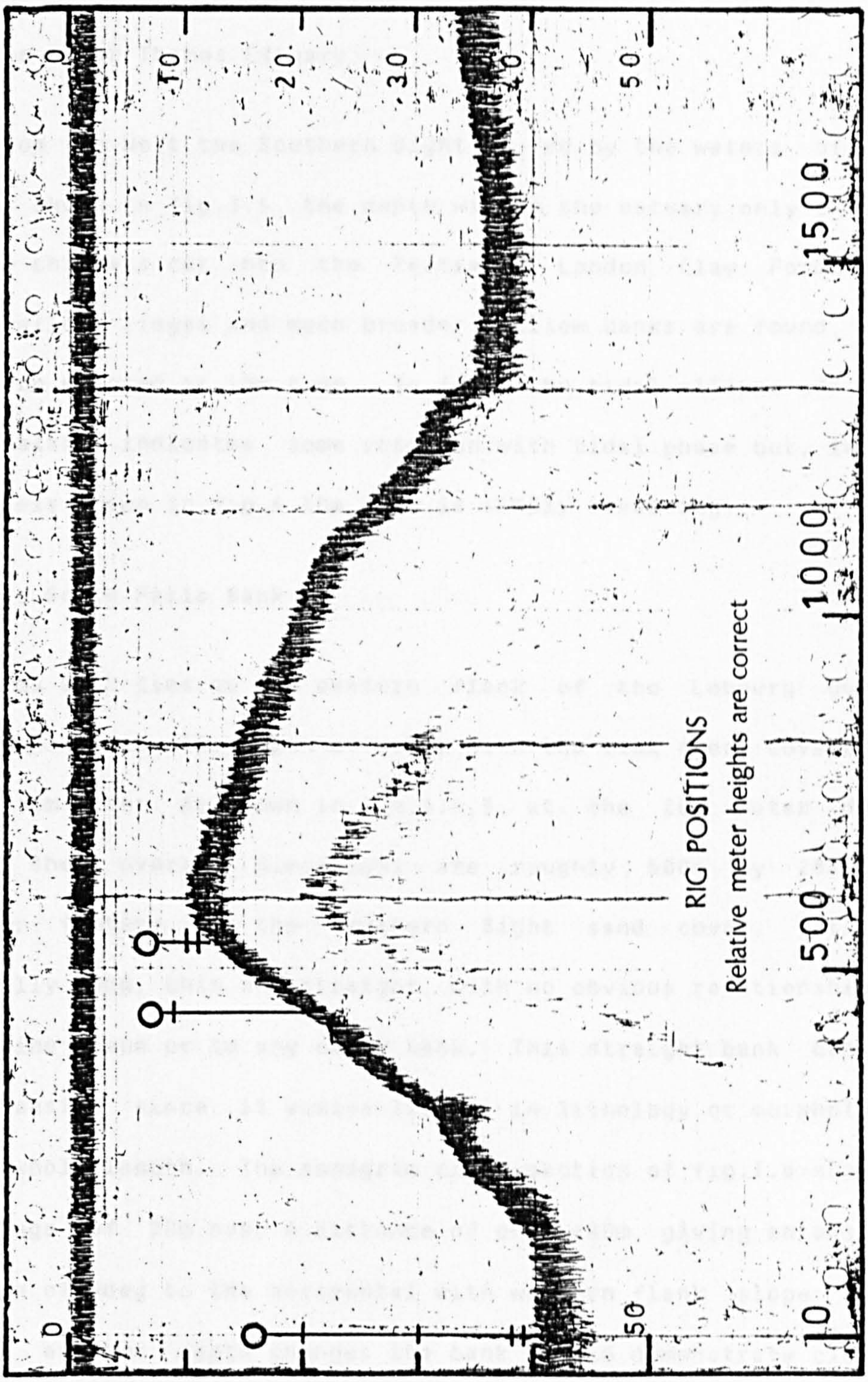

Fig.I.6 South Falls .... Bank cross-section
Depth below sea surface .... metres
Distance from rig 3 .... metres

I.1.3. The Outer Thames Estuary

From the West the Southern Bight is fed by the waters of the Thames. As shown in fig.3,4, the depth within the estuary only exceeds 10m in the channels cut into the Tertiary, London Clay Formation. Narrow shallow ridges and much broader shallow banks are found, some of which are exposed at low tide. In fig.2 the tidal ellipse off the North Foreland indicates some rotation with tidal phase but, in the deep channels shown in fig.4 the flow is simply reversing.

I.1.4. The South Falls Bank

This bank lies on the eastern flank of the Lobourg buried river channel, in 40m depth of water with the bank crest covered by less than 10m water. As shown in fig.I.4,5, at the 20m water depth contour, the overall dimensions are roughly 500m by 28km. A spectacular feature of the Southern Bight sand cover, it is exceptionally long, thin and straight, with no obvious relationship to the coastline shape or to any other bank. This straight bank can be modelled easily since it varies little, in lithology or morphology, along its whole length. The sonogram cross—section of fig.I.6 shows a depth change of 30m over a distance of only 400m, giving an eastern flank slope of 6deg to the horizontal with western flank slope 3deg. With such extreme depth changes the bank should demonstrate clearly the hydrodynamics of a linear sand ridge, and it has the additional simplification of just one varying horizontal dimension. The maximum velocities of the tidal stream associated with this area are given in fig.I.2 as 2.5knots. The tidal ellipse is narrow so the assumption of a simple reversing flow is appropriate.

I.2 THE LINEAR SAND RIDGE PROBLEM

Linear sand ridges, which are also called tidal current ridges (Off,1963), are very large, long and narrow sedimentary bedforms, that are composed of sand. They are aligned at a small angle to the predominant tidal stream direction (Kenyon et al,1981). The problem addressed is that of the genesis and long-term positional and dimensional stability of sand ridges. We first consider the general problem of the formation and mobility of sedimentary bedforms.

I.2.1 Sediment transport and topography

Whereas sedimentary material in the oceans is mainly biogenic, in coastal seas siliceous, particulate matter is a product of erosion. Whilst friction of a tidal stream in shallow water can be considerable, over exposed rock and even the London Clay of the Southern Bight, erosion is slow. However, wave action does actively erode the coastline, particularly in East Anglia. Other loose material within a coastal sea is a product of the weathering of the nearby land mass that is delivered to the sea by river flow over long time periods. In addition, wind and glacial action and the submergence of land areas have provided much of the potentially mobile material of the Southern Bight.

The erosive action of wind waves or a tidal stream over loose fine-grained sediment can be very strong, and rapid modification of the bottom topography is possible. This action of the water flow over a loose boundary can create a variety of sedimentary bedforms on many different lengthscales.

The various bedforms are described by many authors, including Allen(1968), Kennedy(1969) and Dyer(1986). Sand banks may be formed as longitudinal features that separate the deep channels of a river or estuary such as the Thames, as can be seen in fig. I.3,4. However, sand banks vary greatly in size and shape and other methods of formation are possible. The largest and most elongate sand banks are described below.

I.2.2. Tidal current ridges

These bedforms, also called linear sand ridges, are aligned at a small angle to the predominant tidal stream direction. Typically up to 30m in height, they are highly elongate being 1–5km wide and often more than 20 km in length. In his global study of linear sand ridges, Off(1963) showed that linear sand ridges are common within the shallow coastal seas of the submerged continental margins. These areas are subject to resonant tidal motions that can generate very high values for the tidal streams. Off identified several concentrations of these bedforms around the British Isles, many of which lie within or adjacent to the Southern Bight of the North Sea.

The existence, position, size, shape and stability of many shallow sedimentary bedforms can be related to the supply of sand to the region and to the parameters that describe the 2D hydraulic regime in which they are found. For linear sand ridges not one of these factors can be easily explained.

Some banks, such as those near the Dogger Bank are found in deep water, where tidal stream velocities are low, but these may be considered as stable relict banks, that were formed in shallow water before the latest phase of North Sea submergence.

Most of the banks are found in shallow water: the Norfolk banks (fig.I.1a) and the Falls banks (fig.I.5) lie in approximatly 40m water depth with the bank top only 10m below the water surface. We can assume that surface water waves can still have an effect upon these shallow bank tops, since they are all covered in sand waves that show signs of short-term mobility.

The conditions required for the formation of these long banks have not been completely determined. A linear sand ridge is composed of such a large volume of sand that very large transport rates would be required if there were short term instability of size or position. However, since the water velocities of the hydrodynamic regime for the region, away from the banks, are sufficient to entrain the sand grains of which the bank is composed, stability in the long term should not be expected. On the contrary, the combination of wind wave action and turbulent dispersion with the tidal excursion of several kilometres should rapidly destroy any shallow water linear sand ridge.

The noted longevity of these features (Jelgersma, 1979) indicates that a large body of sand must modify the local hydrodynamics in order to ensure its continued existence. Constructive hydrodynamic mechanisms must be present, that will act to counter and reverse the effect of the destructive ones. Any such mechanism may then be sufficient to explain the creation of a bank from some perturbation of the topography (Huthnance, 1982a).

I.2.3. A restatement of the problem

Linear sand ridges are composed of sand of a size that can easily be transported by the wind-waves and tidal streams to which they are exposed. Within the turbulent shallow-water hydraulic regime distinct sandbody features should be dissipated by these mechanisms.

Some constructive hydrodynamic mechanism is necessary for the continued existence of these ridges. It can be seen that an improved understanding of the requirements for linear sand ridge stability of size and position may help to explain bank genesis.

I.3 PRIOR WORK

Early work by Off(1963) identified and described linear sand ridges as a global phenomena associated with the strong tidal excursions of certain shelf seas. The search by Off through available navigational chart data indicated that sand waves and linear sand ridges often form in the same regions, with sand waves close to the normal, and sand ridges nearly parallel, to the peak flow direction.

The theory of linear sand ridge formation by secondary flow was first suggested by Off(1963). His theory required eddies within the flow that would encourage the formation of bands of slower moving water. This would cause the increased deposition of available sand which would then accumulate within these regions. He assumed that any accumulation could then act as a nucleus for further bank formation although no specific mechanism is mentioned and no cross-bank flow was envisaged.

This theory of secondary flow was strongly espoused by Houbolt who investigated the linear sand ridges of the Southern Bight during two cruises in 1963 and 1964. Houbolt(1968) gives detail of the internal structure of these sand bodies, with cross-sections, information on sand grain size, and transport paths inferred from sand wave orientations. Houbolt suggested that linear sand ridges were formed and maintained by contra-rotating helical flows that swept sand up to the ridge crest. This helical flow about an axis parallel to the main flow was investigated by the author in the laboratory and is described in chapter II. On the small scale this phenomenon explains the formation of parting lineations (Allen,1968), and on a larger scale it is known to explain river flow meanders (Scorer,1978).

An alternate explanation was given by Smith(1969). He assumed an anti-clockwise circulation that could trap the sand in order to build a ridge but no on-bank transport mechanism is described. He included a cross-bank component to the flow described as being driven solely by the cross-shoal pressure gradient. He also measured a logarithmic velocity profile on a sand wave crest.

The Smith(1969) investigation of Middle Ground shoal off of Martha's Vinyard, Massachusetts, showed a clear imbalance between ebb and flood tidal streams. This imbalance results in an anti-clockwise circulation around the ridge. Now Middle Ground consists of a sand body over a flat gravel base, and Smith assumed that this sand body was deposited at a time when the hydraulic regime was similar to the present day by an extension of the bank towards the headland. He further assumed that the ridge crest would have reached the surface were it not for the dissipative action of the waves. However, it has not been demonstrated that this flood and ebb imbalance is not a headland sheltering effect. Middle Ground shoal is partially coast-line connected by its close association with the West Chop headland.

A flood and ebb tidal stream imbalance well away from any coastal effect was demonstrated by Caston and Stride(1970) for the Norfolk sandbanks. This data was used to validate the time-meaned currents of the first detailed analysis of the hydrodynamics of a linear sand body given by Huthnance(1973). A bank of infinite length was considered and equations were derived for the time-meaned currents that could be produced by an oscillatory flow. Both type A and type B banks, as identified by (Kenyon et al,1981), see fig.I.7, were dealt with and two separate physical processes were discussed.

The first mechanism was identified as being caused by friction and convection. Here the effect of the friction would be modified in a different fashion when it passed from shallow to deep water to that which prevailed when it passed from deep to shallow water. The time-meaned current produced by this mechanism is in a clockwise sense for a type A bank and anti-clockwise for type B.

The second mechanism is identified as being a result of the Coriolis force. This correlates velocities in the x-direction with displacements in the y-direction so that the friction strength changes due to the change of depth. However, the concept that any change of depth must produce a change in friction is discussed further in the next section. The sense of this current will always be clockwise in the Northern hemisphere for either bank type.

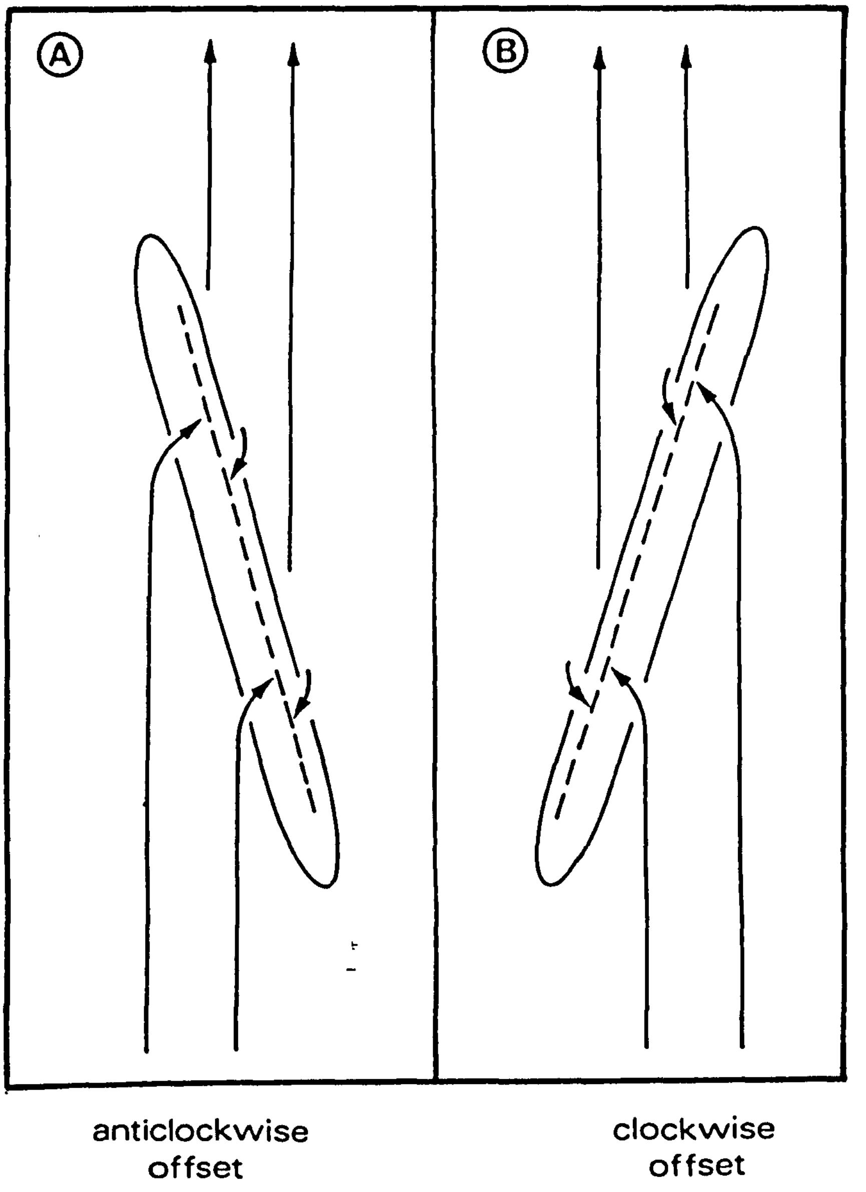

Fig.I.7 Tidal sandbanks .... A and B orientation. The arrows indicate net sand transport direction (after Kenyon et al, 1981).

The theory for the production of these time-meaned currents is compared in Huthnance(1973) with the ebb and flood data of Caston and Stride(1970). No close match was found for the theory and data, but there was qualitative agreement, in that the sign of the transport was shown to be correct. Support for the clockwise or anti-clockwise circulation was given by Caston(1981) and Mcave and Langhorne(1982), where mechanisms were investigated that could transport sand around the tip of a sand ridge and close the circulation.

Further investigation of these ridges by Kenyon et al(1981) confirmed the existence of a cross-bank component to the flow by a consideration of the sediment transport implications of bed-form morphology. It was noted that the orientation of the sand waves on a ridge altered towards the ridge crest to indicate a change in the flow direction more towards the crest. The angle of inclination of a bank to the predominant tidal stream direction was shown to be between 7deg and 15deg. They identified a type A bank, see fig.I.7, with angle of the bank to the peak flow clockwise, and also a type B bank, with an anti-clockwise angle.

The vorticity dynamics of enclosed basins, headlands and linear sand ridges are discussed in Zimmerman(1981). Now the vorticity equation can be derived directly from the equations of motion and continuity by cross-differentiation. In this new form the equations may give more insight into the physical process but the physics remain the same.

It can therefore be seen that the vorticity dynamics of linear sand ridges as expounded in Zimmerman(1981) are essentially a restatement of the hydrodynamics of Huthnance(1973). Nontheless, the use of the combined vorticity and stream-function equations can be a very useful technique for numerical modelling. The hydrodynamics of Huthnance(1973) are extended in Huthnance(1982a) to include the dynamics of bank growth, origin and existence. The sediment transport effects are quantified and a non-linear drag law is used.

Tidal residuals around a Norfolk sandbank were measured in Howarth and Huthnance(1984). Strong agreement between theory and measured data was not found but the measurements do support the theory of clockwise circulation. The data showed no on-bank or off-bank transport and can be considered as good evidence of the lack of a helical flow as suggested by Off(1963). However, the lowest flows measured were at 60 cm above the bed and cannot rule out a near bed-load effect, and one rig with Aanderaa meters at 6m and 17m did show different residuals at these heights. The 17m depth instrument showed a residual towards the bank which is entirely inconsistent with the theory of helical flow.

II PRELIMINARY INVESTIGATIONS

The work described within this chapter is exploratory and pre–experimental. Whereas an experiment is a test of a previously held hypothesis, here phenomena are merely observed and operational techniques assessed. An attempt is made to ascertain the reliability, accuracy and resolution of the values of the oceanographic parameters to be measured.

Field trips were undertaken using the Polytechnic research vessel but the facilities used were not limited to the available Polytechnic resources. I was offered the opportunity to work on partly turbulent flow with Professor Scorer at the Fluid Mechanics laboratory at Imperial College. Although there is no engineering department within the Polytechnic the facilities of the mechanical workshop were available for the construction of an instrument platform.

The concepts that need to be investigated for a better understanding of the stability of a linear sand ridge are; the conditions in a shallow sea that affect sand transport, the effect of a bank upon the velocity profile and the conditions required for the existence of a secondary flow.

II.1 SEDIMENT TRANSPORT

The variation over time of the bedforms described in the previous chapter is an indication of the existence within a shallow sea of sand transport. Any change in size or position of a bedform in a region of sand cover cannot be explained without reference to sediment transport.

Sediment may be silt, which is fine-grained, below 0.06mm, and in company with clay, subject to flocculation. Sand is non-cohesive, with size range 0.06mm-2mm, and this is the fraction that is considered in the investigations that follow.

II.1.1 Sediment motion

Sand grains, which are mainly quartz, settle with a distinct vertical velocity that depends upon; in-situ weight, surface area and the local velocity field. Particles above 2mm, the gravels, cobbles and boulders are less often transported by fluid motion, except by beach processes and storm conditions in shallow water.

There are four velocity fields that are of particular interest, a fluid at rest, a turbulent fluid with a zero mean velocity field, a field with finite mean velocity and a velocity field with vertical shear. The expectation of the existence of a lifting force upon a grain in suspension is different in each case.

In a fluid at rest a single grain will settle at a rate related to its in situ weight and surface area only. The solution for low Reynolds number for the drag on a sphere was first given by Stokes in 1851. It is assumed that an irregularly shaped particle may be modelled by a spherical particle with equivalent fall velocity.

In a fluid not at rest, lift forces may be exerted upon a particle. The effect of irregular shape is that grains, subject to the same flow conditions, and with the same drag and hence the same equivalent diameter, may have different lift forces acting upon them.

In a turbulent fluid with zero mean velocity the local upward velocity perturbations of the fluid will counter and may even reverse the tendency to settle. Thus eddy sizes larger than the grain diameter will have a dispersive effect in the vertical. The finest particles, with negligible settling velocity, will be suspended throughout the water column. Sediment concentration of this finest fraction will therefore be independent of depth. However, the large sand particle will have a finite settling velocity that ensures a bias of the concentration to lower depths. It has been assumed (Yalin, 1977) that the sediment concentration profile is logarithmic.

When fluid is in motion over a loose boundary of sand grains there exists the potential for erosion, by the initiation of sediment motion, as the bed shear stress exceeds a critical threshold value. Where erosion removes more material than is added through deposition there will be a region of scour and where the deposition flux exceeds that of erosion there will be a region of accretion.

The motion of sand grains in both air and water may be divided into a bed load, which is surface creep and saltation, and a suspended load. Surface creep may be by rolling or sliding, while saltation of a grain is by a sudden ejection from the bed surface up into the flow (Bagnold, 1941). Suspension is a result of the entrainment of a saltating grain up into the main body of the fluid where larger eddy sizes act upon the grain to carry it a considerable distance.

II.1.2 The measurement of sand transport

A Davall siltmeter was evaluated for use in the investigation. This instrument showed a multi-valued response to fine sand concentration when tested in the manoeuvring tank in the Navigation Department of the Polytechnic. Since two probes were available consideration was given to modifications that might enable the second probe to generate a reference signal. This would enable a measure of transmissivity or irradience to be made rather than both. Further investigation revealed that such devices already existed but were not recommended for the measurement of fine sand (M. Thorne, personal communication).

A Delft bottle was evaluated for use in the project during the 1979 field trip. The results obtained indicated that this instrument required very skilled operation and that this skill level could only be acquired over several field trips. Interpretation of the records was not easy and an essential requirement was co-deployment with a current meter since the total water flux through the instrument must be measured. This limits the measurement of water velocity to the method used by the Wallingford pump sampling system but with the added burden of a redeployment and bottle cleaning between each reading.

The field work reported in the next section demonstrates the importance of a dense sampling of water velocity. Since resources were limited in terms of personnel and current meters the attempt to assess sediment concentration by direct measurement was abandoned.

The problem of the provision of accurate measures of the concentration of sand in suspenson was not solved. The methods that had been tested were inadequate and no others could be identified that would be significantly better. This undermines confidence in historic sand flux data. The HRS pumped water sampling method may give adequate results in skilful hands but this system could not be made available for the project. Research continues into active and passive acoustic instruments (R. Soulsby, personal communication) and this should improve the situation.

II.2 VELOCITY PROFILE

The movement of sand by water in motion is highly dependant upon the variation of water velocity with depth of water, the velocity profile. The investigation of this variation was by a combination of theory and field work.

Field trips were undertaken to Shipwash Bank, Cutler Bank and the Sunk light vessel, all close to Harwich, which are indicated as stations Sh, Cu and Su in fig.I.3. These trips were used to evaluate the available oceanographic equipment and the levels of accuracy that could be achieved. Braystoke current meter deployment to a known accurate depth was not properly achieved. This could be overcome if the height of an instrumentation cluster could be measured by the inclusion of an echo—sounder or a pressure transducer. Another problem noted during this early field work was that of depth penetration in a fast tidal stream and for later work this was tackled by the use of heavy sinkers or the use of a bottom mounted rig.

A bottom mounted rig should be a good solution to the problem of near sea-bed measurement. Deployment from the ship was subject to ships motion such that the current meter followed a path in the vertical that was unknown. High in the water column, where velocity change with change of depth was small, measurement was not affected. However, near to the bed, where change of velocity was large with change of depth, the resultant integrated velocity values had no defined meaning.

II.2.1 Theoretical

We considered the hydrodynamics of shallow sea flow and followed the approach adopted in (Yalin, 1977) and (Schlichting, 1960) for the models of rough and hydraulicly smooth turbulent flows. We discuss, in an order of increasing complexity of the variation of topography, some of the forms that the velocity field may take.

a) 1-D LAMINAR FLOW

Low Reynolds number laminar flow exhibits the parabolic velocity profile (Yalin,1977) and this solution is used for model validation in the next section. Even at the turn of the tide, when the velocity in a simple reversing flow passes through zero, residual turbulence levels will prevent the establishment of a laminar flow regime in a shallow sea. However, the laminar flow solution for the flow around a sphere is applicable to individual sand grains with low velocities relative to the surrounding fluid. Furthermore it has often been assumed (Yalin, 1977) that a thin laminar sub-layer exists as a turbulent flow approaches the bottom boundary.

b) 1-D TURBULENT FLOW

For a 1-D steady state flow pattern that only varies in the vertical, the profile is given by II.(01) and this is applicable to any channel flow where width >> depth and the boundary is rough.

Now z_0 is the height above the bed of zero velocity, as estimated from the velocity profile, and this is used as a measure of bottom roughness. It is however, an artifact of the effect of the topography upon the flow and not of the topography itself. As such, it is, of course, not properly defined for a zero velocity field, since velocity is zero everywhere. However, it is assumed to vary little with changing velocity field values and this is supported by fig.IV.6. It can be found by extrapolation from velocity measurements at, at least two, different heights above the bed.

The relationship between z_0 and measured roughness value k was demonstrated by Nikuradse (Schlichting, 1960). For both smooth and rough turbulent flow the velocity profile is integrated between $z_{min} = k$ and $z = h$ to give

$$\frac{u}{u_*} = \frac{1}{K} \ln\left(\frac{z_0}{k}\right) + B \qquad \text{II.(01)}$$

where

$$B = \frac{1}{K} \ln\left(\frac{u_* k}{\nu}\right) + 5{\cdot}5 \qquad \text{II.(02)}$$

which is curve Sa in fig.II.1, a plot of the variation of B with log of grain size Reynolds number $u_* k / \nu$. Thus for a given sand roughness, as velocity is increased, the flow regime is first smooth, then transitional and lastly rough turbulent flow.

c) 2-D FLOW, x-variation

Flow over topography that changes in the along stream direction only will be governed by continuity. For any 2-D steady flow that has a variation of u in the vertical and in the x-direction, the form of the sea bed, and its relationship to the free surface, is governed by the Froude number F_r, which is the ratio of the fluid velocity u and the phase velocity c_s of a shallow water wave. For subcritical flow, where $F_r < 1$, two different bed forms may exist. If the sea bed deformation $\Delta <<$ water depth h then ripples will be formed and Δ will not be a function of h.

However, if Δ is not much less than h then $\Delta = f(h)$ and dunes will be formed. For critical and supercritical flow, where $F_r > 1$, anti-dunes will form with wavelength and amplitude strongly correlated with L and η for the free surface (Yalin, 1977). This problem of specifying the flow and bed interaction has been tackled by many authors (Kennedy, 1969) and (Fredsoe, 1974).

d) 2-D FLOW, y-variation

We now consider a 2-D steady flow with u variation in the vertical and in the y-direction. This form is crucial to the main line of investigation for the thesis. No previous theoretical work was found that discussed in detail what flow might be expected for a topographic variation normal to the mainstream.

On the very smallest scale it has been assumed (Allen, 1968) that parting lineations are a result of a secondary flow, that is, vortices with axis the mainstream direction.

One aspect of normal topographic variation that has been considered is that of channel flow sinuosity. It has been well established that river meandering is associated with secondary flow phenomena (Shlichting, 1960).

Flow over 3-D topography is complex and can induce a transfer of vorticity from one component to an othogonal component. Bluff obstacles trap vortex lines but gentle topographies bend and retard them (Scorer, 1978).

e) FRICTIONLESS FLOW

In the limit as the Reynolds number tends to infinity, viscous frictional effects are contained within a small turbulent boundary layer and the main body of the flow may be considered to be irrotational. There are two applications for this method in a shallow sea. Firstly, the upper layer of the flow may be modelled in this way with a considerable simplification for a 3-D flow. Secondly, particles with high velocities may be analysed thus and we can use results from aerodynamic theory to estimate the lift force on a particle on the sea bed or in suspension.

The existence of a force associated with rotating bodies was first demonstrated by Magnus in 1853. It depends upon the generation by the circulation of an asymmetry in the boundary layer separation zones. A numerical model of the interaction of the Magnus force with a logarithmic velocity profile was produced. No results are presented here since this work did not figure in the main investigation.

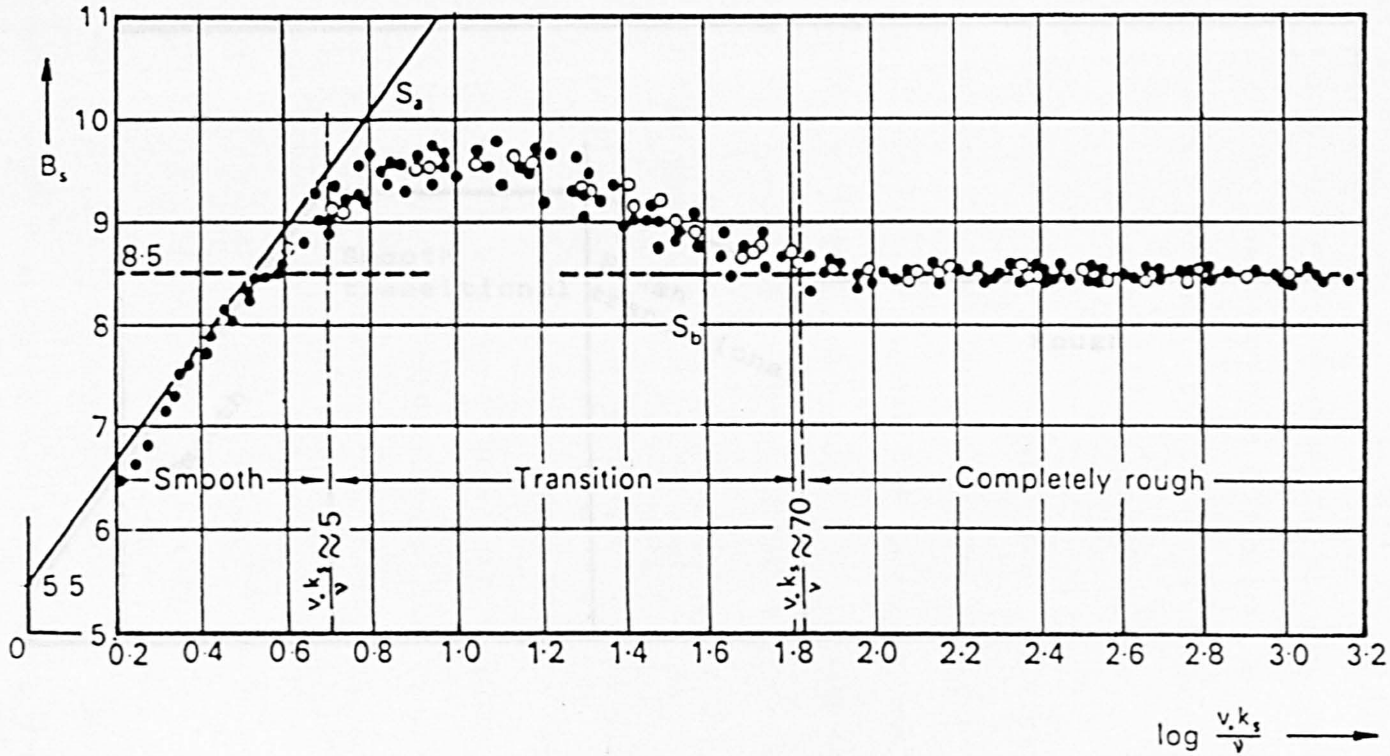

Fig.II.1 Nikuradse B-curve

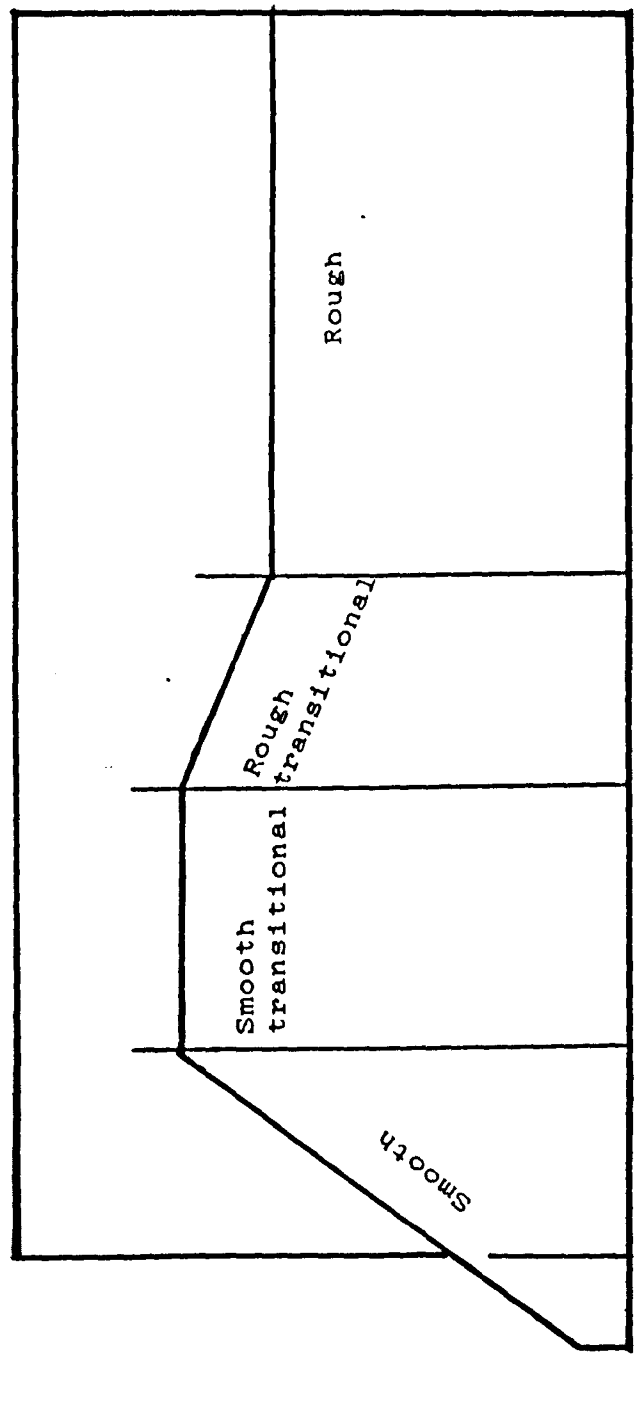

Fig.II.2 Simplified B-curve

II.2.2. Computational

a) Low Reynolds Number Flow

Laminar flow was investigated by the numerical solution of the vorticity and stream function equations which were solved for a 1-D channel flow and compared with a parabolic profile, the theoretical solution.

The Jacobi, Gauss-Seidel and Successive Over Relaxation schemes were implemented and the parabolic solution used for the stretched mesh dimension. This laminar channel flow modelling was a useful exercise but cannot be used as a description of the main body of the flow of a shallow sea since this is always turbulent.

However, for the flow about a single grain, laminar flow is a useful model because the density difference between quartz and water is not large and hence settling velocities can be very low. The next stage was to model the flow around a sphere in spherical coordinates. This problem is discussed in (Schlichting, 1960) where some results from (Jenson,1959) are presented. The work on the flow around a single grain was not taken any further.

b) Turbulent Flow

The combined equation II.(01) for rough turbulent and smooth flow is solved. A simple iteration scheme is used to solve for u_*, which occurs twice in this equation if the flow regime is smooth. The Nikuradse curve for B in fig.II.1 is simplified as shown in fig.II.2 where the transitional curve is approximated to by straight lines.

These define a value of B = 9.4 that we call the smooth-transitional value between $u_* k / \nu$ = 5.5 and 12.0, and the linearly interpolated value between 12 and 70 which we refer to as the rough-transitional region. The initial value of B = 8.5 assumes rough flow and the initial value of u_* = 1 is inaccurate. Nevertheless, convergence to a correct solution for both smooth and transitional flow solutions is rapid and rough flows are correct on the first iteration. The model takes no account of any form roughness such as ripples or dunes. We can expect that, with these higher effective roughness values, rough flow will be the norm for a shallow sea.

Output from the program was plotted showing velocity profiles for different velocities at 1m and different sand roughness values with a linear plot below the viscous sub-layer depth. For the rest of the investigations, no turbulent regimes other than rough flow were assumed and no plots from this modelling exercise are presented here.

II.2.3 Instrument platform design

The previous fieldwork had indicated that cycling of a single current meter for a velocity profile was not the best use for such a resource. All near sea bed velocity values achieved so were very low quality. Now inaccuracies of the profile high in the water column will have no large effect upon calculations of sand flux and can be discounted. However, loss of accuracy in depth measurement and velocity values near the bed will have a disproportionate effect upon calculations for the mass of sand transported in a flow regime.

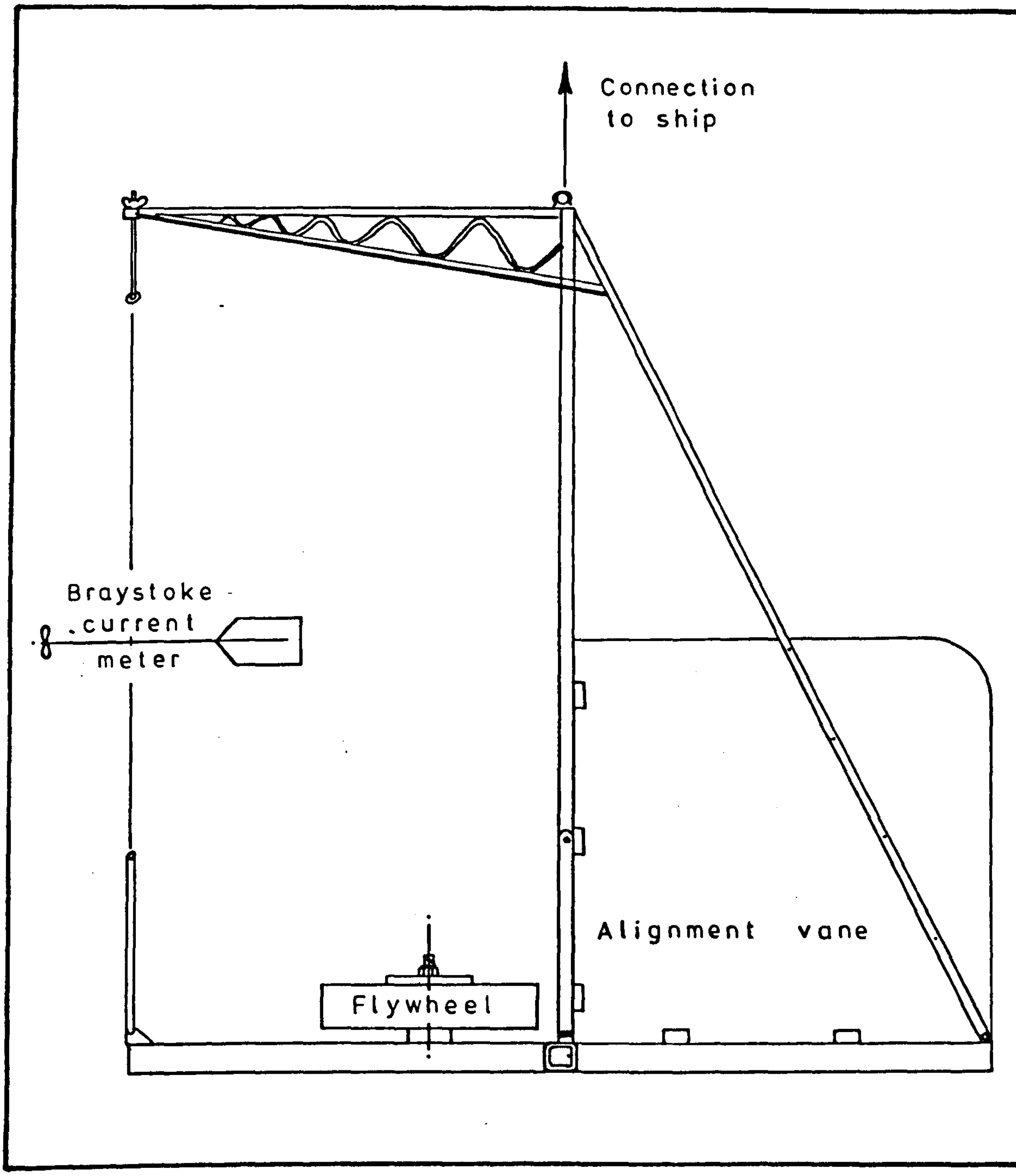

Fig.II.3 U100 Bottom rig

It was therefore decided to build an instrument cluster framework that would rest upon the sea bed. This frame was called the U100 rig since its main function was to record the water velocity at 100cm above the sea bed although the salinometer and siltmeter could also be mounted at 1m.

No resources were available for an in situ data logger, which made it necessary to use a tethered frame with direct reading aboard the support ship or boat. No modifications could be made to the Braystoke which must retain its normal operational capability. A design criterion that was considered to be of prime importance was that records should not be affected by support turbulence.

The regions of interest in the Thames Estuary and Southern Bight all have a degenerate tidal ellipse such that the flow is simply reversing. Although this bi-directional flow must be catered for it must not be forgotten that the moored ship will change position with the change of tide. The design requirement is therefore for an instrument that is uni-directional.

Values free from local effects can be achieved if we ensure that all support and rigidity are placed downstream from the current meter. The C-shape that this suggests is only slightly compromised in the final design shown in fig.II.3. This used a heavy square-section tube cruciform for the base with an alignment fin of marine plywood although sheet steel was the preferred material. The weight was centrally placed to be under the suspension point. A horizontal halo of steel rod, mounted on the upper current meter attachment point, ensured the framework could tumble without damage to the Braystoke.

II.2.4 Fieldwork in the Thames Estuary

The problems of depth penetration and measurement were tackled using a large sinker and the near sea bed capability was provided by the use of a bottom resting framework.

II.2.4.1 The Edinburgh Channels stations

This investigation made use of the first of these new techniques. The maintenance of these navigable channels, the main eastward and southward route from the Thames estuary, is of considerable importance (Cloet,1964). This region could have made an interesting study and the extreme bank mobility, indicating large sand fluxes, would have simplified sediment concentration measurement.

From the chart fig.I.4 it can be seen that for an ebb tide in the North Edinburgh channel and for the flood in the South Edinburgh channel the curvature induces a secondary vorticity. We can postulate that, for such an asymmetry of the flow, the secondary vorticity has acted to build up the mass of the central Shingles Patch. This bi-directional effect is related to the uni-directional effect of the central ridge that was noted in the double river bend experiment.

Some preliminary deployments within the region were tried in order to assess the potential for a full investigation. The two stations worked on the Shingles Patch in between the two channels were not sufficient for a major investigation but the ship could not be moored any nearer to the mainstream.

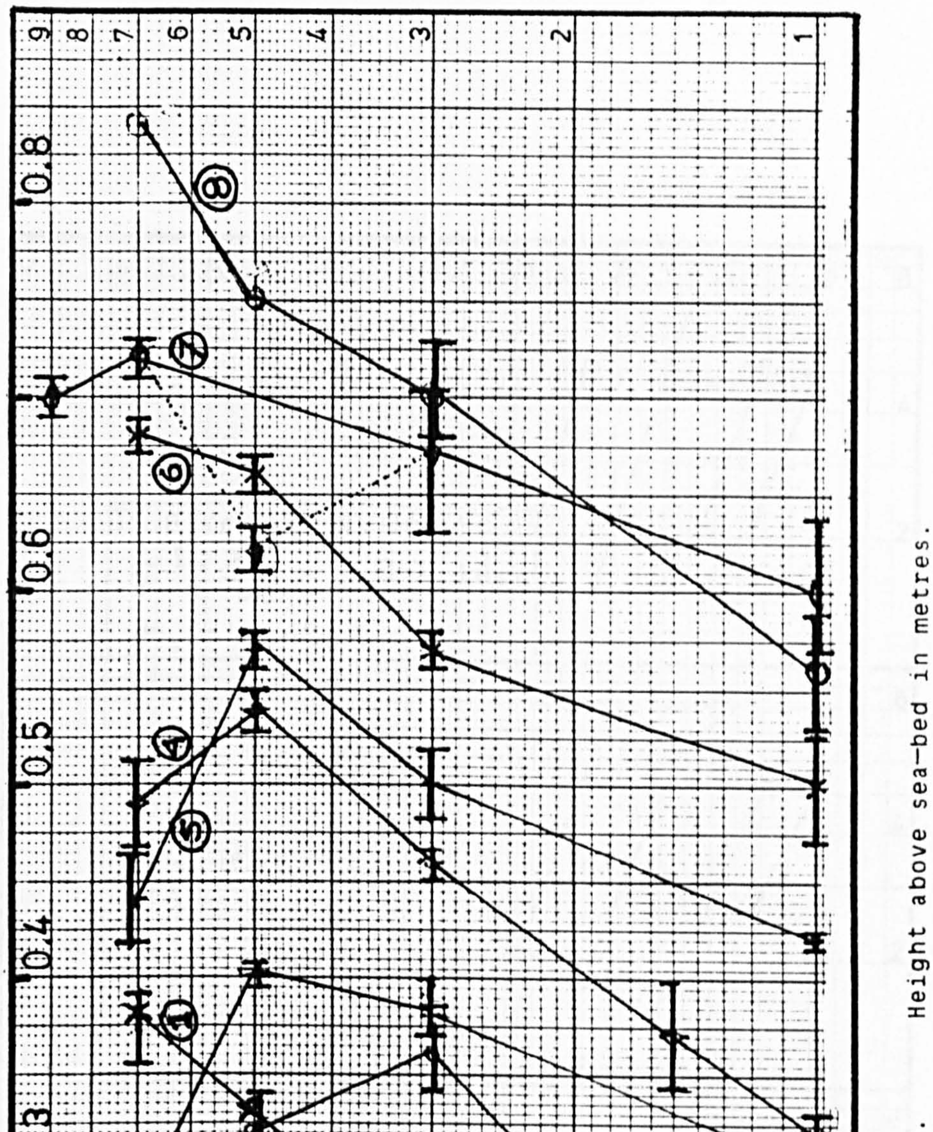

Fig.II.4 Edinburgh Channels — E2 velocity profiles
Single current meter data, downwards
deployment direction for profile 1.

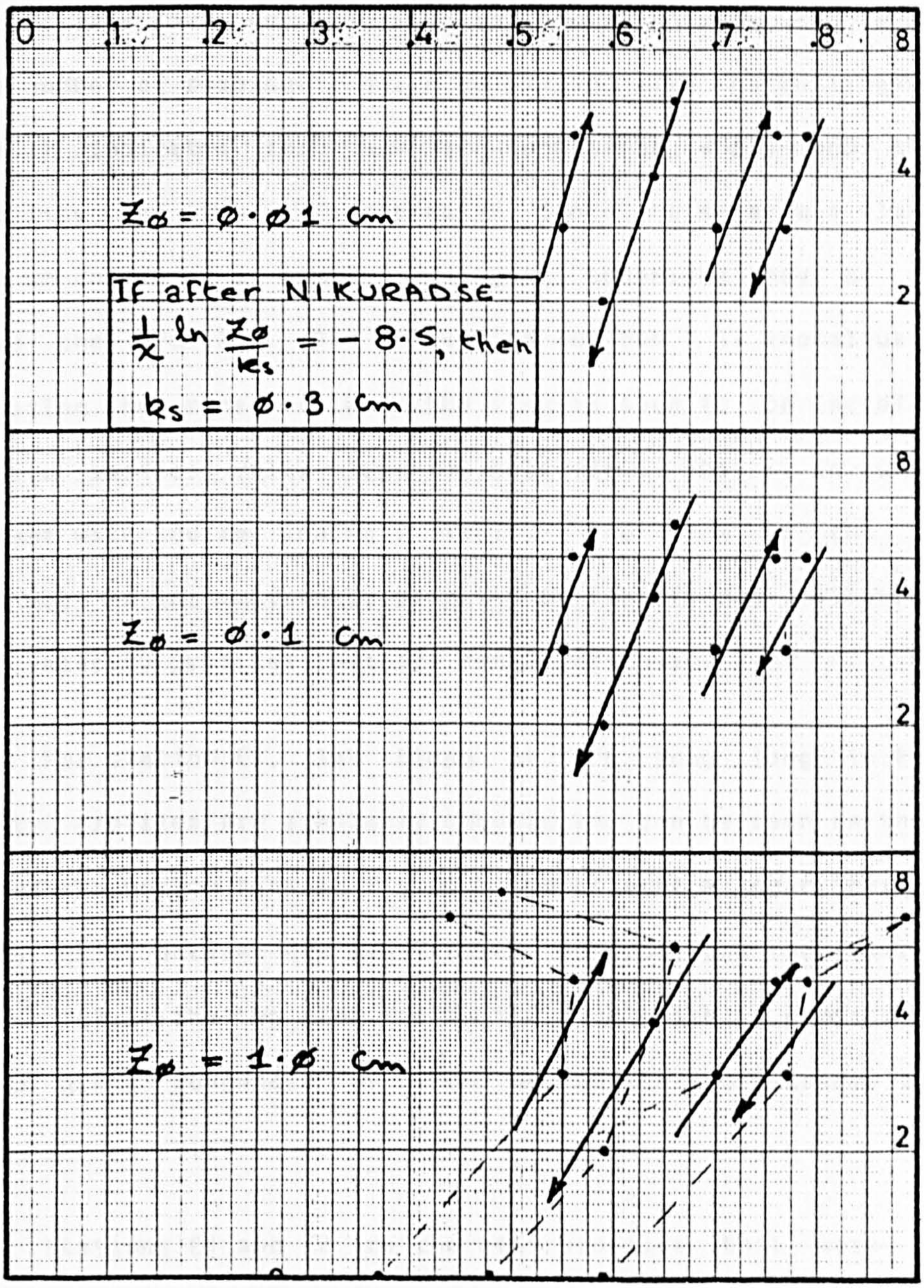

Water speed in metres/sec.
Height above sea-bed in metres.

Fig.II.5 Edinburgh Channels − E1 velocity profiles
Single current meter data, arrowheads
indicate the deployment direction.
Dotted lines show the measured profiles.
Logarithmic profiles are fitted for
three different Z_o values.

For station E2, lat 51deg 31.9'N long 1deg 19.13'E, the fig.II.4 velocity profiles are chaotic. The error bars should indicate the turbulence level but here they only serve to show the difference in the number of readings(1–5). A comparison with the Wallingford data fig.II.11 indicates that similar conditions apply and that the variability in time is a problem. Since the meter was alternately cycled up and down, a simple averaging technique may be used to improve the profiles. The 5m reading for run 7 is anomalous with no explanation. For runs 2–4, when the flow is seen to be accelerating, the near surface value lags the bulk flow. This is in qualitative agreement with Soulsby and Dyer (1981). The flow on the Shingles Patch may be intermittently affected by the stronger mainstream flow giving velocity profiles that are not logarithmic.

For station E1, lat 51deg 31.78'N long 1deg 16.8'E, the velocity profiles are similarly chaotic and can be seen as the dashed lines of the bottom plot in fig.II.5. We attempt a logarithmic profile fit to this dataset but must reject the upper and the lower values. The best fit is the top plot for z_o = 0.01cm which is compatible with a sand grain roughness of 0.3cm. We can therefore assume that some form roughness exists.

Stations E1 and E2 are the best profiles that were achieved using the cycling of a single current meter and they are not very satisfactory. The extra work needed to use a large weight reduced the number of values available to form the average for each observation. Some better method is needed to estimate bed shear stress τ_o and for a known z_o value this may be achieved using a bottom mounted rig.

The complexity of working in the Edinburgh Channels region indicated that some new region should be decided upon. It was decided that a shallow water region should be used for measurement since it would be possible to moor the ship out of the navigable deep water routes. A long thin ridge of sand would be more easily measured and modelled since the variation is effectively 2D.

II.2.4.2 The Knob Shoal investigation

This investigation utilised the U100 rig described in section II.2.3. The name Knob Shoal is not on the charts and was coined for the shallow section of a long ridge of sand which incorporates Tizard bank and trails WSW from Long Sand (fig.I.3,4). The high point of the bank is Station K, lat 51deg 31.25'N long 1deg 9.8'E, which lies 3cables NNW of the NE Knob buoy.

The flood tide over Knob Shoal may be affected by the wake from the Tizard Bank but on the ebb tide the flow should be undisturbed. The contouring of fig.I.4 is deceptive, the topography is not a simple sand ridge but a series of sand waves and small linked banks as can be seen from the survey runs of fig.II.6.

Deployment of the U100 rig was from the main derrick in the bows using the anchor winch. Once in the water the frame orientation is very stable with a forward tilt and it appears to take the ground well. The rig was first deployed with a full instrument cluster of Braystoke, salinometer and siltmeter. The water velocity readings were limited by the attempt to collect other parameters. The temperature and salinity values showed insufficient variation to be of interest.

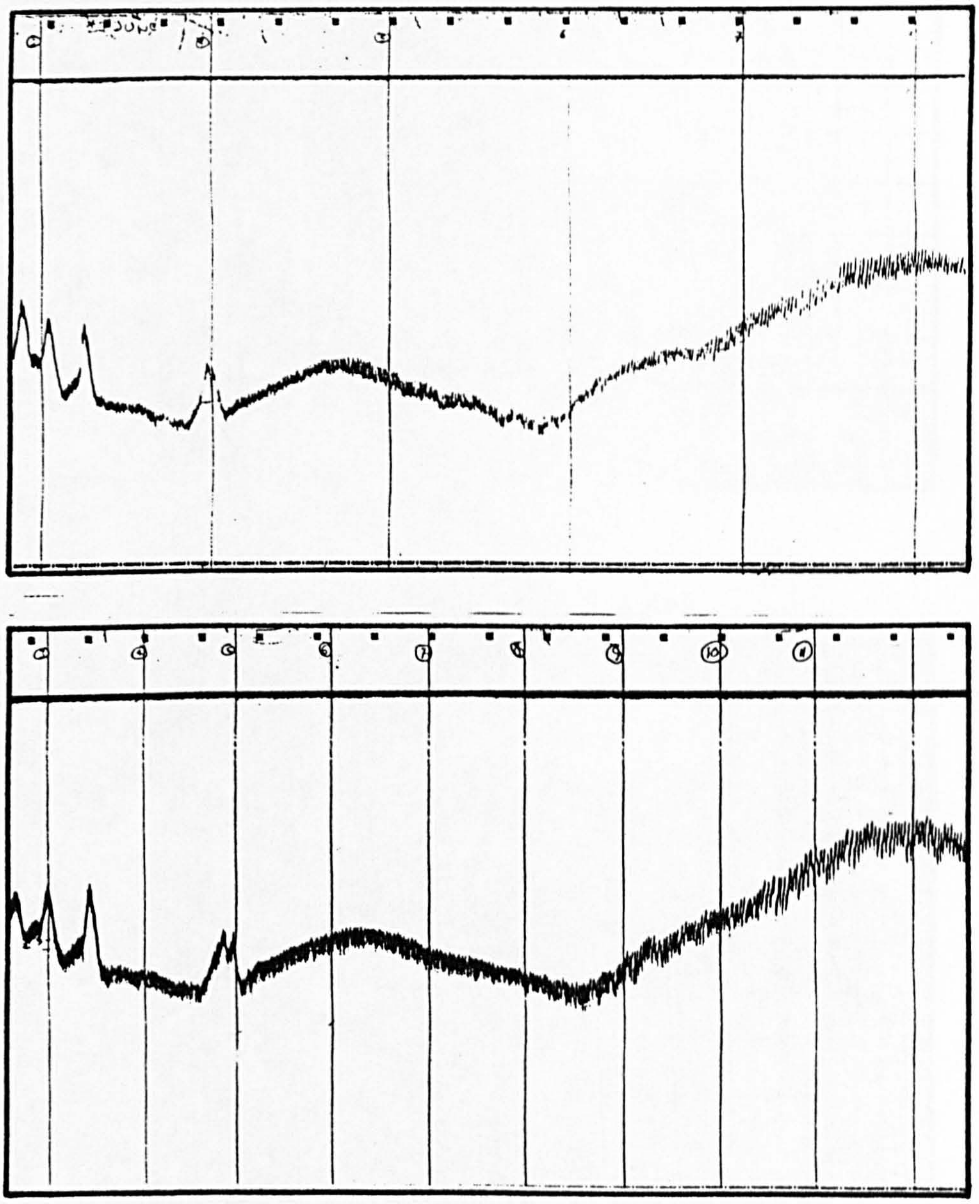

Fig.II.6 Knob Shoal — 1979, 1980 survey runs along the central ridge.

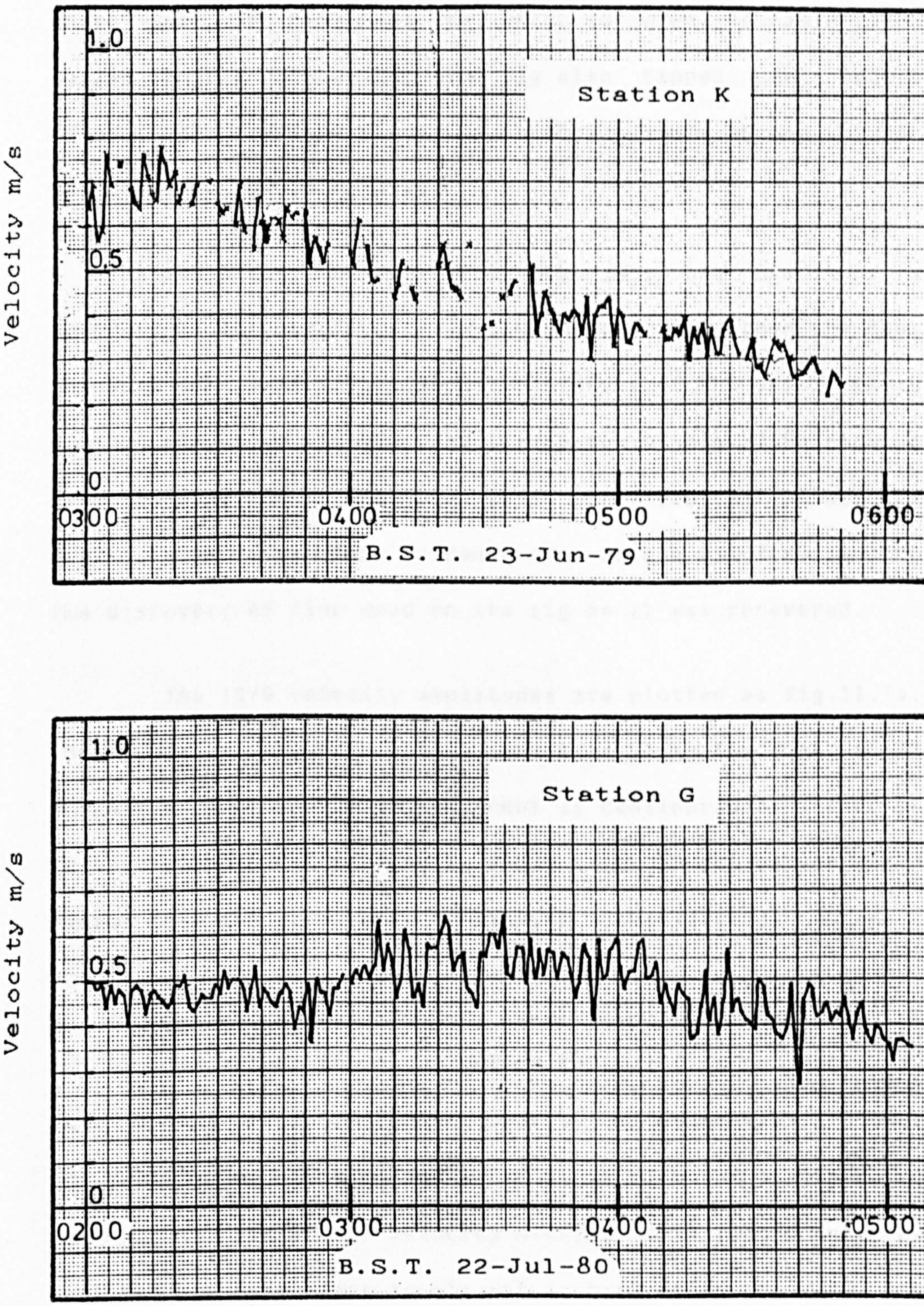

Fig.II.7 Velocities at 1 metre ... Stations K and G

With wind across the tide the ships moored position was not stable and there were no personnel to watch for when the cable tightened and pulled the rig to one side. The rig also tipped over but this was noted in the readings since the direction would become very stable and unrelated to the ships head.

The deployment of 1979 with just the Braystoke was more successful. The single cable was more manageable than the cable bundle and with some surface buoyancy the effects of the ships motion could be decoupled from the rig. The survey run of fig.II.6b shows no change from the 1978 run of fig.II.6a which indicates a stable bank with little sand flux. This evidence of a stable bed-form is supported by the discovery of fine weed on the rig as it was recovered.

The 1979 velocity amplitudes are plotted as fig.II.7a. Values for direction vary from 240deg, which is along the bank, to 270deg for which the cross-bank flow component is considerable. The Braystoke can resolve measures of bearing to 10deg only, so the values for direction cannot show the fine scale variation demonstrated by the velocity values.

The record commences before maximum flow and decreases for the last 2.5hrs. The variations over a 10min timescale are considerable and justify the decision not to continue with the single current meter cycling to obtain a velocity profile. This record could perhaps be analysed for turbulence levels but is too short to show the tidal variation. This 3hr length record shows the maximum that was achieved within a 12hr day. This has to include the deployment and recovery time and the passage to and from a safe port, in this case Sheerness.

A 25hr dataset is an absolute minimum for any serious scientific measurement of a tidal cycle but overnight working was not possible. Several other stations were worked using the U100 rig with similar results to those presented and similarly constrained to less than 3hr duration.

In 1980 the U100 rig was deployed at station SF on the South Falls bank for a comparison with the NERC designed rig (fig.III.1). This was not achieved since the ship was forced to to shelter within the Goodwin Sands by bad weather. The opportunity was taken to moor at station G for the record shown as fig.II.7b. This demonstrates that with no interruptions 1 reading per minute is possible. However, to achieve only 1 data dropout in over 3hr data collection requires a high degree of operator concentration.

A data logger is a definite requirement if data collection is to be stretched to a full day or longer. The record itself is of interest with a clear measure of turbulence levels. The tidal variation is not clear however and this, like the records from the Shingles Patch, supports the view that the maximum tidal streams are prevented from penetrating shallow regions while the smaller velocity values near the turn of the tide do penetrate and are comparable with the deep water values. A longer record may have demonstrated a square wave form for the velocity record but the tide did not turn during the 3hr observation period.

This attempt to measure the natural flow of a shallow sea was quite successful. Although water velocity initially appeared to be a problematical parameter, the capacity for accurate measurement at a known depth has been demonstrated. The numerical modelling of a 2D turbulent flow complements this experimental work. The concept of a logarithmic profile will be incorrect in detail for instantaneous values of the flow but the smooth and rough turbulent flow profiles are useful tools for analysis and comparison with measured flows.

Rather than continue to work with the very limited data that has been collected during the field trials it was decided that further experimental work should be planned. The complexity of modelling and the difficulty of practical work ruled out the Edinburgh Channels as a region for study. The work in a new direction would build upon the most successful early work at the Knob Shoal site.

II.3 SECONDARY FLOW

The work above on the velocity profile assumed that only the amplitude of the velocity vector can vary with change of depth below the surface. This primary flow is strictly two-dimensional (2-D), with a defined mainstream direction. Secondary flows are a particular class of 3-D flows that are a small perturbation of this 2-D flow by the inclusion of a streamwise component of vorticity (Scorer,1978). The helical flow suggested by Houbolt(1968) as a mechanism for sand ridge creation is of this type.

II.3.1. Laboratory work

This work was done, with Professor Scorer, on the Armfield Engineering recirculating flume in the Theoretical Hydrodynamics Laboratory of Imperial College (University of London).

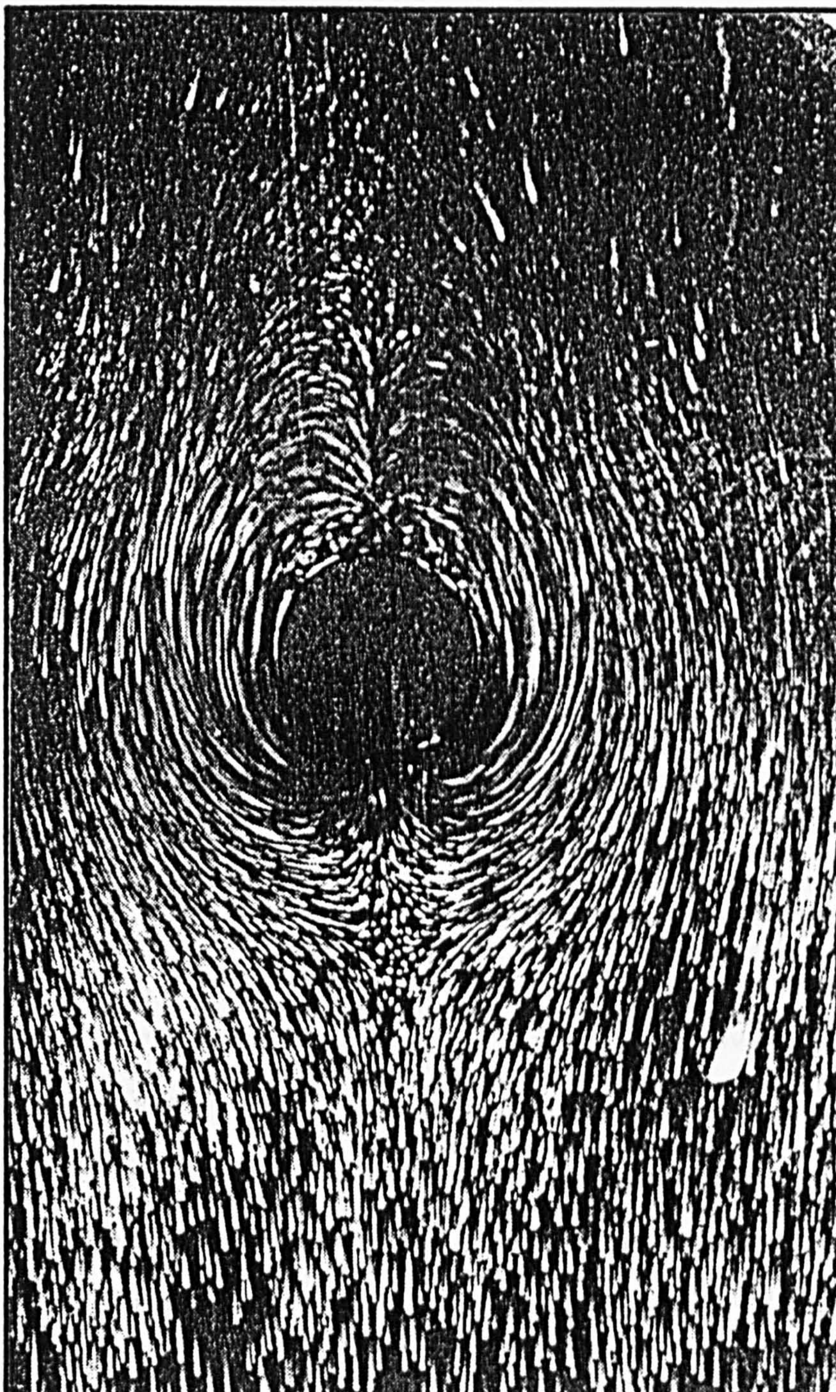

Fig.II.8 Flow visualization :
Horseshoe vortex around a cylinder

The aim was to study the effect of secondary flow upon fixed and loose boundaries, and to relate this to sediment transport and sand ridge growth. The flow visualization technique for fixed bed flow used dense white paint to mark the dark blue plastic bed. With time point markers extend far downstream whereas sprayed markers show the 2-D vector field of the bottom layer. An application of this technique is shown in fig.II.8, which shows the flow around a vertical cylinder of circular cross-section. The author performed this experiment for different flow values to show that the position of the 2-D convergence produced by the horseshoe vortex is quite stable and not a strong function of flow velocity.

For future research a useful extension of this experiment would be to produce visualizations of secondary flow around a sphere, both on and close to the bottom surface. However, whereas the cylinder remains in position within the flow because of its weight, some method of support must be found that could achieve positional stability for a sphere without the effect of the support modifying the flow pattern. This could be achieved by using a stiff wire rear support, which might modify the alternate rear vortices but should show the horseshoe vortex correctly. Measurements of lift and drag could also be made using this support method.

The second fixed bed experiment was a flow visualization around a single 45deg bend in a 10cm width channel with inner bend is of 20cm radius. Fig.II.9a,b show a weak double vortex system in the flow before the bend and a cross stream component directed towards the inner bend. For fig.II.9c the main flow was marked and can be seen to

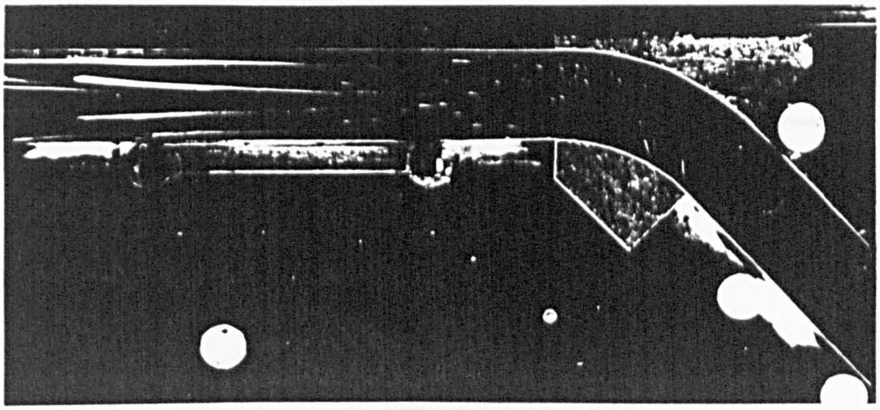

(a) First application. Upstream point markers show channel flow double helix. Sprayed markers show accretion at inner bend.

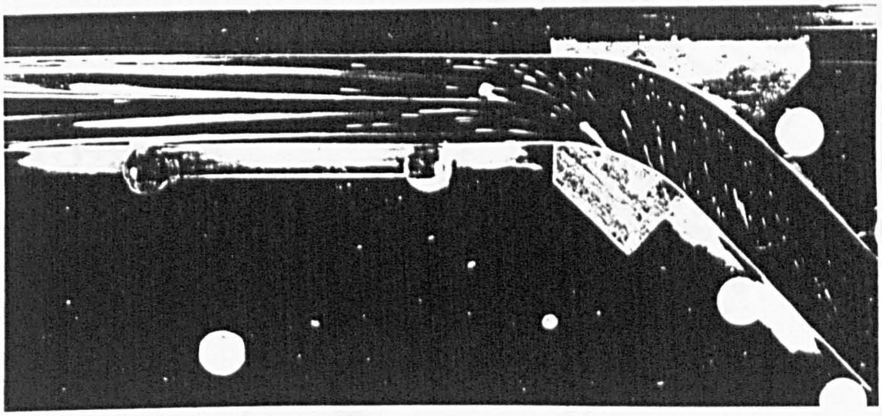

(b) Second application. Heavy point markers at bend. Sprayed markers at and round bend.

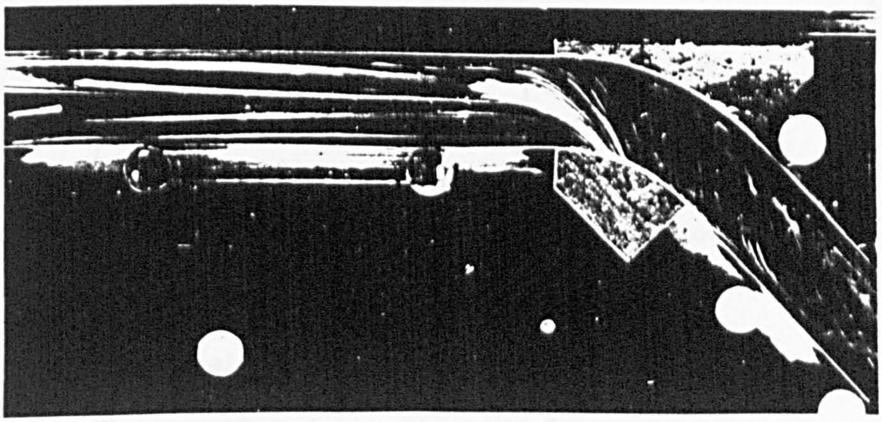

(c) Third application. Extra upstream marker. Previous heavy markers at bend have coalesced. All streak lines increased in length. Main flow is marked, showing turbulence with no cross stream component.

Fig.II.9 Flow visualization .... Channel bend

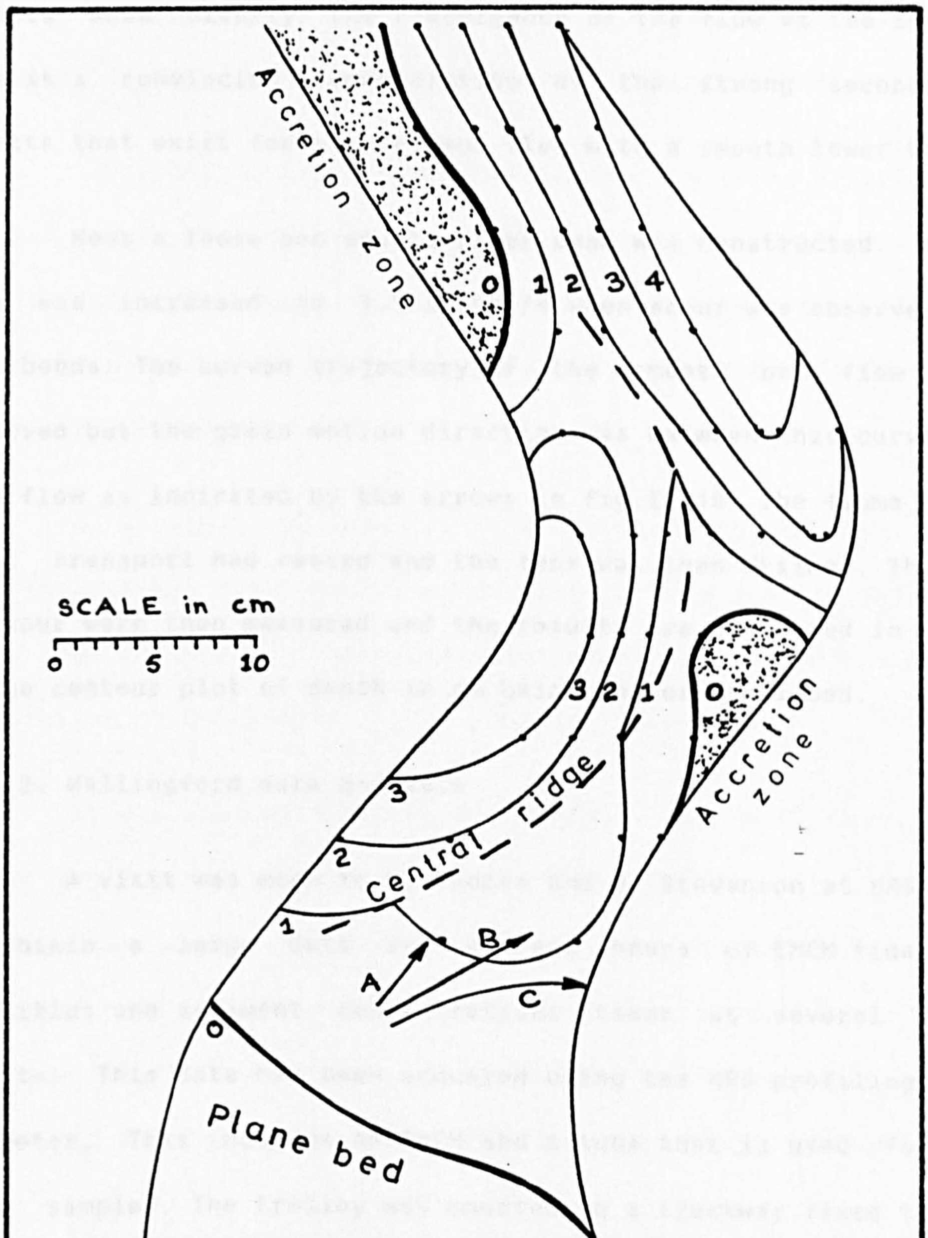

Contours are centimetres below plane bed.

A – Main stream direction.

B – Single grain : Observed tragectory

C – Smooth bed : Observed tragectory

Fig.II.10 Loose bed flow .... Channel double bend be highly turbulent with no cross stream component. Point and sprayed markers show clearly the convergence of the flow at the inner bend. This is a convincing demonstration of the strong secondary flow effects that exist for a turbulent flow with a smooth lower boundary.

Next a loose bed double river bend was constructed. The flow rate was increased to 3.5 litres/s when scour was observed through both bends. The curved trajectory of the smooth bed flow was not observed but the grain motion direction was between this curve and the main flow as indicated by the arrows in fig.II.10. The flume was run until transport had ceased and the tank was then drained. The regions of scour were then measured and the results are presented in fig.II.10 as the contour plot of depth in cm below the original bed.

II.3.2. Wallingford data analysis

A visit was made to M. Thorne and J. Stevenson at HRS in order to obtain a large data set of six hours of EMCM tidal current velocities and sediment concentrations taken at several different heights. This data had been acquired using the HRS profiling sediment fluxmeter. This includes an EMCM and a tube that is used for pumped water samples. The trolley was mounted on a trackway fixed to one leg of the Maplin Tower, which was on the sand flats near Southend, very close to station M on fig.I.3,4.

The data consisted of a final analysis of the calibrated values in the form of a computer printout and a magnetic tape of the files of the raw data as millivolt readings from the EMCM. The records commence with a 4—integer header which gives a zero code followed by the run number, G.M.T., and the height in centimetres. This is followed by a series of u, v values, the number of which is dependent upon the length of observation (~800 for a 4min record).

Two problems were tackled using the raw data. Firstly, it was assumed that the raw data would be used in the estimation of turbulence levels. Steps were taken to provide the capability to do a spectral analysis. Routines were coded to perform an FFT and some test transforms were output.

As a validation exercise it was decided to try to duplicate the calibrated data set by extracting it from the raw data. It was found that while the u absolute value was nearly correct as a direct translation of millevolts to m/s, the sign was wrong.

It was obvious that the calibration had not been a simple matter and further consultation with HRS confirmed this. The EMCM had suffered from drift during the experiment and a difficult validation analysis had been required. This used the comparison of turbulence levels of the EMCM and a wave-rider buoy. The analysis of the raw data was halted and further work concentrated upon the calibrated values.

The calibrated values for u and v with time and height were hand coded from the printout of the J. Stevenson analysis. This data set has an unusually high density of data points for each vertical velocity profile. It was decided to utilise this information to specify what part of the flow can be modelled as a vector rotating in the horizontal with its associated velocity profile. The residual flow can then be analysed as a secondary flow.

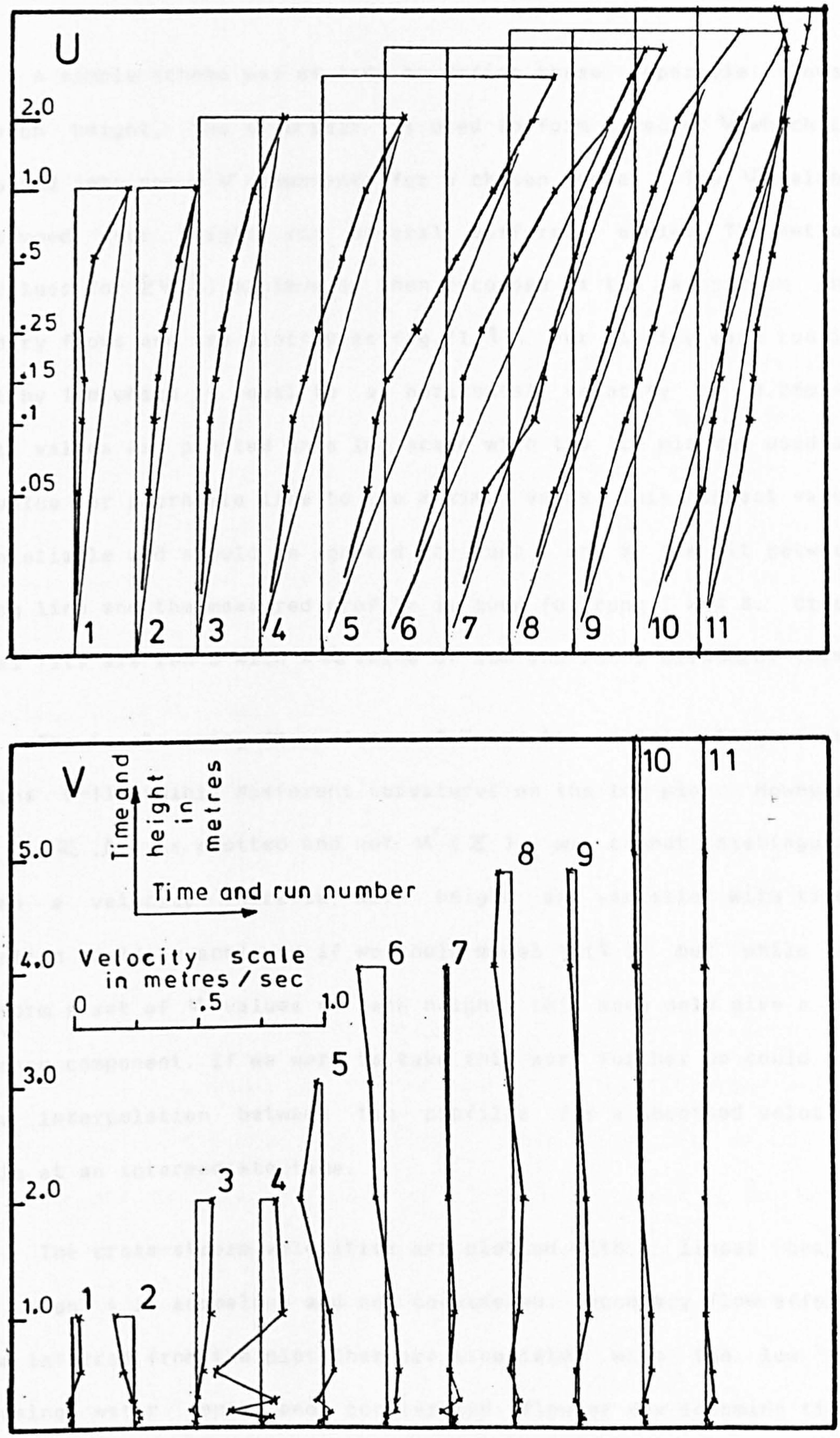

Fig.II.11 Maplin .... Velocity profiles

Mainstream and normal velocities

A simple scheme was devised to define these separable flows. For each height, the u, v pair is used to form a vector V which is decomposed into new u', v' components for a chosen angle. The v' values are summed over height for several different angles. The set of u', v' values for $\Sigma v'(h)$ minimum is then recorded as the mainstream and secondary flows and are plotted as fig.II.11. For clarity each run is offset by 1cm which is equal to a horizontal velocity of 0.25m/s. Height values are plotted on a log scale with the 1cm minimum used as a z_0 value for a profile line to the maximum value. This highest value is unreliable and should be ignored for runs 1 and 8. The fit between the log line and the measured profile is good for runs 7 and 8. Other partial fits are run 5 with a z_0 value of 5cm and run 9 with z_0 of 10cm.

The accelerating flow of runs 1–6 and the decelerating flows of runs 9–11 exhibit different curvatures on the log plot. However, since $u'(z,t)$ is plotted and not $u'(z)$, we cannot distinguish between a velocity increase with height and variation with time. Separation could be achieved if we could model $u(t)$, but while we can form a set of u' values at each height, this does only give a low frequency component. If we were to take this work further we could use linear interpolation between two profiles for a smoothed velocity profile at an intermediate time.

The cross-stream velocities are plotted with a linear height scale. Run 4 is anomalous and not considered. Secondary flow effects may be inferred from the plot that are associated with the low and increasing water depth and accelerated flow of the incoming tide. However, the plot is of $v'(z,t)$ and, if we assume the variation to be time dependent only, these values are consistent with those that could be produced by turbulent eddies with a time-scale of ~10min. These profiles cannot therefore be claimed as evidence for the existence of a secondary flow.

The plots appear to show the largest v' values high in the water column. This does not indicate that eddy values are larger with height above the sea bed. It is an artifact of the summing method used for separation. However, if we summed for the cross-stream mass flux minimising $\Sigma v'(\Delta z)$, where Δz is height above a previous reading, the effect would change. This method would show greater variations low in the water column for runs 1-6 but little difference for 10,11.

II.3.3. Secondary flow phenomena

The powerful effects of secondary flow have been noted. Scour at a loose boundary in a river meander or before a bluff obstacle is considerable. If a secondary flow is present at a linear sand ridge it should have an important effect upon sediment transport patterns.

The laboratory investigations confirm the importance of secondary flow phenomena. At the smallest scale the horseshoe vortex about a sand grain may give a lift effect close to the bed. It can be seen that where the bulk flow is described by the balance of two large forces that have a different variation in the vertical, a secondary flow will occur. However, field measurement of secondary flow would require simultaneous readings at many vertical positions. The effect may be small and obscured by the tidal stream, so that the direct measurement of secondary flow velocity vectors may not be worthwhile.

III LINEAR SAND RIDGE TIDAL FLOW

The field work on Knob shoal, using the bottom mounted U100 rig described in chapter II, had demonstrated the feasibility, but also the associated difficulties, of measuring parameters, at a known height above the sea bed, using direct reading meters from a moored ship. A preferred method of measurement would be by self-recording meters suspended between a heavy weight and a sub-surface buoyancy buoy. This method, essentially a deep sea mooring adapted for shallow water, had been used off the U.S. coast (Gadd et al,1978).

Knob Shoal is not a complete bank, only a spur of a large sand bank complex. Only on the ebb tide, when the shoal would not be affected by the wake of the other banks, could measurements hope to show a bank-like behaviour. It was hoped that another bank, as smooth on the top as Knob shoal, could be found somewhere in the Thames Estuary or Southern Bight. The Shipwash bank has been well studied (Davies, 1974) and shown to consist of sand waves along the whole of the crest length. This seems to be a characteristic of many of the banks in the region.

In 1979 Dr. B. D'Olier was awarded NERC facilities in order to investigate the geology of the Southern Bight down to the Dover Straits. This work combined well with an investigation of sandbank crest morphology and a fluid flow experiment. A field trip was undertaken to look at sand banks, sand waves and other bathymetric features of the Southern Bight and Outer Thames Estuary. To support this work I was to initiate the design of a rig to look at the flow over a sand bank.

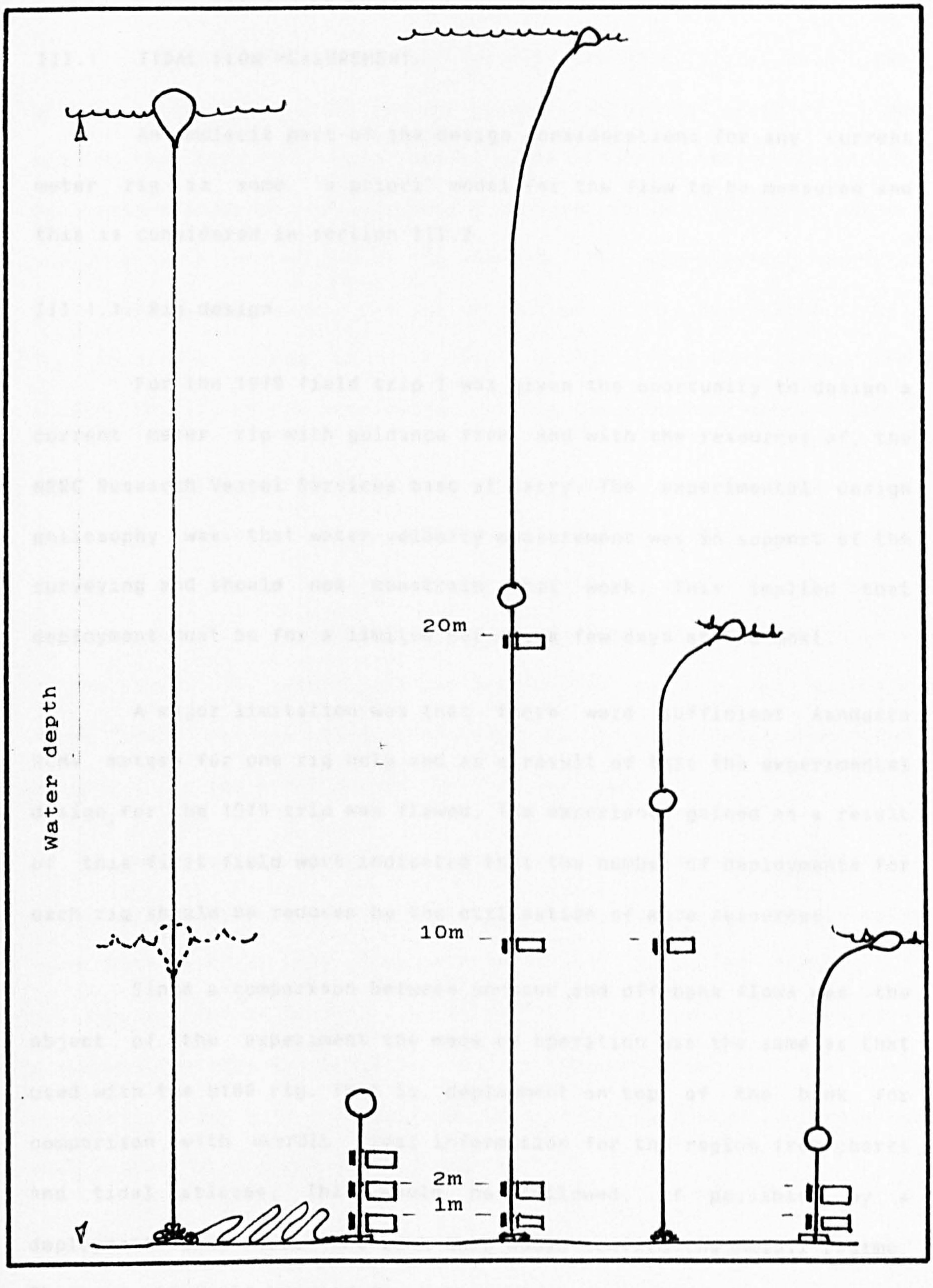

Fig.III.1 Aanderraa current meter rigs - 1979,1980

III.1 TIDAL FLOW MEASUREMENT

An implicit part of the design considerations for any current meter rig is some 'a priori' model for the flow to be measured and this is considered in section III.2.

III.1.1. Rig design

For the 1979 field trip I was given the oportunity to design a current meter rig with guidance from, and with the resources of, the NERC Research Vessel Services base at Barry. The experimental design philosophy was that water velocity measurement was in support of the surveying and should not constrain that work. This implied that deployment must be for a limited period, a few days at the most.

A major limitation was that there were sufficient Aanderra RCM4 meters for one rig only and as a result of this the experimental design for the 1979 trip was flawed. The experience gained as a result of this first field work indicated that the number of deployments for each rig should be reduced by the utilisation of more resources.

Since a comparison between on-bank and off-bank flows was the object of the experiment the mode of operation was the same as that used with the U100 rig. That is, deployment on top of the bank for comparison with overall tidal information for the region from charts and tidal atlases. This would be followed, if possible, by a deployment away from the bank that would confirm the overall regime. The same rig would be used for both deployments and must therefore be capable of being deployed in say 10m and 50m water depths.

A U-mooring was used as detailed in fig.III.1, with 100m ground line, chain clump and spar buoy. A pinger was attached to the rig, to aid recovery if this latter tackle should be lost. The design was rather crowded, it contained 3 Aanderaa current meters at 1m, 2m and 3m above a lead weight at the sea-bed. The sub-surface buoyancy buoy immediately above the top meter gave a total rig height of 5m. The imperfect nature of this rig design resulted from the incompatibility of the requirements at the two different water depths.

It was expected that the top meter would be contaminated by wind wave action for the deployment in only 10m of water. The intention was that a comparison between the lowest and the top meter would provide an estimate for a correction factor for wind wave contamination. The intercomparison between the on-bank and off-bank flows would be for different tides which would make comparison difficult and for short records not very accurate.

The 1980 rig designs benefited from the experience of the 1979 field trip, which had demonstrated that rig deployment and recovery were both arduous and time consuming and that the number of deployments should therefore be minimised. These new rig designs were a response to this knowledge and to an increase in the available resources. This time 7 Aanderaa current meters were made available so that several rigs could be deployed.

The strategy to be followed was that all rigs would be deployed at once and all recovered after the same period. A self-imposed constraint was that since the area of study was a North Sea fishing ground at no time would the rigs be left unattended.

Only a days sidescan survey work remained to be done in this region so the maximum allowable observation period coincided with the minimum sensible observation period of 25 hours. The highest data rate for an Aanderaa was used, 1/2min between samples, which gave a 3 days operating limit.

Three rigs were designed – one for the bank top in 10m water depth, another for the bank side or flank in 20m and a third completely away from the bank in 40m water. Although U-rigs were the norm for NERC designs, Phil Taylor suggested that an I-rig design would be appropriate for my needs and this recommendation was followed. The designs used are as given in the diagrams in fig.III.1.

Top Rig

This was intended for a charted LAT depth of 7.5m and with 5m spring tide range mean sea level h is 10m. Aanderaa's were mounted at 1m and 2m above the anchor weight. This was ~1000lb lead weight so that vertical accuracy of meter positions could be maintained. This equipment was supported on a wire rope below a 27inch subsurface buoyancy buoy to which a surface buoy was attached by a floating rope.

Flank Rig

This rig was to be deployed in 20m water on the bank sides where there are sand waves. Accurate vertical measures relative to some indeterminate level within the sand wave field on the flank would not be useful, so a chain clump was used here instead of the lead weight. Below the surface buoy a subsurface buoy supported a single current meter at mid-depth, 10m above the bed.

The Off-Bank Rig

This rig was the most complex and also the most important one. With good results from this rig we could hope to define the nature of the tidal regime undisturbed by the bank. We needed to be able to validate the logarithmic assumption used in the 1st model or to demonstrate a shallow water Ekman veering of the flow. On the ebb a lee wave effect from the bank might be seen.

This main rig was deployed in 40m water below a surface buoy. Between the subsurface bouyancy and the lead weight 4 Aanderaa's were suspended at heights of 1m, 2m, 10m, and 20m above the sea bed. This chosen spacing was optimal for the delineation of a logarithmic profile.

For the 1981 rig design criteria, the experimental region was unchanged and the success of the 1980 data collection suggested that the rig design should not be changed. However, the I-rig design with a small surface buoy does risk some wave-contamination and it means that the rig may be difficult to find for recovery. The advice from RVS was to use the U-rig anchoring method this time and this modifies the deployment method.

The rig design between bottom weight and sub-surface buoyancy is unchanged and is described above. No flank rig was used this time, just two off-bank rigs and two on-bank rigs.

III.1.2 Field trips

From previous work by Dr. B. D'Olier, it was known that the upper surfaces and flanks of many banks were, like Shipwash, sculpted, by the water flow, into a continuous series of sand waves. It was considered essential that a sand bank should be found that had a region with no sand waves at the bank crest. If such a region could not be found, it would not be possible to separate the effects of bank top water velocity from that of the flow variation over the sand waves. This would require a much more extensive measurement program than could be mounted using just Polytechnic resources.

The NERC research vessel 'John Murray' was used for the 1979 field work. A survey was undertaken in order to find a sand-wave free region. Sufficient information was available to eliminate many of the banks beforehand. Echo-sounder runs were commenced along the remaining sand ridge crest lines. Considerable difficulty was experienced in maintaining a survey line since the tide often pushed the ship off course. The last runs were along the Outer Gabbard and the Falls bank group and were nearly completed before the required region was found at position Lat 51deg 17.5'N Long 1deg 45'E.

An echo-sounder and side-scan sonar survey of the area were completed and the rig was deployed on top of the bank. The very crowded rig design (so many meters on a short rig length), made for a tricky deployment, but the rig was successfully laid on the bank top. While on station,it was noted that there was a considerable cross-bank component to the flow. This was identified as the reason why the maintenance of a survey line along the bank had been so difficult.

A Radar watch was kept on the rig while adjacent areas were being surveyed. The weather now deteriorated until no useful work could be achieved. Shelter was taken in Dover Outer harbour. It was expected that the main threat to the rig, which was trawling, would be stopped by the gale.

However, upon our early return to the site next day, a fishing vessel was noted to be navigating along the length of the bank, without its tackle in use. No rig markers were found. The pinger that had been included for just this eventuality did not show on the equipment provided. The site was identified by Decca co-ordinates and the rig ground-line was trawled for for several hours. It was decided that no more boat time could be used and recovery attempts were abandoned. The difficulty experienced while navigating along the bank crest is very clear qualitative evidence for a cross-bank flow component. However, no quantitative data was obtained that could be used for comparison with a mathematical model or simulation.

A useful result of this work was the identification of a uniquely suitable region for the investigation of the flow over a Southern Bight sand ridge. The trip had demonstrated the value of the site finally chosen, subject to it being shown that the gap that had been found in the continuous sandwave coverage was a permanent feature. If it proved to be a stable feature of the area the description of bank flow by a measurement programme would be possible. It was decided that this region, the South Falls, shown in fig.I.5, should be explored further, particularly as a further deployment was possible during 1980.

The 1980 field work again made use of the NERC research vessel 'John Murray'. The departure was delayed by gales but heavy weather was forecast for the whole of the research period. The ship left Milford Haven to round Land's End in a Southerly gale in order that what weather windows there were could be used for research rather than for making a passage. Fortunately, most of the work of preparing the current meters and tackle had been completed by RVS Barry staff before the passage commenced. The main group of scientists was embarked at Dover just 1 day late and deployment work commenced immediately.

The bank top region previously identified was re-surveyed and found to contain the same gap in the sand-wave coverage of the bank top. The three rigs described in the previous section were deployed with one on the bank, another just west of the bank crest on the flank and the third further west, completely off the bank. The deployment positions relative to the bank are marked on the echo-sounder profile of the bank given in fig.I.6.

The sea was rough by the time the deployment was finished and the weather deteriorated during the 25 hours of data collection. It appeared that the weather would deteriorate further and so the rigs were recovered at this time, albeit with some difficulty. The Aanderaa meters were checked and found to be working well. The timing of the in-situ clocks in 2 of the meters had drifted by $\sim$10 seconds so that the 1/2min sample periods were less well synchronised towards the end of the measurement period. The rest of the field trip was used by Dr. D'Olier for the acquisition of geological profiles to the East of South Falls and along the Belgium coast.

The data return from this 1980 field work was exceptionally good and it more than compensated for the lack of data in 1979.

The 1981 cruise once again made use of the NERC research vessel 'John Murray'. We embarked at Dover on 5th May and immediately commenced seismic surveying. The hydrodynamic measurement program detailed below started on 8th May.

The SF1 bank top region was surveyed again and little change was found. In particular, there were still no sand waves in this area. The four rigs described in the previous section were deployed with one to the East (A), off of the bank, two on the bank (B),(C) and the forth (D) further West, also off of the bank.

TABLE IV.3.A

A	B	C	D
51 17.9'N 01 44.7'E	51 17.7'N 01 45.6'E	51 17.7'N 01 45.4'E	51 17.5'N 01 46.2'E

Upon recovery, certain of the rigs had suffered damage; one rig was wrapped around with a large blue industrial polythene bag! There was obvious damage like the complete loss of one Savonius rotor and some bent rods. It was hoped that this had occured on recovery and not on deployment. The meters themselves were checked and found to be in working order.

III.1.3 Data preparation

The initial form for the 1980 collected data was seven 3inch diameter 1/4inch width magnetic tapes. These were returned to RVS Barry where they were translated onto paper tapes which could be read by the fast paper tape reader at City of London Polytechnic computer centre straight into datafiles on the DEC10. Although this is rather old technology, it was much easier than the acquisition of the Wallingford data, which was by 1/2inch 9-track magnetic tape with all the problems of tape formats.

A file of data values for each current meter was kept on the DEC-10 archiving system. The minimum retrieval time for archived material was 24hr and a maximum of only 4 data files could be worked on at one time.

It was extremely unfortunate that, during a fallow period for this research of a few months in 1983, contact with the Polytechnic Computing Service was lost when both the DEC-10 and its archiving system were withdrawn from service. Hence, the data and processing programs were not availale for some of the later work on the thesis.

Work planned on the spectral analysis of the data for an investigation of turbulence levels could not be attempted and no plots of the data other than the initial along-bank and cross-bank velocities could be provided.

III.1.4 Data processing

No software existed locally for the processing of the Aanderaa data so this had to be written. The output format details are described in the RCM4 operating manual. The 6 information channels are; a reference number, temperature, conductivity, pressure, current direction and current speed and the six 10-bit integers of each record are coded in a compact (FFI-PS) binary code. A double coefficient power series formula is used, with data from tests at Barry, to calculate the individual sensor calibration.

Programs were written for the extraction from each main file of the data values for the individual parameters and a new file was written for each of the calibrated parameters. Prior to the data analysis these files were printed for a first scan to check data quality and then plotted. Raw data plots are shown in fig.III.2-6. Both the water speed and direction of fig.III.3-5 had to be smoothed with a 9-point running average (4.5min time smoothing) in order that the variance should not dominate the signal.

The 1981 collected data set was treated in the same fashion as the 1980 data-set. The 1/4inch RCM4 magnetic tapes were transcribed by RVS Barry as before. Unfortunately the data return this year was poor - there was a very high data drop-out. The processing method used is described above and only the water velocity data was plotted as amplitude and direction in fig.III.7.

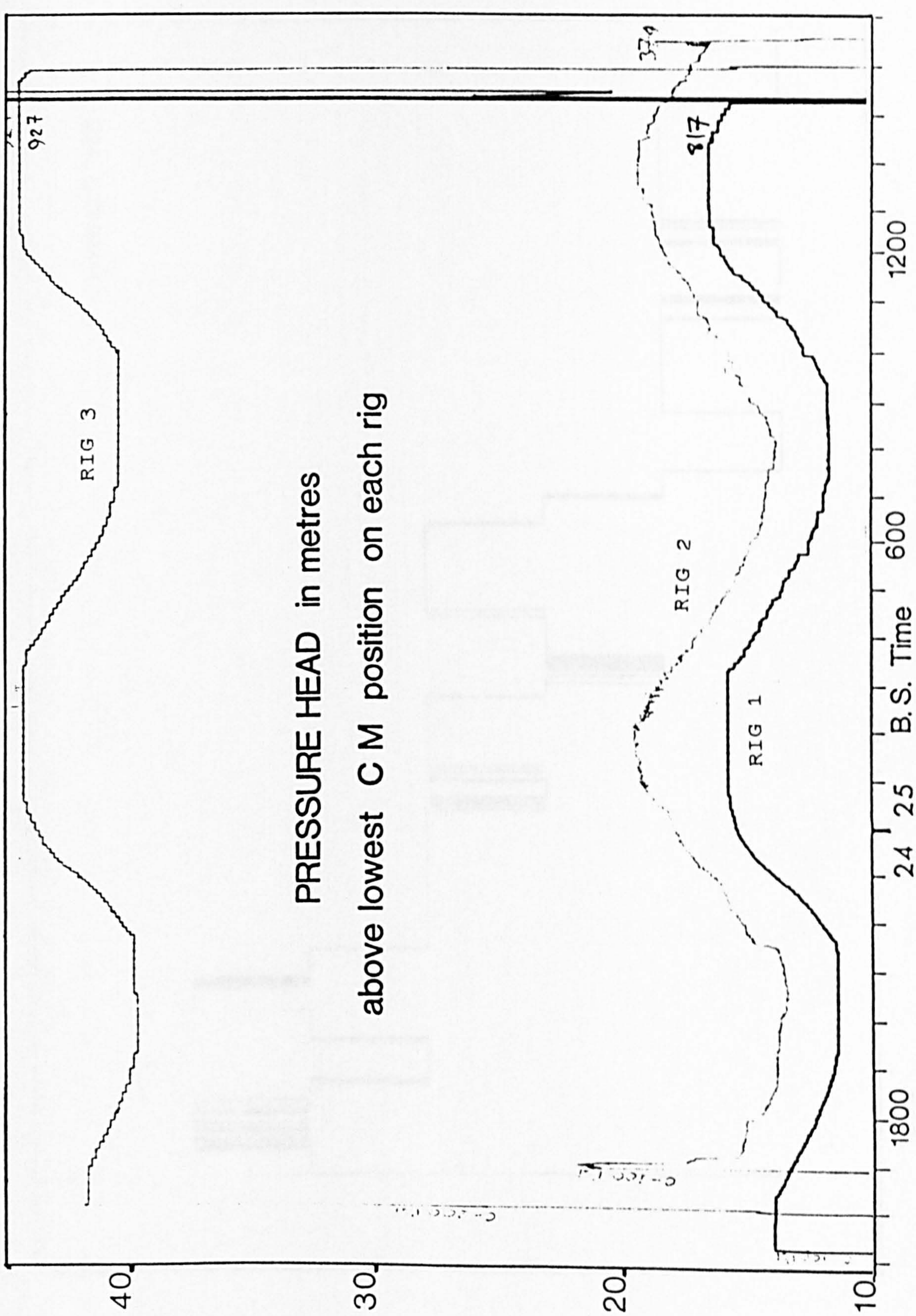

Fig.III.2a 1980 data — Pressure head,
water depth in metres.

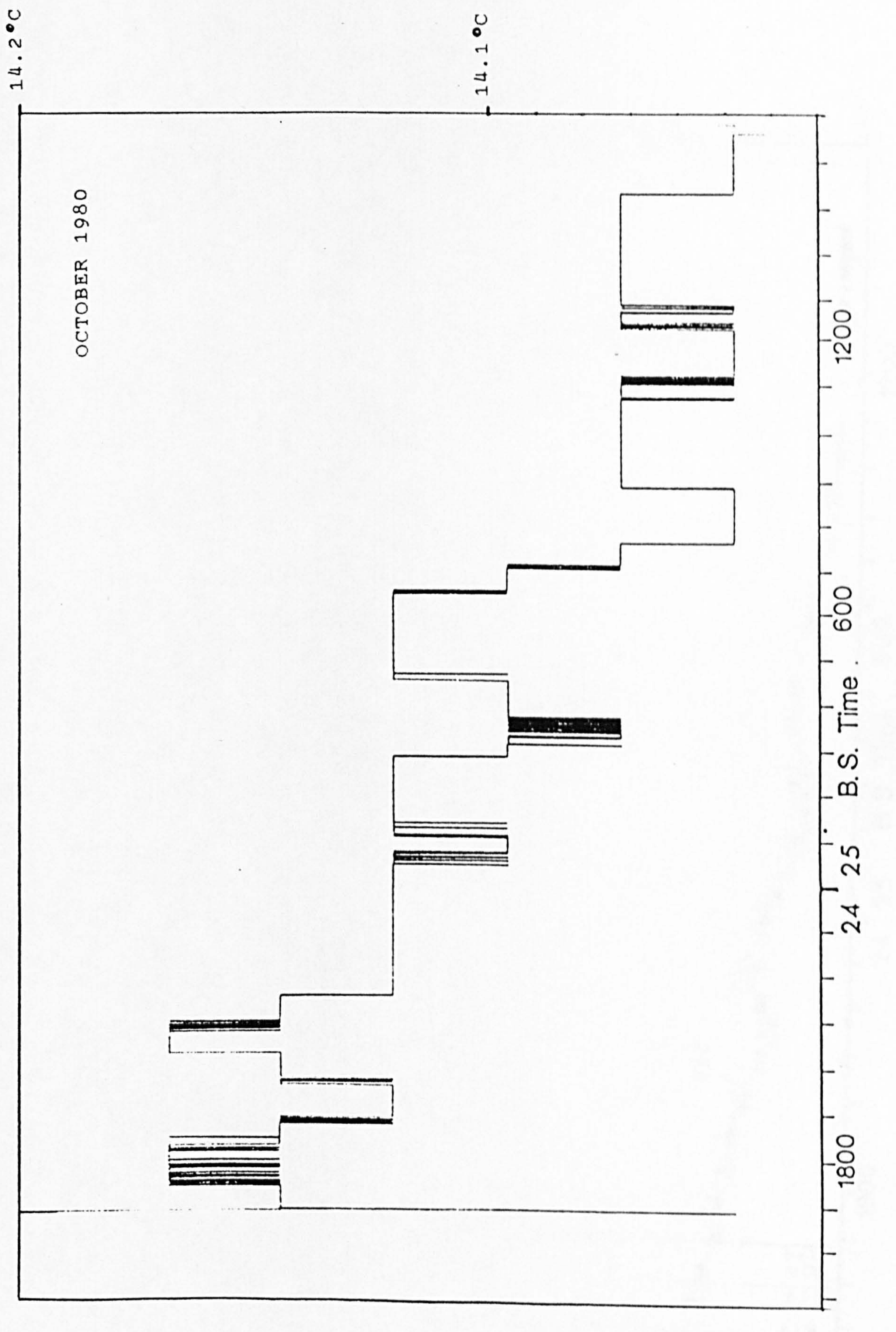

Fig.III.2b 1980 data — Temperature at RIG 2

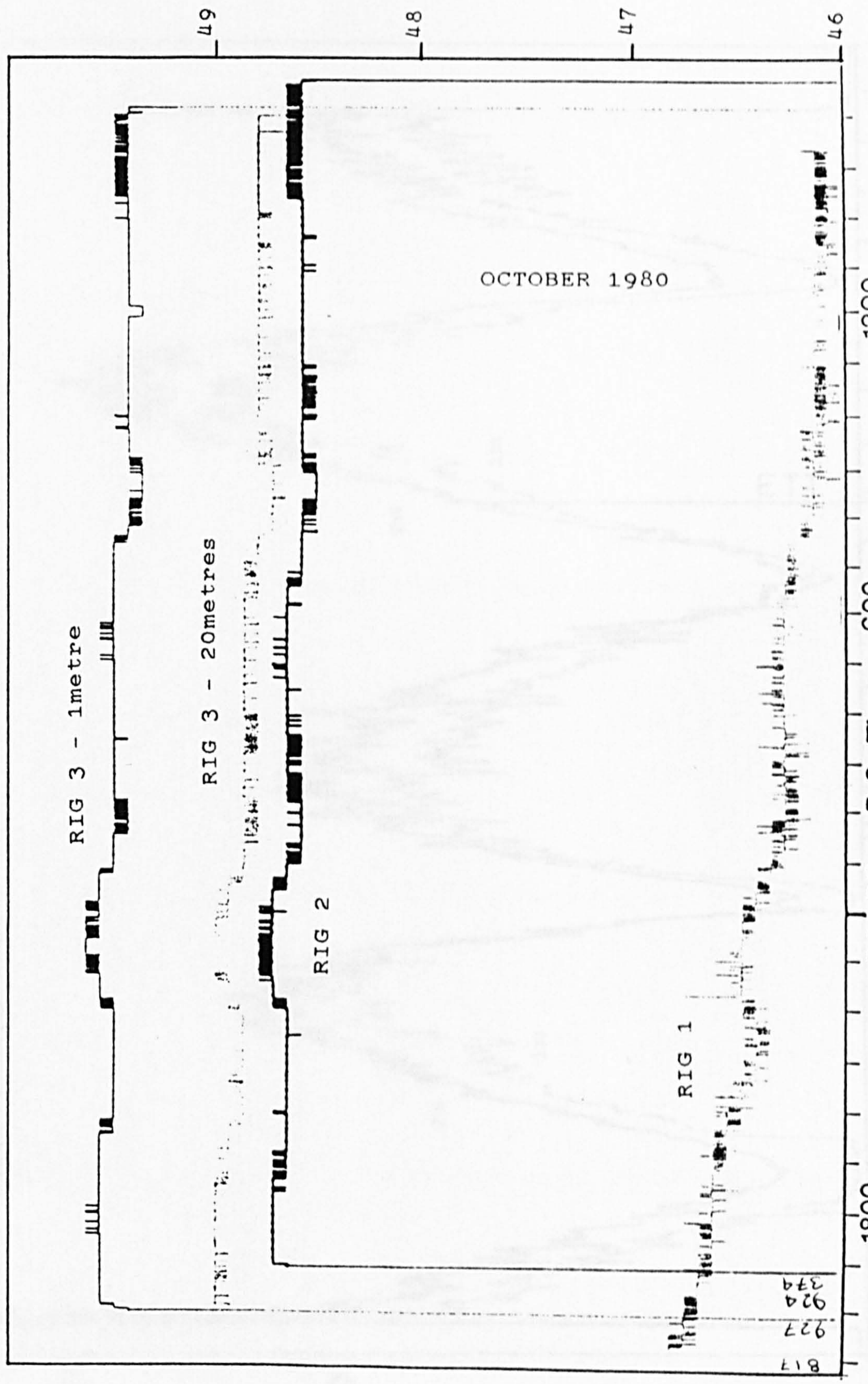

Fig.III.2c 1980 data — Conductivity

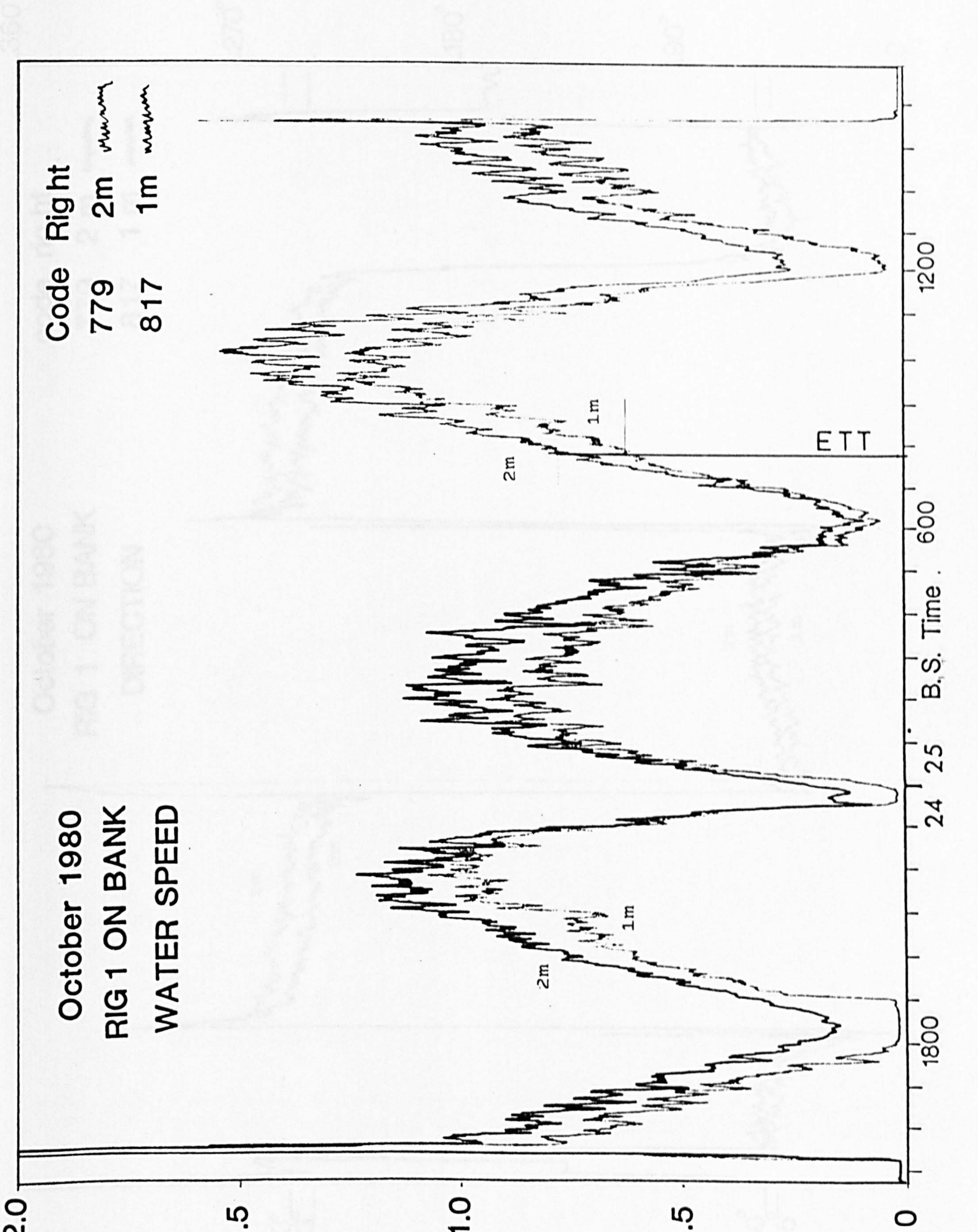

Fig.III.3a 1980 data - RIG 1 Water speed (m/s)

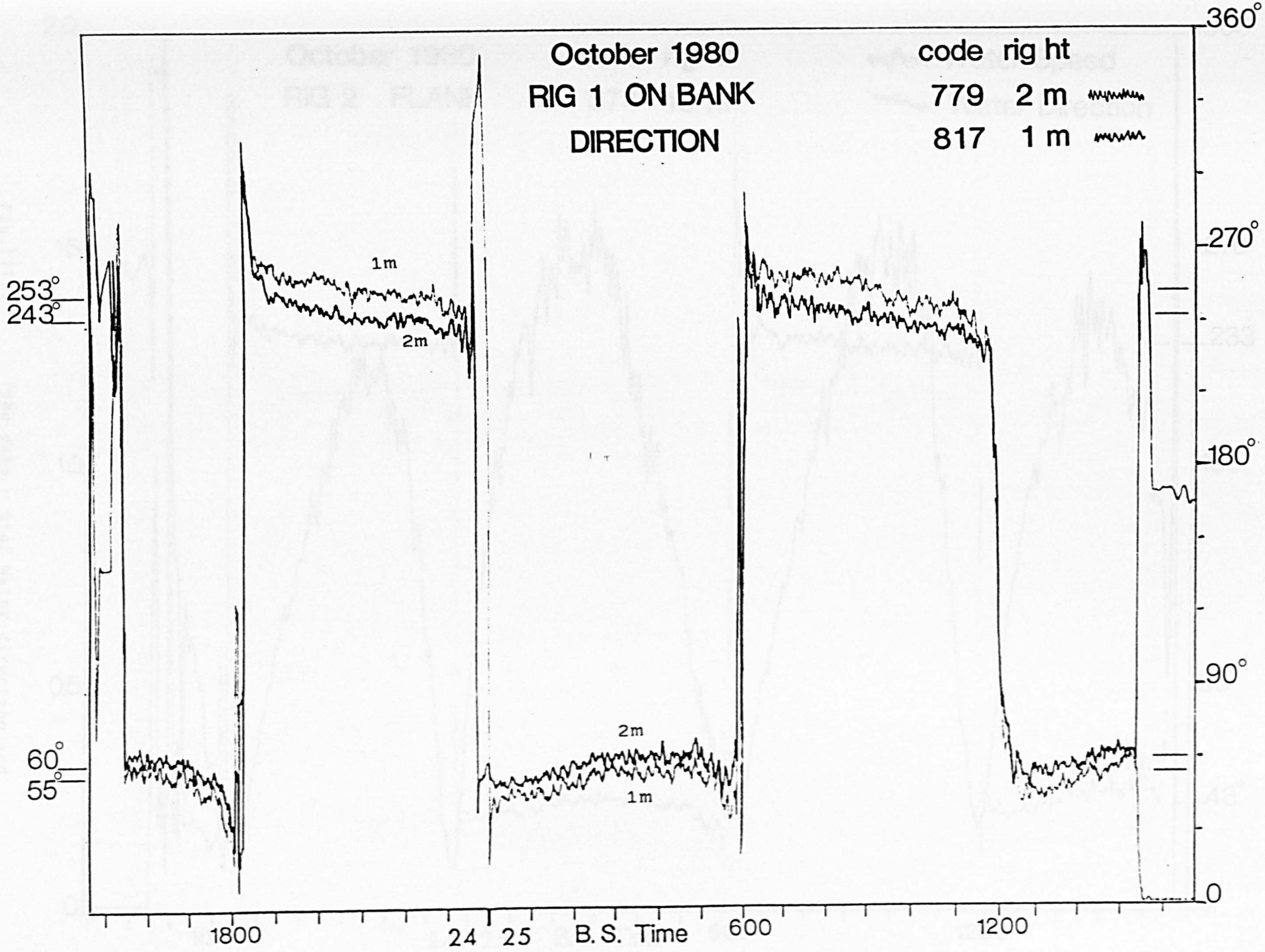

Fig.III.3b 1980 data - RIG 1 Water direction

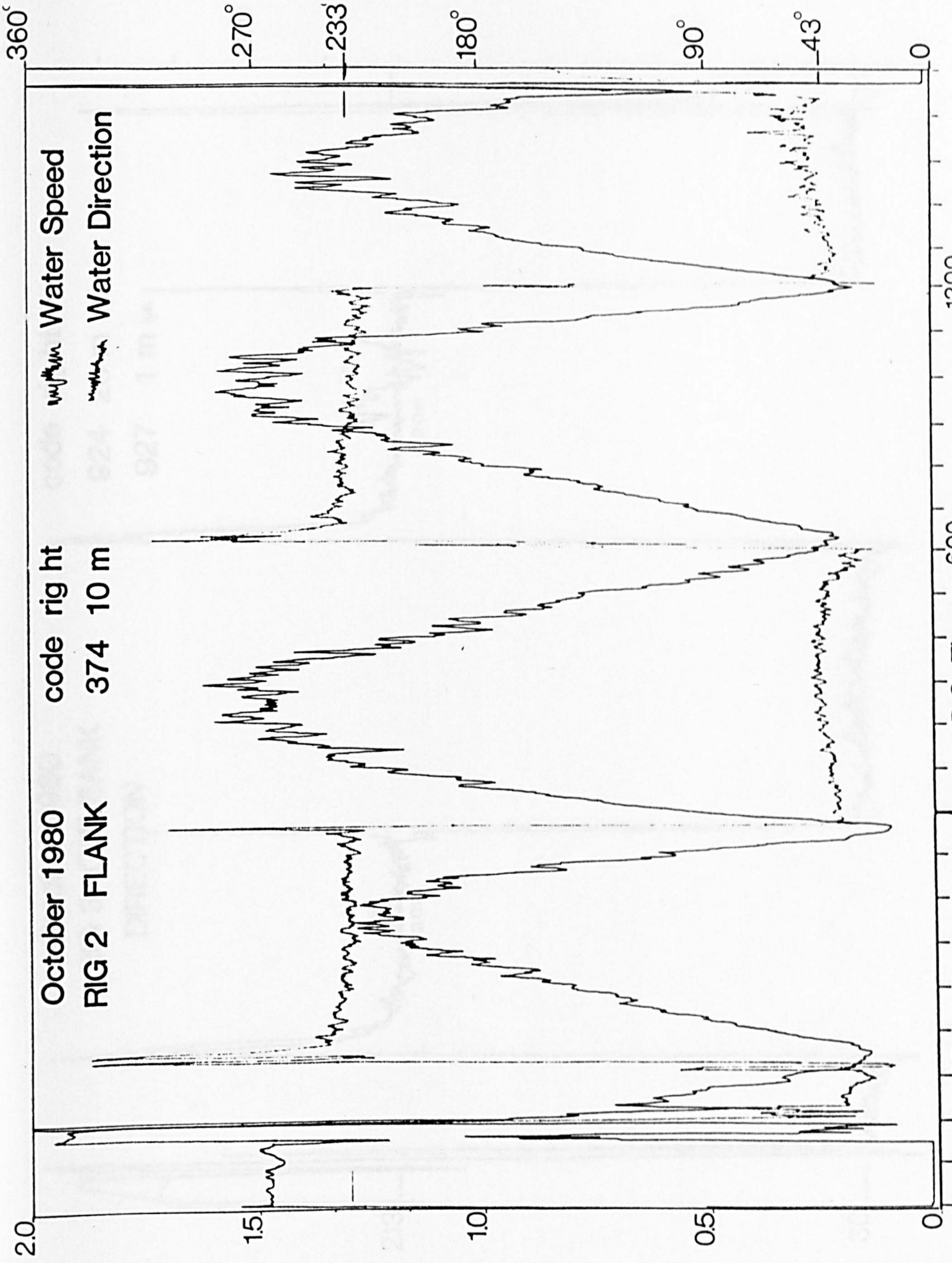

Fig.III.4 1980 data – Rig2 Water direction and water speed (m/s).

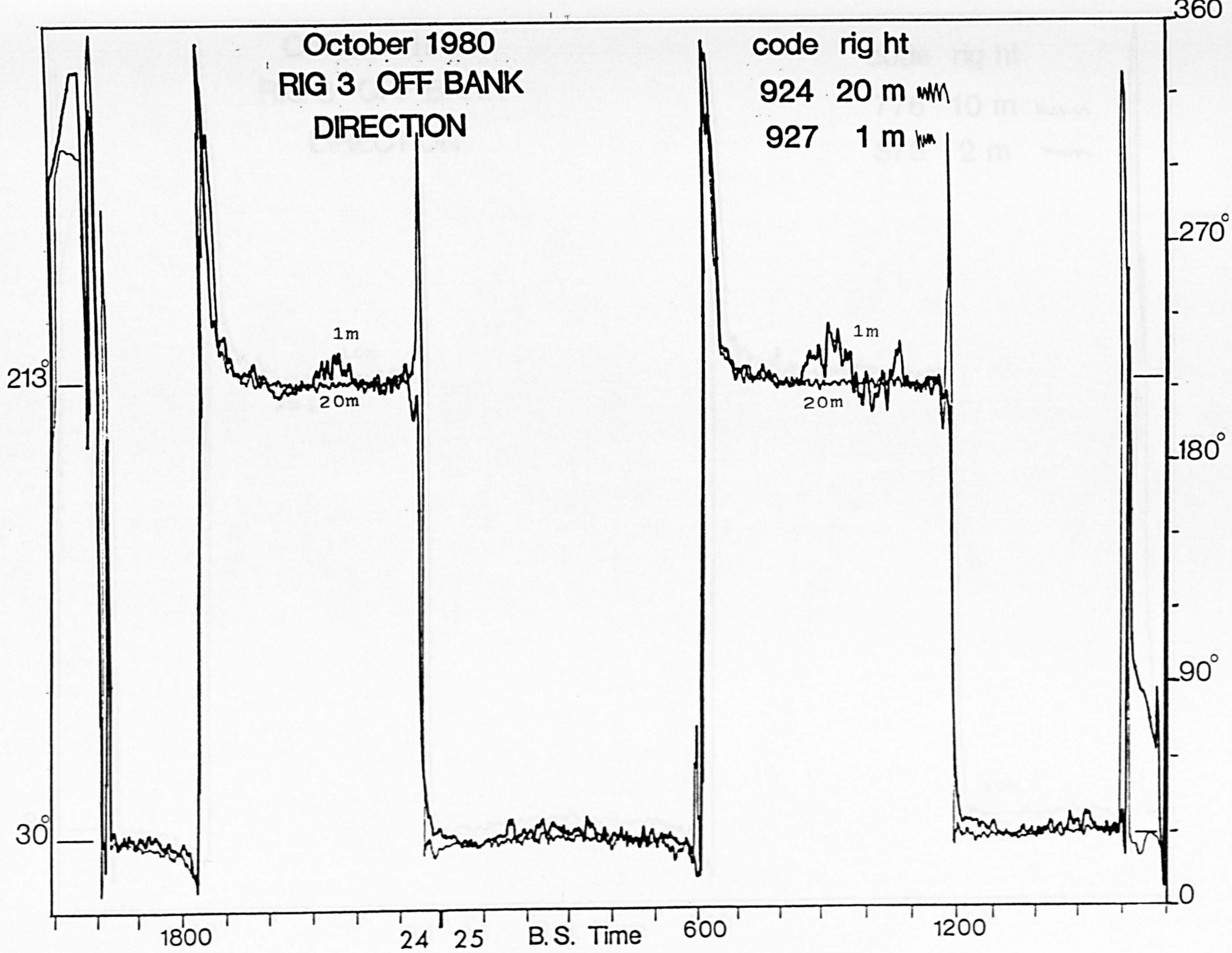

Fig.III.5a 1980 data - Rig3 Direction 1m and 20m

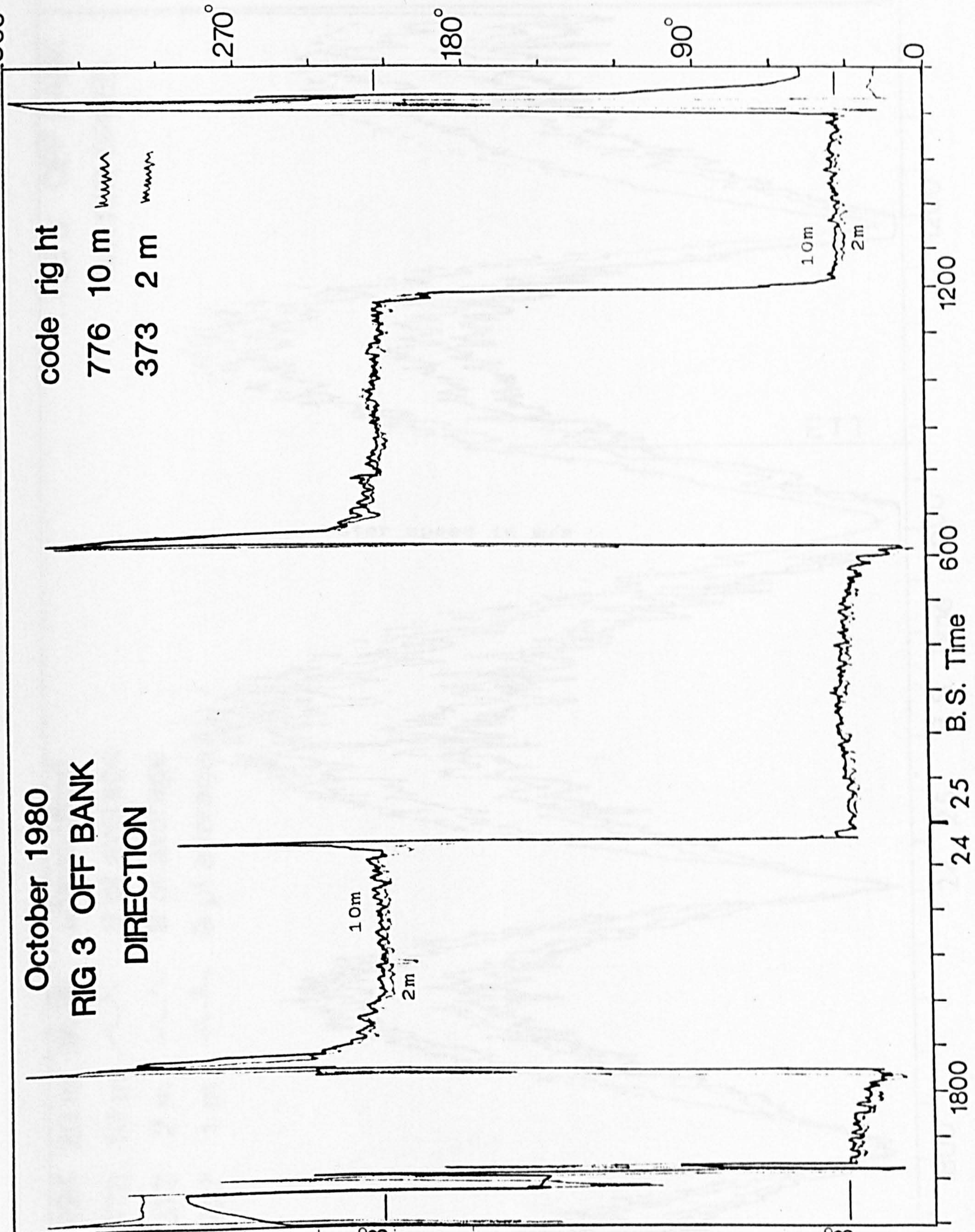

Fig.III.5b 1980 data — Rig3 Direction 2m and 10m

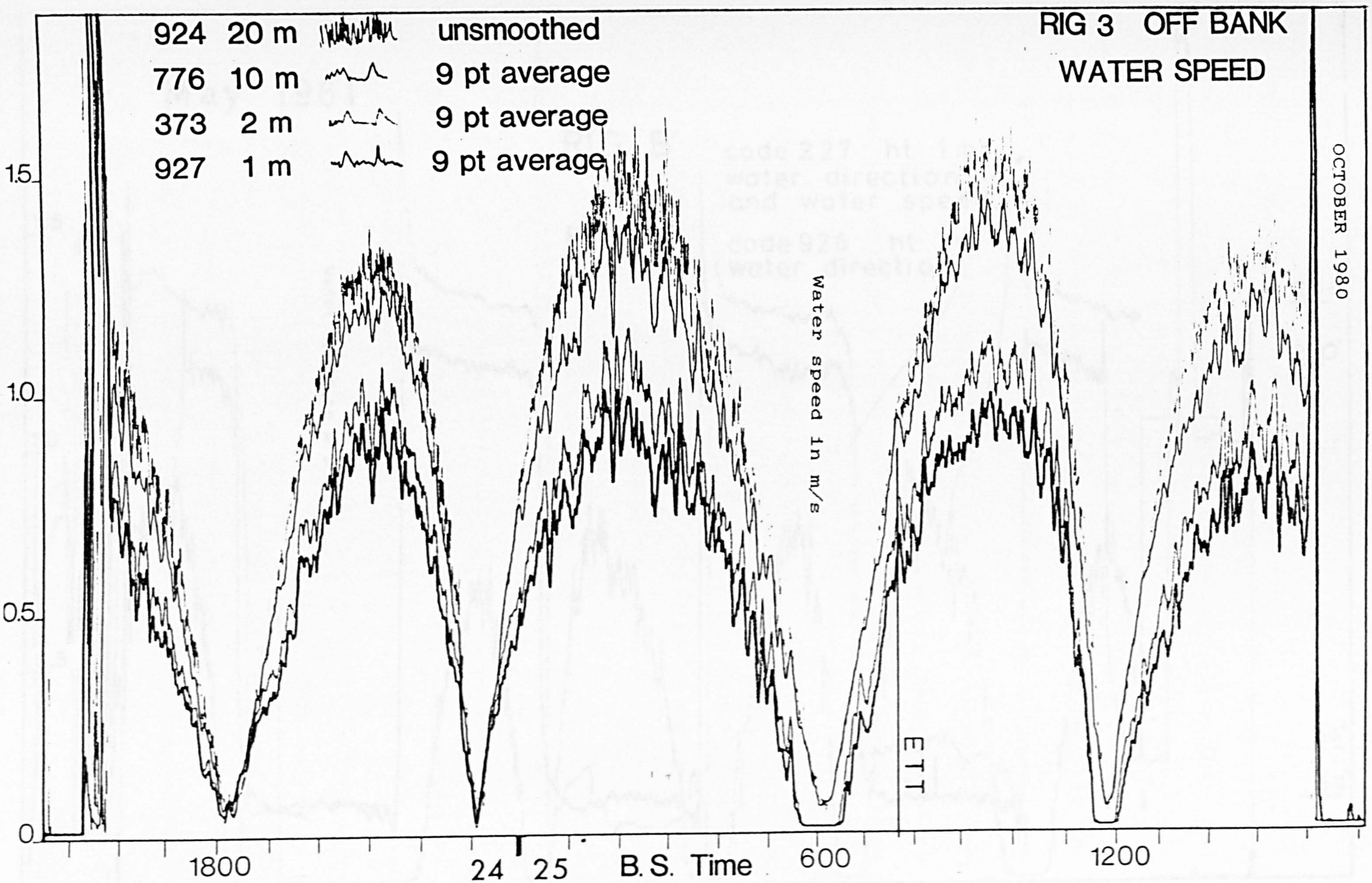

Fig.III.6 1980 data - Rig3 Speed 1m,2m,10m,20m

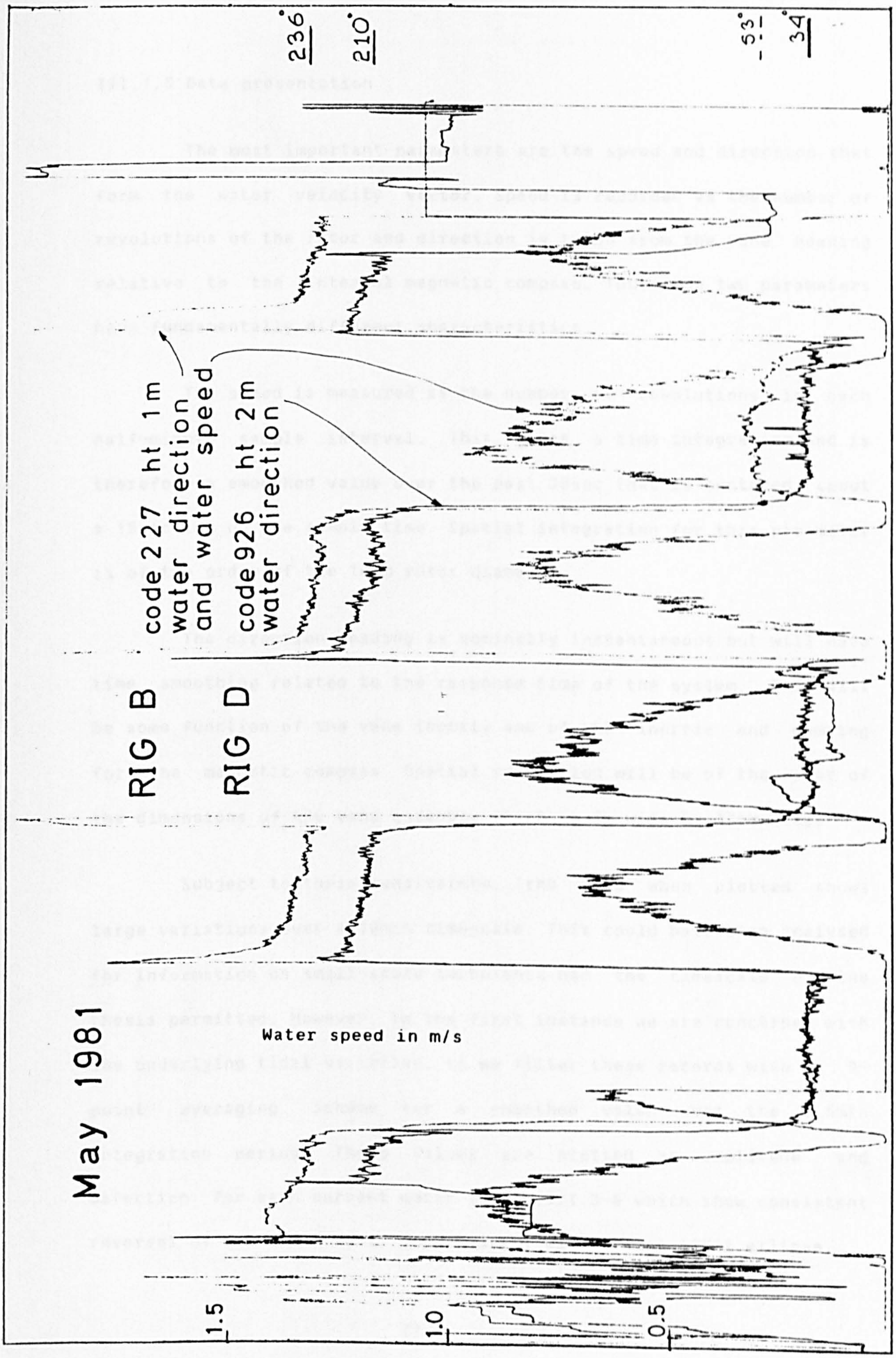

Fig.III.7 1981 data — B, D Speed and direction

III.1.5 Data presentation

The most important parameters are the speed and direction that form the water velocity vector. Speed is recorded as the number of revolutions of the rotor and direction is taken from the vane heading relative to the internal magnetic compass. Thus, the two parameters have fundamentally different characteristics.

The speed is measured as the number of revolutions in each half-minute sample interval. This gives a time integration and is therefore a smoothed value over the past 30sec that is centered about a 15sec lag on the sample time. Spatial integration for this parameter is of the order of the 10cm rotor diameter.

The direction reading is nominally instantaneous but will have time smoothing related to the response time of the system. This will be some function of the vane inertia and of the inertia and damping for the magnetic compass. Spatial resolution will be of the order of the dimensions of the vane assembly which is 1m wide by 37cm deep.

Subject to these constraints, the data when plotted shows large variations over a 10min timescale. This could have been analysed for information on small-scale turbulence had the timescale of the thesis permitted. However, in the first instance we are concerned with the underlying tidal variation, so we filter these records with a 9-point averaging scheme for a smoothed value over the 4.5min integration period. These values are plotted as amplitude and direction for each current meter in fig.III.3-6 which show consistent reversal of the flow, as if for a river, with a flat tidal ellipse.

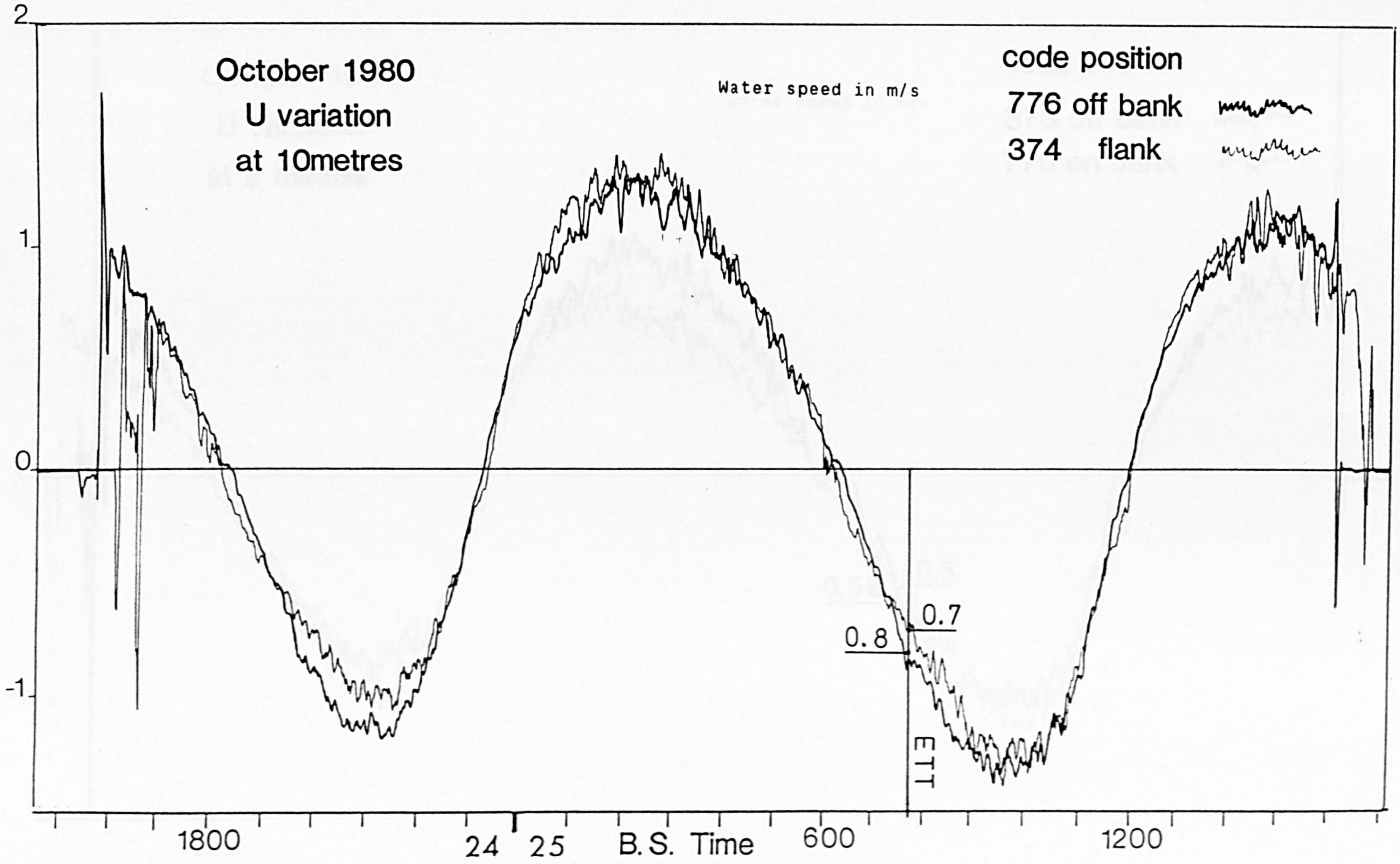

Fig.III.8a 1980 data - Along-bank velocity U at 10m 78

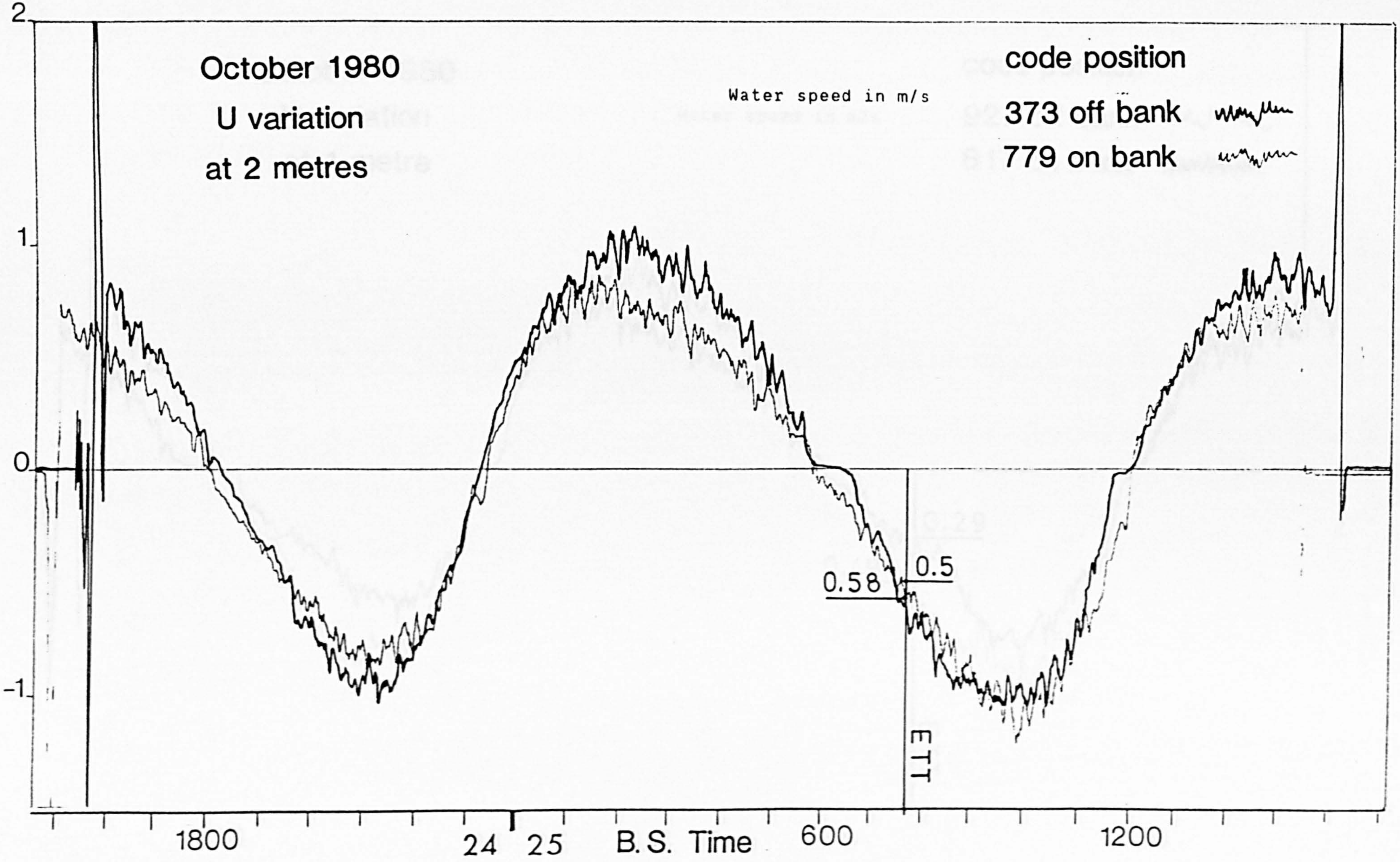

Fig.III.8b 1980 data - Along-bank velocity U at 2m

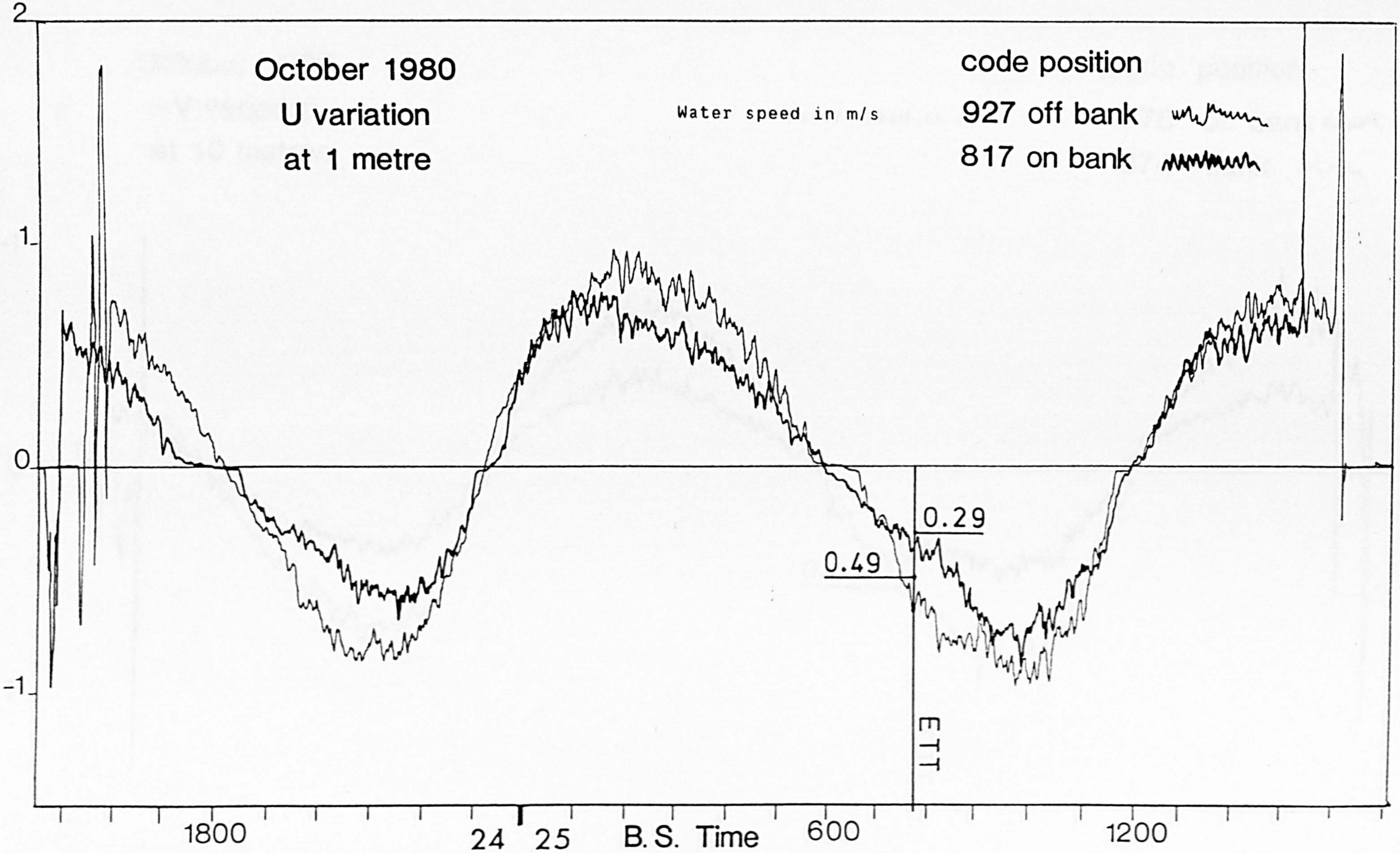

Fig.III.8c 1980 data - Along-bank velocity U at 1m 80

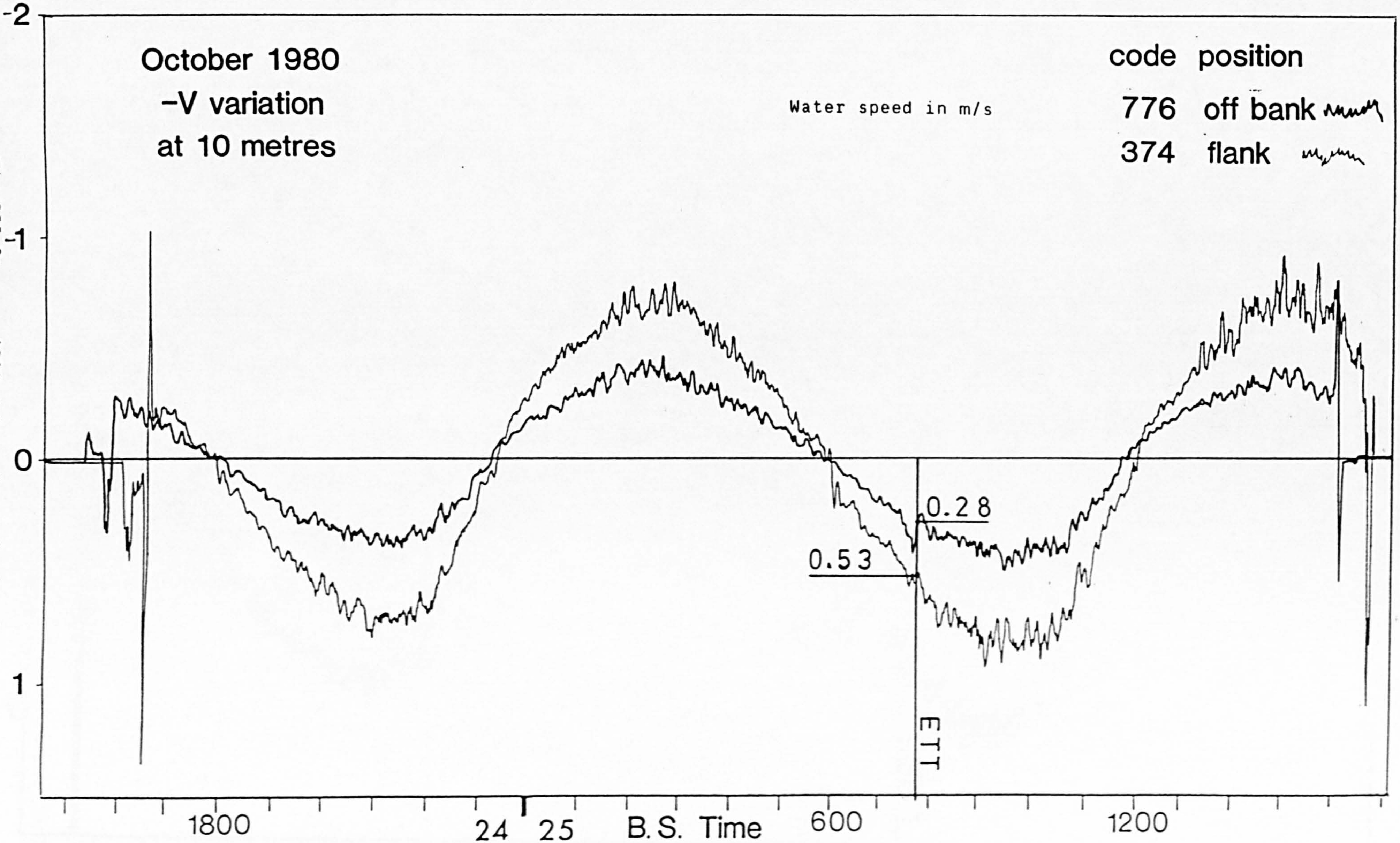

Fig.III.9a 1980 data – Cross-bank velocity V at 10m 81

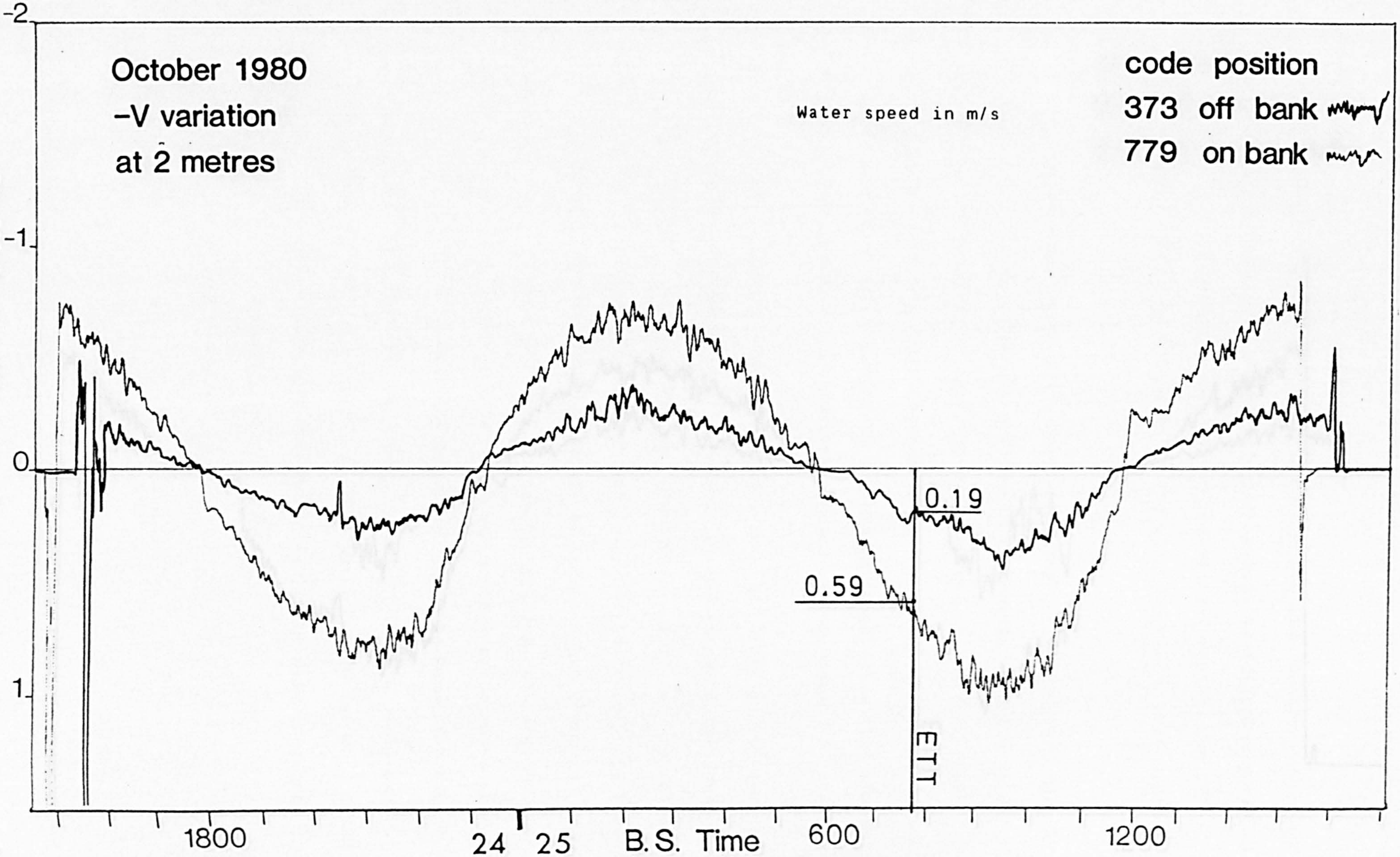

Fig.III.9b 1980 data – Cross-bank velocity V at 2m

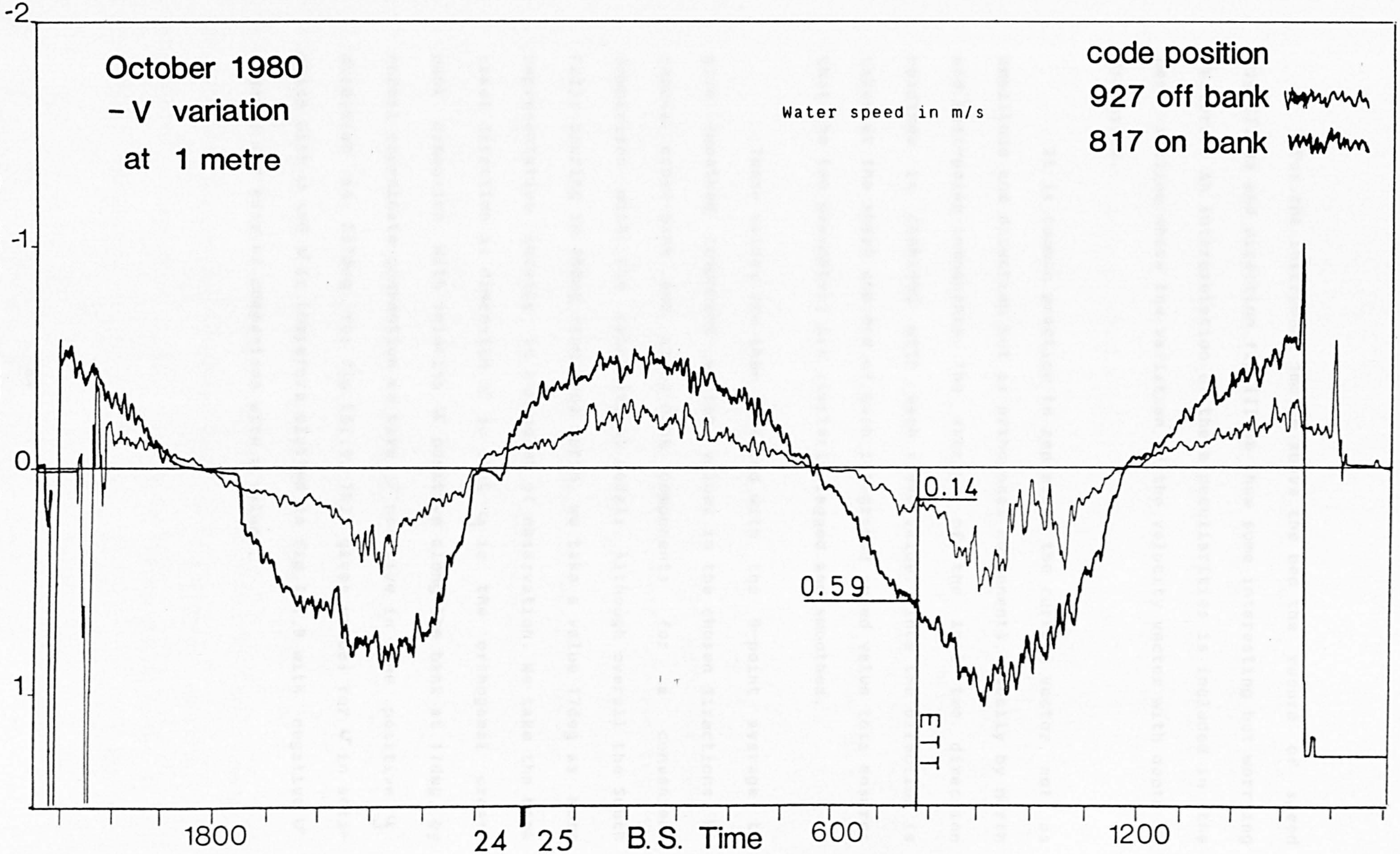

Fig.III.9c 1980 data – Cross-bank velocity V at 1m

For the instrument 1metre above the bed the record of speed fig.III.3a and direction fig.III.3b show some interesting but worrying features. An interpretation of these peculiarities is included in the next section where the variation of the velocity vector with depth is discussed.

It is common practice to represent the current vector, not as amplitude and direction but as orthogonal components, usually by north and west-going components. The average of the last two direction readings is combined with each speed value. Since the direction is taken at the start and end of each integrated speed value this ensures that the two parameters are similarly lagged and smoothed.

These values are then filtered with the 9-point average to give smoothed component vector values in the chosen directions. We choose cross-bank and along-bank components for a convenient comparison with the mathematical models. Although overall the South Falls bearing is 15deg from True north, we take a value 17deg as more representative locally to the point of observation. We take the bank crest direction as dimension x so that y is the orthogonal cross-bank dimension. With velocity u positive along the bank at 17deg, by normal coordinate convention we take v positive in the positive y direction as 287deg for fig.III.8. This gives values for v in anti-phase with u and v is therefore plotted in fig.III.9 with negative v upwards for ease of comparison with u values.

The data return from the 1981 cruise was so low that very little in the way of analysis could be attempted. The processed data plots are shown in fig.III.7. There was not sufficient information to produce comparative plots for u, v on and off the bank, nor to compare easterly and westerly tidal flows.

The most useful aspect noted from this data is the nature of the turbulence characteristics. Although time and resources did not permit a proper quantitative spectral analysis of either of the datasets, a qualitative feel for the turbulence characteristics can be got from a comparison of the amplitude and direction plots of fig.III.3–6 and fig.III.7.

Some reassurance can be found from the fact that the 1981 data is not notably different from the 1980 data, even though the weather was much rougher during the 1981 observation period. This does suggest that the turbulence levels noted in both data sets are due to tidal friction rather than waves, but we could not be certain that the 1980 data set is free from wave contamination without further work.

III.1.6 Data anomalies

Careful study of fig.II.3b suggests that the variation is not a simple veering with depth. There is an apparent veering on the flood tide but a backing with increasing depth on the ebb tide. This is not the expected pattern for Ekman veering. If it were true then it might represent a flow separation in one of the directions. However, as mentioned in section III.1.5, aspects of the record at 1metre give some cause for concern.

In particular, measured water speed of fig.III.3a between the 1st and 2nd turns of the tide, may be reduced from its true value. The 1metre rotor was slow to start and both 1metre and 2metre rotors slowed to a minimum value while the direction plot fig.III.3b still indicated a steady flow. The 2metre rotor then recovered before again approaching a minimum which this time coincided with its vane turning. This problem of speed reduction was also noted for the 2metre rotor between the 3rd and 4th turn of the tide and is shown in fig.III.8b.

Problems with the direction plot fig.III.3b are even more serious. While the 2metre vane turns correctly with the 2metre speed at a minimum the 1metre vane turned 10minutes later when the recorded water speed at 1metre was 10cm/s. This indicates that there is some serious obstruction of the rotation of the instrument as a whole which must compromise any conclusions that depend upon the exact values for direction of the 1metre vane.

My interpretation of these peculiarities is influenced by the 1981 rig recovery when one instrument emerged with a blue plastic fertilizer bag wrapped firmly around the rotor. This does suggest a considerable quantity of debris at the sea-bed over the whole region. Any such material or even seaweed clumps could cause speed reduction. However the speed might also be reduced by a fouling of a link in the rig that could accentuate the angle of the Aanderaa past the point at which it can operate correctly. It is difficult to see how this could have happened for the 2metre instrument of the off-bank rig. However, the 1metre instrument for both on and off bank rigs was shackled directly to the lead weight. If this link fouled and the Aanderaa was tilted the vane could touch the sea bed! If the vane was touching this could easily give an impression of a 'banana'-shaped tidal ellipse beneath the simply reversing flow of the 2metre vane.

No plots are providedof the 'interesting' dynamics that these measurements suggest, since it is most likely that the values merely indicate the difficulties of current measurement close to the sea-bed. Instead we concentrate upon some 3-D aspects of the records that we do have confidence in.

III.2 TIDAL FLOW MODELLING

Some initial assumptions must be made about bank flow in order to design the rig and the associated experiment.

III.2.1 A first model for water flow over a sand bank

For a circular bank the flow direction is immaterial by definition. For the flow over the central region of a finite, but very long, bank, it is convenient to separate the flow into a cross-bank and an along-bank component, and to consider these components individually as limiting case flows.

Now, for a long bank, cross-bank flow is very well defined. It must be constrained, by continuity, to flow faster over the bank top. The effect is similar to that over a sand wave or ripple. For shallow sea regions, away from coastal and drying areas, the Froude number will be small compared to unity and any associated surface deformation can be neglected for most purposes.

The along-bank flow vector for a long bank is much less well defined. It is not clear what connection there may be between flows at different depths, and horizontal mixing may be important. However, for the Southern Bight, the greatest cross-bank slope found is 6 deg so that $\partial h/\partial y$ is small.

We therefore assume that with water depth varying by a factor of four the effect of these different depth scales will be more important than the rate of change of depth. Thus for the Reynolds stress terms changes in the values for vertical mixing are of more importance than horizontal mixing. For a zero-th order assumption we take cross-bank flow as 2-D continuity, with logarithmic vertical profle,

$$\frac{\partial (h v)}{\partial y} = 0 \qquad \frac{\partial v}{\partial z} = \frac{1}{K}\frac{v_*}{z} \qquad \text{III.(01)a}$$

and we take along-bank flow as described by a 2-D plane bed flow with logarithmic vertical profile,

$$\frac{\partial u}{\partial y} = 0 \qquad \frac{\partial u}{\partial z} = \frac{1}{K}\frac{u_*}{z} \qquad \text{III.(01)b}$$

Now this is just a kinematic model, we have yet to consider the dynamics of this assumed flow regime, and in particular the horizontal diffusion of momentum.

The 1979 experiment sought to confirm this flow regime by the measurement of water velocity amplitude and direction as it changed over a bank. A bank with a smooth top surface was necessary in order to avoid the inclusion within the experiment design of the measurement and modelling of the flow over a sand wave field.

III.2.2 A second model for water flow

In order to gain insight into the physical mechanisms that govern bank flow we must create a dynamical model. That is a model for the bank subject to the constraints of the conservation of mass and momentum. Mass balance is expressed by the mass conservation equation

$$\frac{\partial \rho}{\partial t} + \nabla.(\rho V) = 0$$

For an incompressible fluid this reduces to the continuity equation

$$\nabla \cdot V = 0 \qquad \text{III.(02)}$$

Momentum balance is expressed by the Navier-Stokes equation for a turbulent fluid with the Reynolds stresses represented by eddy viscosity terms as

$$\frac{DV}{Dt} + 2\Omega X V = -\frac{1}{\rho}\nabla P + A\nabla^2 V \qquad \text{III.(03)}$$

The equations that we derive here are similar to those of Huthnance(1973). However, we will be restricted to only two tidal cycles for the measurement period so we do not study the tidal residuals but look at the variation within the tidal cycle.

The Huthnance model used cross-bank limits at plus and minus infinity with an imposed tidal flow angled to the bank. This analytical model is appropriate for the study of residuals to which it is applied. However, for a numerical model of the tidal cycle we need a different specification with finite limits.

We consider a constant latitude $2 \times y_{max}$ width channel flow on an $f-$ plane. We use the Coriolis term to give the cross channel component of the flow in a natural and easily implemented form. We have an infinitely long bank and therefore take all parameters as invarient in x, except for P which is linear in x such that $\partial P / \partial x$ is constant. This does imply infinitely large positive and negative pressures at plus and minus infinity, but this convention has often been used for fluid dynamics modelling (Lamb,1906).

Of course, for the real bank flow that we model, $\partial P / \partial x$ is oscillatory with a value that is slowly varying and so only locally constant. It is perhaps easier to think of the flow as quasi-stationary, and when we vary $\partial P / \partial x$ in time this can be interpreted as a spatial variation in η.

However, although this may seem less ambiguous we must remember that the tidal wave is 500km wavelength and the bank, although very long and thin for a bank, is only 20km. Thus the concept of a tidal wave travelling along the bank is only a first order approximation.

The bottom topography is described by $h(y)$, the depth below the mean sea level and we take $\eta(y)$ to be the height of the sea surface above this reference mean level. Thus total water depth is $h+\eta$. A simple form of bank topography is illustrated in fig.III.10.

III.2.2.1 The Equations

Now equation III.(03) may be written

$$\frac{\partial u}{\partial t} + v\frac{\partial u}{\partial y} - fv = -\frac{\partial p}{\partial x} + A_z\frac{\partial^2 u}{\partial z^2} + A_y\frac{\partial^2 u}{\partial y^2}$$

$$\frac{\partial v}{\partial t} + v\frac{\partial v}{\partial y} + fu = -\frac{\partial p}{\partial y} + A_z\frac{\partial^2 v}{\partial z^2} + A_y\frac{\partial^2 v}{\partial y^2} \qquad \text{III.(04)}$$

since all terms in $\partial/\partial x$ are zero by the x-invarience of the topography. We integrate over the depth for a 1-D model in the y-dimension. The bottom friction term must therefore be parameterised in terms of u, v, p, the available depth-averaged parameters. This is of great importance for the form of the dynamics.

For this second model of bank flow we use the parameterization from Huthnance(1973)

$$A_z\frac{\partial^2 u}{\partial z^2} = -\frac{ku}{h} \qquad \text{III.(05)}$$

and ignoring non-linear terms

$$\frac{\partial u}{\partial t} - fv = -\frac{\partial p}{\partial x} - \frac{ku}{h} \qquad \text{III.(06)a}$$

$$\frac{\partial v}{\partial t} + fu = -\frac{\partial p}{\partial y} - \frac{kv}{h} \qquad \text{III.(06)b}$$

Now from the continuity equation III.(02), following Phillips(1966) and Gill(1982), we use a rigid lid approximation for the y-direction, to remove the p/g term

$$\frac{\partial p}{\partial t} + \frac{\partial}{\partial y}(hv) = 0 \qquad \text{III.(06)c}$$

Equation III.(06) was used below for a numerical model.

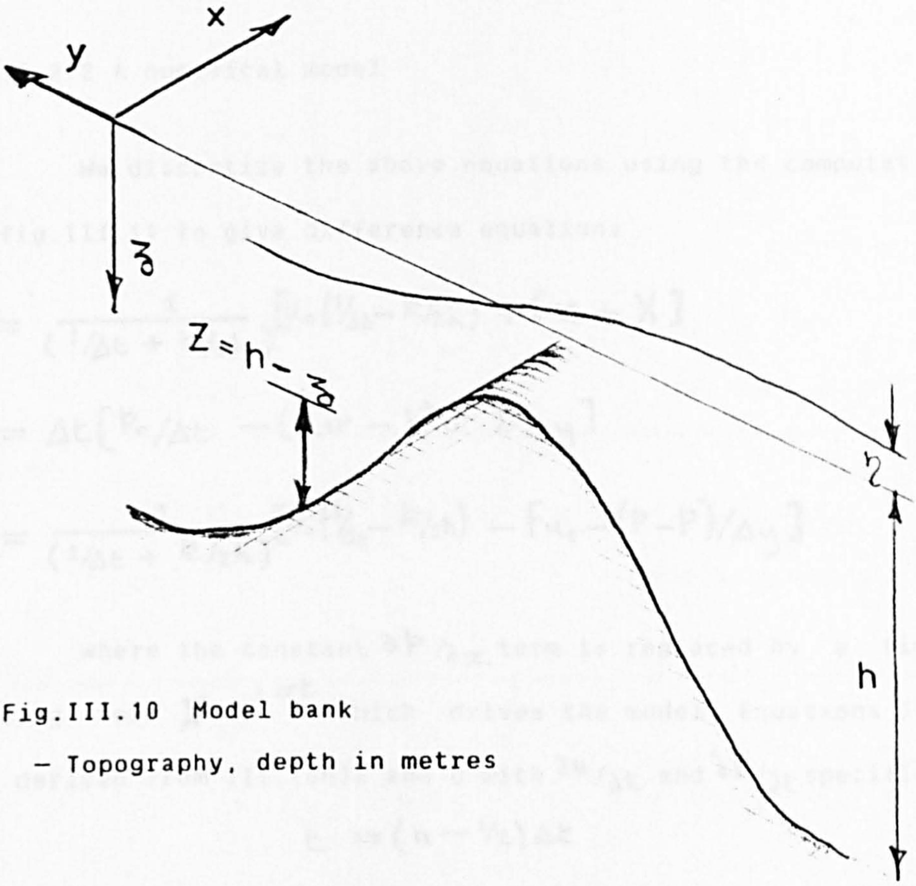

Fig.III.10 Model bank

— Topography, depth in metres

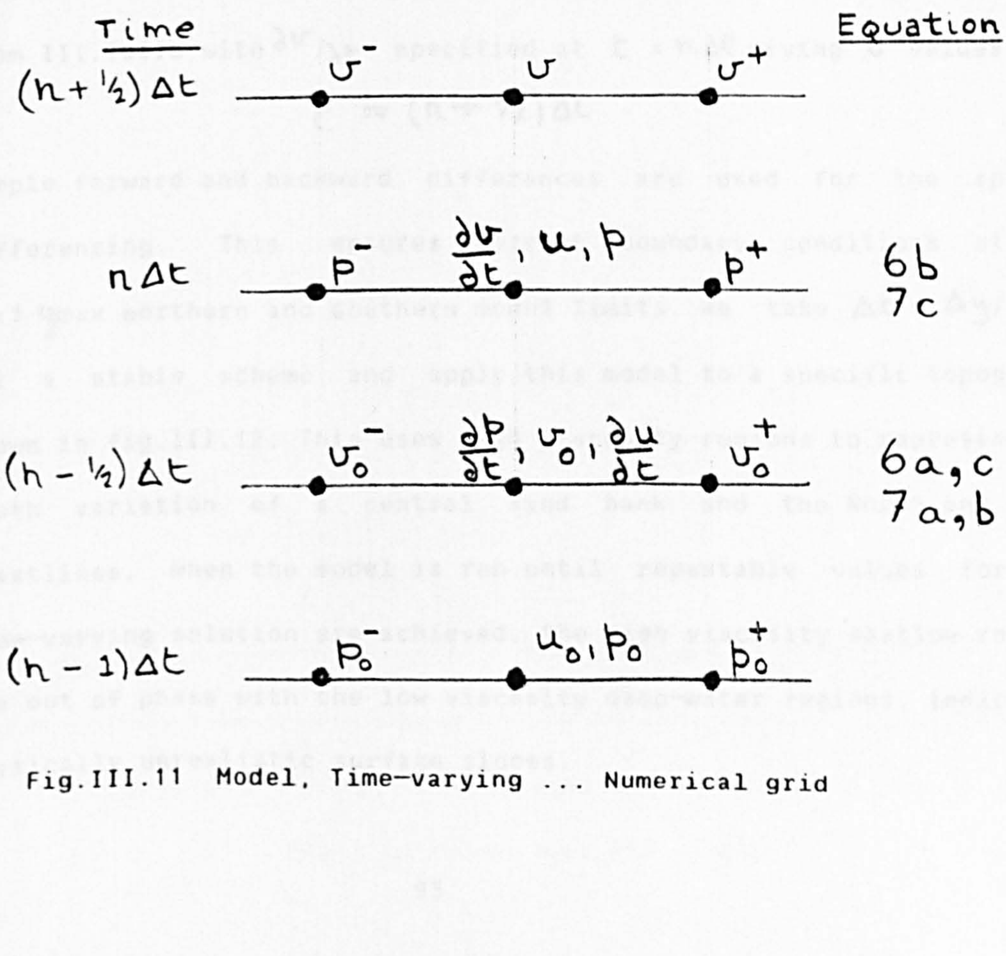

Fig.III.11 Model, Time-varying ... Numerical grid

III.2.2.2 A numerical model

We discretize the above equations using the computational grid of fig.III.11 to give difference equations

$$u = \frac{1}{(1/\Delta t + k/2h)}\left[u_0\left(1/\Delta t - k/2h\right) + f v_0 + X\right]$$

$$p = \Delta t\left[p_0/\Delta t - (hv - h^+ v^+)/\Delta y\right]$$

$$v = \frac{1}{(1/\Delta t + k/2h)}\left[v_0\left(1/\Delta t - k/2h\right) - f u_0 - (p - p^-)/\Delta y\right] \qquad \text{III.(07)}$$

where the constant $\partial p/\partial x$ term is replaced by a time-varying forcing term $X = e^{i\sigma t}$ which drives the model. Equations III.(07)a,b are derived from III.(06)a and c with $\partial u/\partial t$ and $\partial p/\partial t$ specified at

$$t = (n - 1/2)\Delta t$$

to give values for u and p at $t = n\Delta t$ such that we have a central difference scheme in time. Equation III.(07)c is similarly derived from III.(06)b with $\partial v/\partial t$ specified at $t = n\Delta t$ giving v values at

$$t = (n + 1/2)\Delta t$$

Simple forward and backward differences are used for the spatial differencing. This ensures correct boundary conditions at the $y = \pm y_{max}$ northern and southern model limits. We take $\Delta t = \Delta y/2$ to get a stable scheme and apply this model to a specific topography shown in fig.III.12. This uses high viscosity regions to represent the depth variation of a central sand bank and the North and South coastlines. When the model is run until repeatable values for the time-varying solution are achieved, the high viscosity shallow regions are out of phase with the low viscosity deep-water regions, indicating physically unrealistic surface slopes.

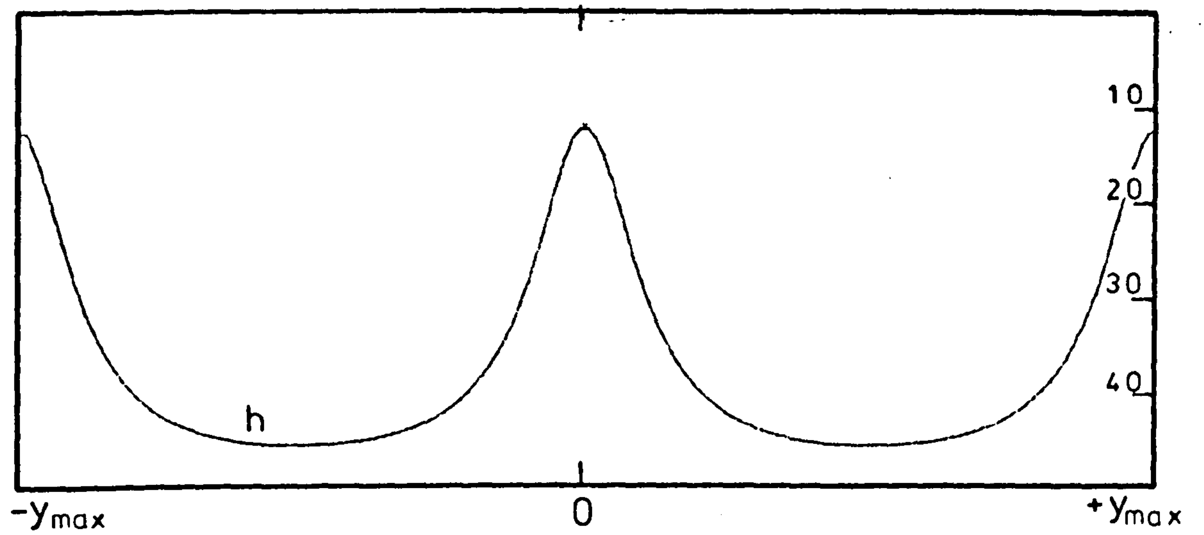

Fig.III.12 Model, Time-varying ... Cross-section

depth in metres

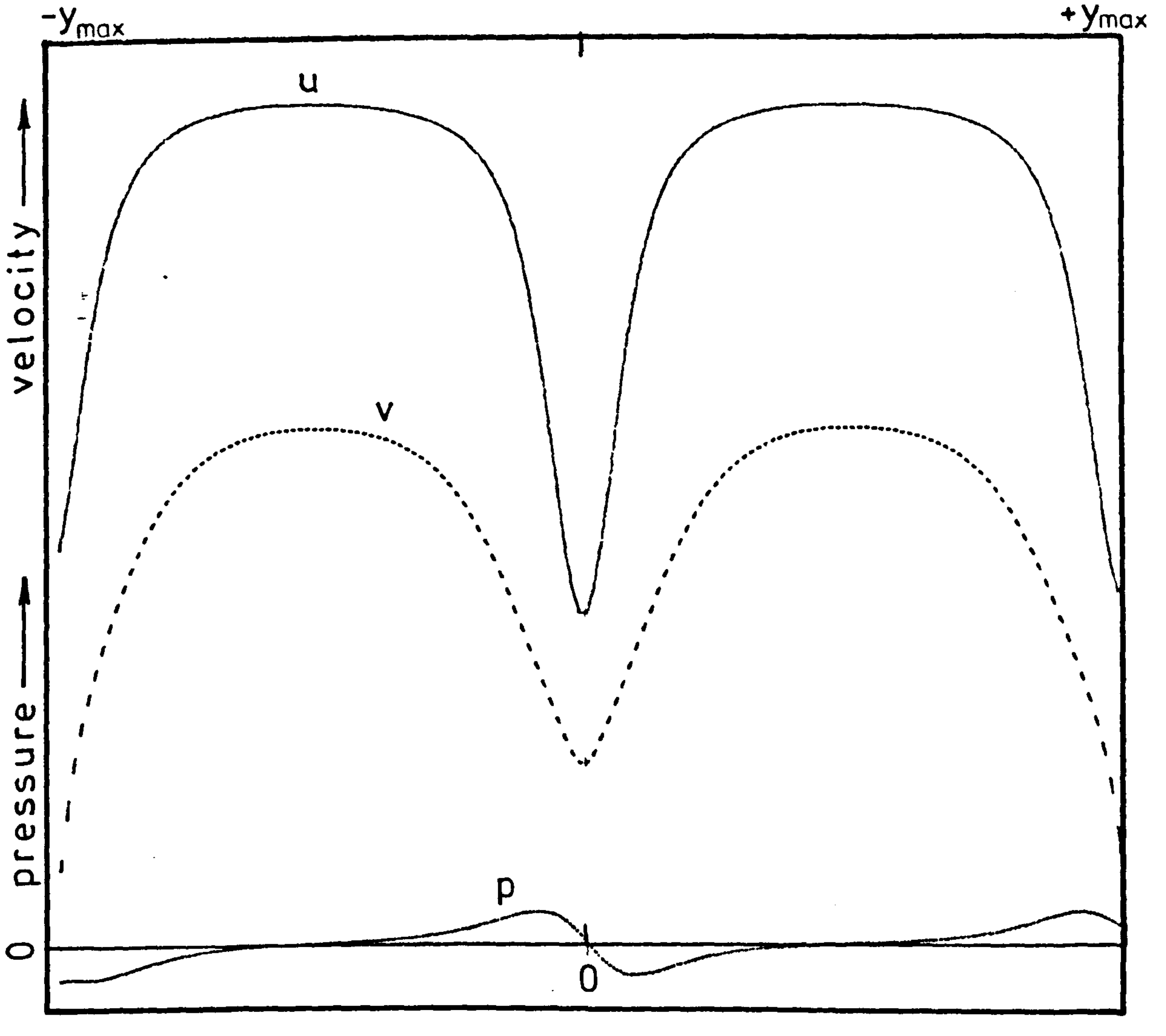

Fig.III.13 Model, Time-varying ... Numerical results

Plots of velocities and slope

This mode is possible for any wavelength on a bank of infinite length but for the South Falls bank, with 20km length, we must expect different behaviour, since the bank length is only 1/25 of the 500km tidal wavelength. In fact, for a 1/2km bank width with a wavelength over 1km, this model will give unacceptably high values for $\partial p/\partial y$ that must invalidate the assumption of no horizontal mixing.

The transient solution given in fig.III.13 compromises the model by using the fact that it starts in phase to produce a solution in phase. The timescale taken is appropriate for the spatial lengthscale. However, the variation of v with y for this solution is incorrect for any finite flow values since it is contrary to continuity of cross-bank mass flux. The plot represents infinitesimal flow conditions associated with the set-up of the very small $\partial p/\partial y$ trapped surface wave at the bank crest. Attempts to introduce realistic parameter values for the region considered gave rise to numerical instabilities.

For the chosen parameters, the numerical model transient behaviour does not represent a valid bank flow. It may be that further research into this model will reveal a form of transient behaviour that does give valid bank flow solutions. It can be seen that there are problems with the numerical model in this form and this is discussed further in chapter V.

No further modelling was undertaken before the field trip of 1980 and the flow assumed for rig design purposes was the same as before. It was intended that the experiment would give some guidance for the expected variation of the along bank velocity.

III.2.3 A third model for water flow

We now need some new model that will match the measured flow. When the measured velocity vector is resolved into along-bank and cross-bank components, a clear picture emerges. Cross-bank velocities in fig.III.9 are constrained by continuity to be inversely proportional to water depth, so that

$$h v = \text{constant} \qquad \text{III.(08)}$$

However, along-bank velocity vectors on and off the bank, at the same height above the sea-bed, do not show in fig.III.8 sufficient variation to warrent the inclusion of any cross-bank variation of along-bank velocity in the model. Therefore, to first order, we take

$$u(y) = \text{constant} \qquad \text{III.(09)}$$

The above relations are derived empirically, by inspection of measured values. The theoretical model should be able to reproduce the same relationships for the variables with appropriate values for equation constants.

III.2.3.1 The numerical model reconsidered

For our present purpose, the model is still of some use to give us relative plots of u, v, p. We reject time-varying forcing to take the forcing term X constant. In this form, the solution will approach a time-independant solution described by the steady-state equations.

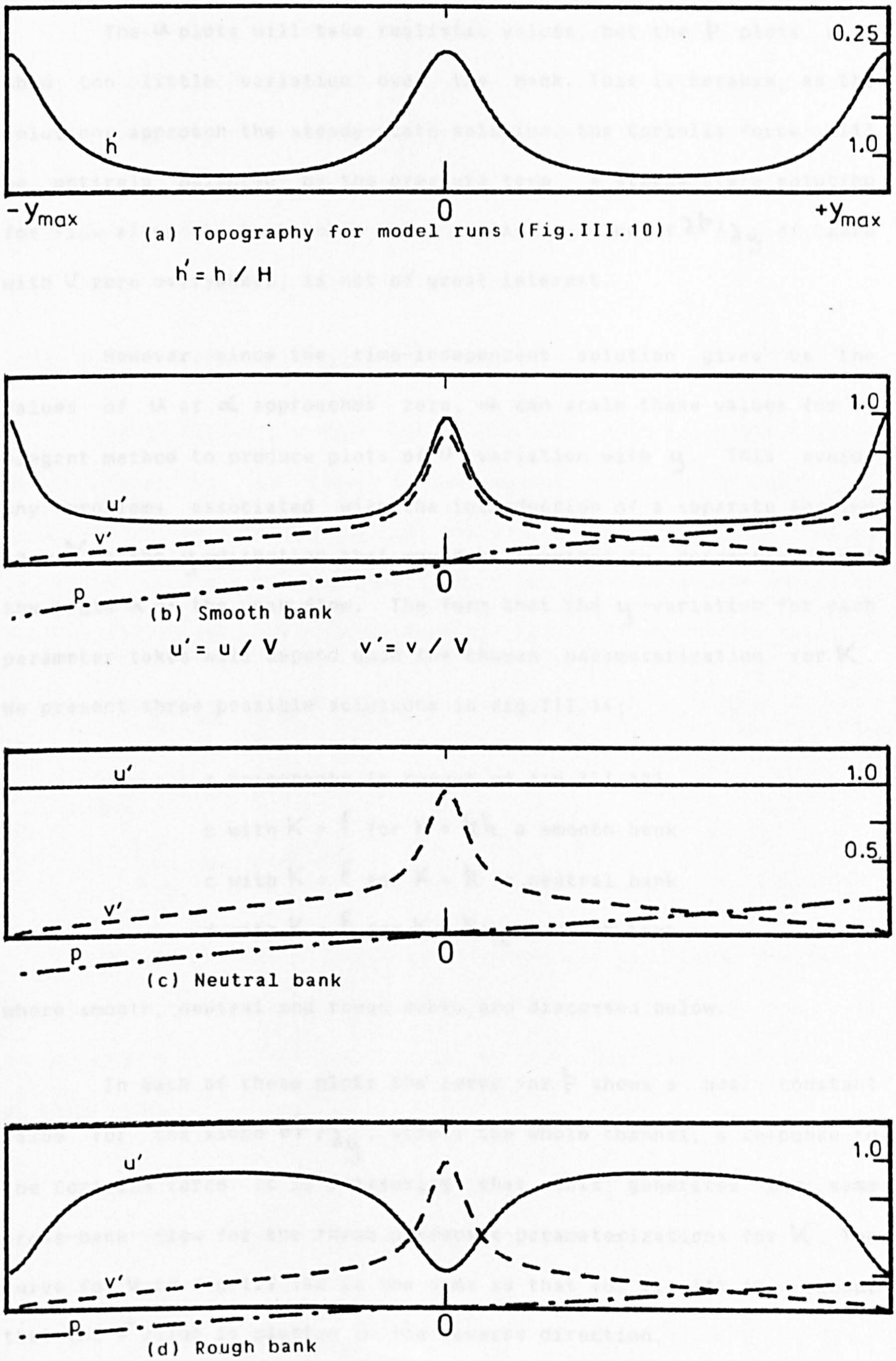

Fig.III.14 Model, Steady-state ... Numerical results

Plots of velocities and slope

The u plots will take realistic values, but the p plots will show too little variation over the bank. This is because, as the solutions approach the steady-state solution, the Coriolis force will be entirely balanced by the pressure term. A steady-state solution for flow along the bank only, which implies a value of $\partial p/\partial y$ of zero with v zero everywhere, is not of great interest.

However, since the time-independent solution gives us the values of u as α approaches zero, we can scale these values for an elegant method to produce plots of v-variation with y. This avoids any problems associated with the introduction of a separate forcing term Y in the y-direction that would be required to correctly model the angle α of the peak flow. The form that the y-variation for each parameter takes will depend upon the chosen parameterization for K. We present three possible solutions in fig.III.14;

a topography (a repeat of fig.III.12)

b with $K = f$ for $K = kh$ a smooth bank

c with $K = f$ for $K = k$ a neutral bank

d with $K = f$ for $K = k/h$ a rough bank

where smooth, neutral and rough banks are discussed below.

In each of these plots the curve for p shows a near constant value for the slope $\partial p/\partial y$, across the whole channel, a response to the Coriolis force. It is reassuring that this generates the same cross-bank flow for the three different parameterizations for K. The curve for u in fig.III.14d is the same as that for fig.III.13, except that the v value is plotted in the reverse direction.

These solutions are considered as a guide only since the reality of the numerical model has been questioned. The values for v are very small, and would be zero for a steady-state when Coriolis would be balanced completely by $\partial p/\partial y$. In order to validate the results we reconsider equation III.(06), using a separation of tidal wave and water velocity variation timescales.

III.2.4 The steady-state equations

South Falls is a type A bank (fig.I.7), with an anticlockwise axial offset(α) of 17deg to the regional direction of peak tidal flow. For any α > 10deg, spatial variation of water velocity values is on a faster timescale than that of the tidal variation which can thus be considered invariant in time giving the steady-state equations

$$X = uK - fv$$
$$\frac{\partial}{\partial y}(hv) = 0$$
$$\frac{\partial p}{\partial y} = -Kv - fu \qquad \text{III.(10)}$$

We do not obtain analytical or numerical solutions for these equations. The simplicity of form is such that we can find relationships by inspection. First we consider the equations in general terms.

For III.(10)a the forcing, surface slope X, is opposed by friction and Coriolis (v is negative for type A bank).

From III.(10)b, for any K to f relation, continuity dominates and for $p/g \ll h$ we have

$$\frac{\partial}{\partial y}(hv) = 0 \qquad \text{III.(11)}$$

which is in rough agreement with measured values although we do not try to match the more exact relation

$$(h+\eta)\,v = \text{constant} \qquad \text{III.(12)}$$

For III.(10)c the surface slope $\partial p/\partial y$ is here a response to a balance between the forces of friction Kv and Coriolis fu. For $K > f$ this balance is small giving $\partial p/\partial y$ much less than X.

We can see that, in general, equation behaviour must be dominated by the parameterization for K and its relation to X and f. Whereas equation III.(10)b generates the main constraint upon the flow as expressed by III.(11), equation III.(10)a defines the dynamic forcing for the flow.

We now take typical South Falls values for the more particular arguments that follow. For height we use H=40m for the off-bank water-depth, and consider that h varies between this value and 10m at the bank top. We take maximum water velocities of u=1m/s so that v=1m/s on the bank top (from fig.III.9), and hence v=0.25m/s off of the bank (from III.(11)). Now f has the value 0.0001s^{-1} so that fv has this value on the bank top but fv = .000025m/s^2 off the bank. Since the tidal range is 5m, η is 2.5m and from g = 9.81m/s^2 we have that p is 25m^2/s^2. Now a general value for the tidal wavelength in the Channel is 500km. We estimate $\partial p/\partial x$ from $p\,2\pi/L$ as X = 0.00031m/s .

In fact, the Dover Strait acts as a throttle for the flow, and much larger values are expected here. We take a typical value of $X = 0.001 \mathrm{m/s^2}$ with an upper limit of $X = 0.01 \mathrm{m/s^2}$. Thus $K > f$ for all solutions and we take, without loss of generality, $K = 10f$ for the following argument.

We now consider values and parameterizations for the only free variable K to seek a solution for III.(10)a that yields $\partial u/\partial y = 0$.

Smooth bank, $K = kh$ is the least likely constraint and it implies that the flow responds to the bank as it were smoother than the surrounding deep water and equation III.(10)a becomes

$$u = \frac{X}{hk} + \frac{fv}{hk} \qquad \text{III.(13)}$$

where since the first term varies as $1/h$ and the second term varies as $1/h^2$ then u will increase over the smooth region for any k value.

Rough bank, $K = k/h$ is the constraint that was used for Huthnance(1973) and it is inherently likely. It implies that the bank acts as an element of roughness within the flow giving

$$u = \frac{hX}{k} + \frac{f(vh)}{k} \qquad \text{III.(14)}$$

here the second term is constant as required with the first term fluctuating. We might say that we have u = constant for small X, giving $K \leq f$, BUT X is the forcing function for the flow! This implies that there is a balance between friction and Coriolis force.

We might believe this just for the bank top if the flow is driven by a bulk force balance off of the bank, but this equation defines the flow in the region of the bank as well. We surely expect channel flow to be dependant upon values for the forcing term.

Neutral bank, $K = k$ for no constraint at all at the bank gives

$$u = \frac{X}{k} + \frac{fv}{k} \qquad \text{III.(15)}$$

where the first term is constant and the second fluctuating to give u = constant if and only if $K > f$ with $k = X$. This implies, paradoxically, that although the bank is not an area of high friction relative to its surroundings, it must exist within a region of relatively high friction.

We have found two different forms for the friction term and before deciding between them we should query our initial assumptions.

Firstly, we have ignored all of the non-linear advective terms. Tidal charts show no significant change of velocity over the bank length so it is reasonable to ignore the $u\partial u/\partial x$ and the $u\partial v/\partial x$ terms. The $v\partial v/\partial y$ term may affect the trapped surface wave and so should be included in equation III.(10)c. However, the $v\partial u/\partial y$ term for equation III.(10)a will be zero for u = constant as measured.

Secondly, for the small latitude change of the model, f is constant of course but, do we assume that X cannot vary over the bank? If we could take $X' = \frac{X}{h}$ then u=constant for III.(14) only, and III.(15) could be rejected with the rough bank the best solution.

Initially, it does seem quite reasonable to accept that the forcing term X is reduced over the bank, but this term is in fact along-bank surface slope. This assumption would imply a lowering of the water surface at the bank nose with an equivalent raising at the bank tail. This would generate large compensating flows at the bank ends that are not noted on the charts. We must therefore hold to the assumption that X does not vary across the bank.

While we have considered that X is constant for the duration of the 10minute timescale required for the flow to cross over the bank, it is in fact varying sinusoidally in time to give values close to zero at the change of the tide. Thus the argument above for $K > f$ is not a strong one since we have considered the maximum conditions only. However, we cannot extend an argument defined in terms of the maximum flows to smaller values because of the linearization of the friction term.

There is no compromise between the concept of a rough or a neutral bank, only one term or the other can be constant and we must choose between them.

The curve for u for the rough bank, in fig.III.14d, suggests that some complex current system must exist at the bank ends to resolve the reduced u value within the region of high viscosity and no evidence for this is noted on the charts.

Furthermore, for the rough bank, if we take the measured u value as valid, then $K < f$ and we have a balance between Coriolis and friction. This is the basic assumption for Ekman flow and we should expect a veering of the flow with depth for any region where this balance holds.

The measured flow of fig.III.5a demonstrates that there is no veering between 1m above the bottom and 20m above the bottom in 40m water depth. Thus we may confidently assume that the flow is frictional and that the main balance of forces must therefore be between the forcing term and the friction term. Thus the bank must be frictionally neutral with only local effects upon the flow and no overall affect on the bulk flow dynamics.

We have shown that $K > f$ and this will affect the nature of the surface slope in the y-direction. Equation III.(10)c must be modified to include an advective term as argued above

$$\frac{\partial p}{\partial y} = -Kv - fu - v\frac{\partial v}{\partial y} \qquad \text{III.(16)}$$

and we can see that the constant cross-channel slope will be modified over the bank by the second and third terms. The bank acts like a leaking channel boundary — water accumulates upstream of the bank to give rise to trapped topographic Kelvin waves.

IV GRAVITY WAVE EFFECTS

Waves have a considerable effect on beaches and sand bars in storm conditions and although water depths are greater over sand banks an investigation would not be complete without consideration of the effect of surface waves on the bank and vice versa. The waves can transport sediment and wave breaking will increase turbulence to affect the hydrodynamics.

We therefore consider the variation over the bank of wind wave amplitude, speed and frequency. The stimulus for this work was the Seasat image fig.IV.1 of the Southern Bight. Much of the work in this section was presented as a paper at the 15th Liege Colloquium on Ocean Hydrodynamics in May 1983.

Many different effects can cause modulation of the image from a Synthetic Aperture Radar signal. This means that image interpretation is not easy. We show that the image at South Falls can be explained as a variation in water surface roughness. That is, a variation of the gravity wave amplitude and/or wavelength.

The Seasat Synthetic Aperture Imaging Radar was designed for a maximum response from ocean waves and the apparent topography of fig.IV.1 was a surprise. The microwave signal can penetrate at most only 1cm below the sea surface, so it must be assumed that the sea surface shape itself responds to the topography of the sea bed over which it flows.

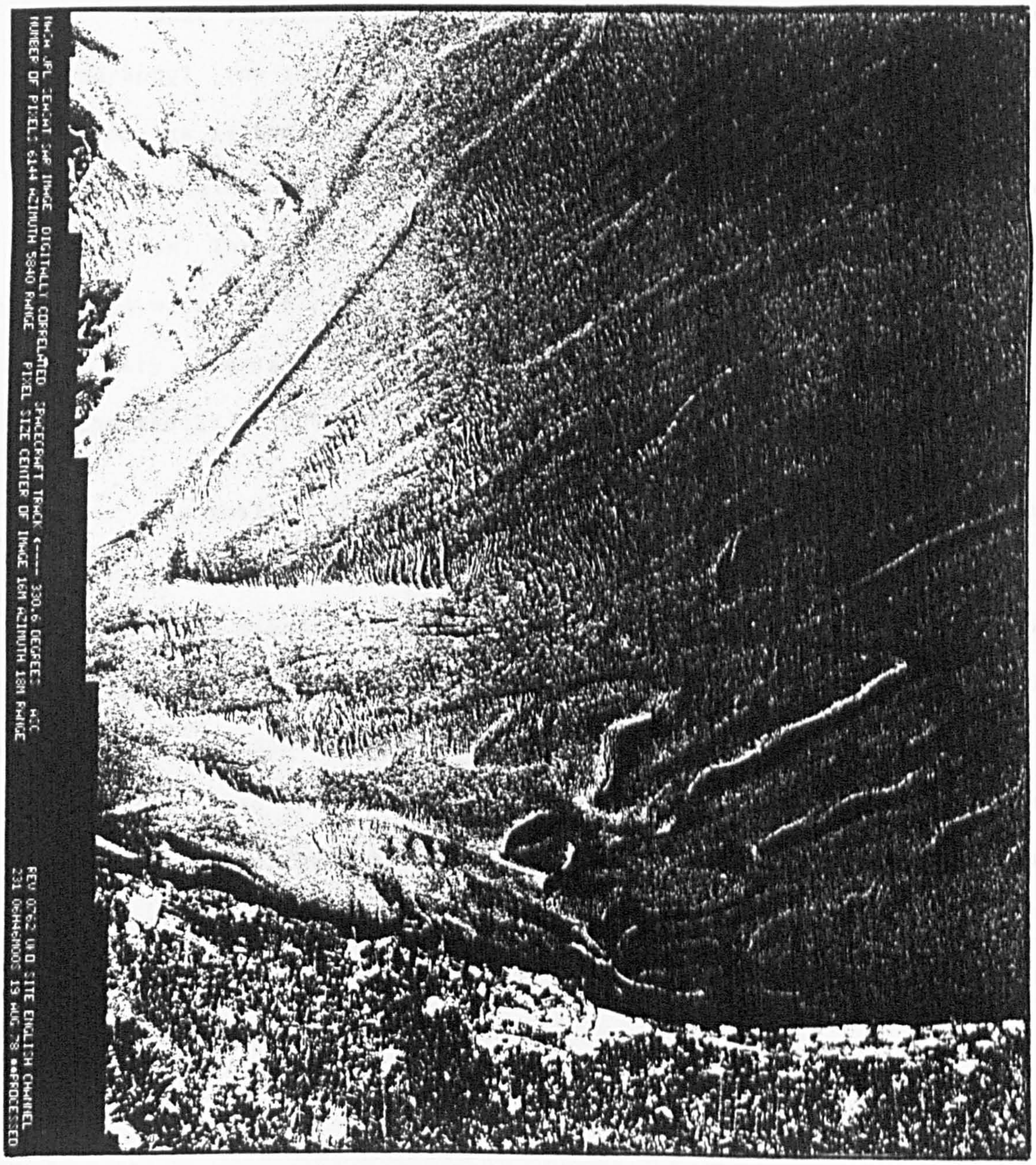

Fig.IV.1 Southern Bight — Image from Seasat SAR (courtesy of JPL, Pasadena, USA)

The sandbanks and sandwaves of the region are clearly shown. The South Falls and the Goodwin sands are on the top left of the image.

What relationship is there between this image and the real topography? The image has the appearance of an optical picture of the sea bed, as if there were 'faces' inclined away from the spacecraft and in shadow while others shine brightly as if by specular reflection. The effect is limited to shallow water and so presumabley surface water velocity is the main parameter, since by continuity this must vary inversely with depth. This is confirmed for the South Falls by the models of chapter III.

Any small amplitude real topography, with no slope that is greater than the angle of illumination, can be assumed to return a backscattered signal in proportion to some function of slope, say $f(\partial d / \partial x)$. If so, a side-illuminated shape, when viewed from above, would show a sudden change from maximum to minimum brightness at a sharp peak. This effect is noted in the image at the South Falls bank. As a first approach to modelling the phenomena we integrate the signal G, for the pseudo-bathymetric depth d. We fit this curve to a measured cross-bank profile to show the relationship between real and apparent bathymetries.

IV.1 Coincidence

We have echo-sounder traces of the bank cross-section and compare them to the shape of the image brightness. We look for the relationship between them in order to fix the bank position on the image and to explain the brightness variation.

Not having access to the digital values, a film of the optically processed image fig.IV.1 was digitised on a scanning

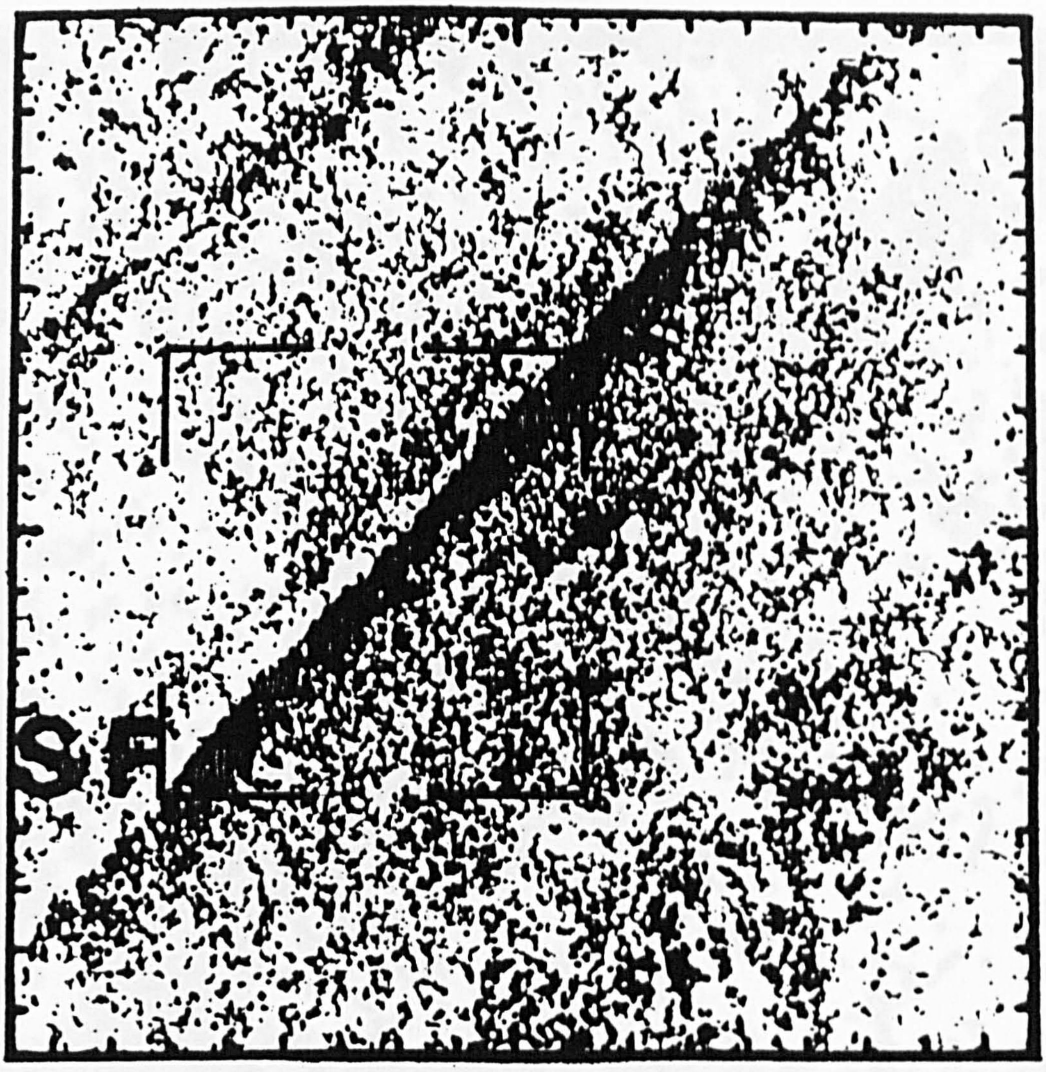

Fig.IV.2 Southern Bight — Image: Submatrix 1 is from the top left of Fig.IV.1. Here SF indicates the tail of the South Falls. The feature east of the bank does not resemble a mobile vessel track. A chart wreckmark approximates its position.

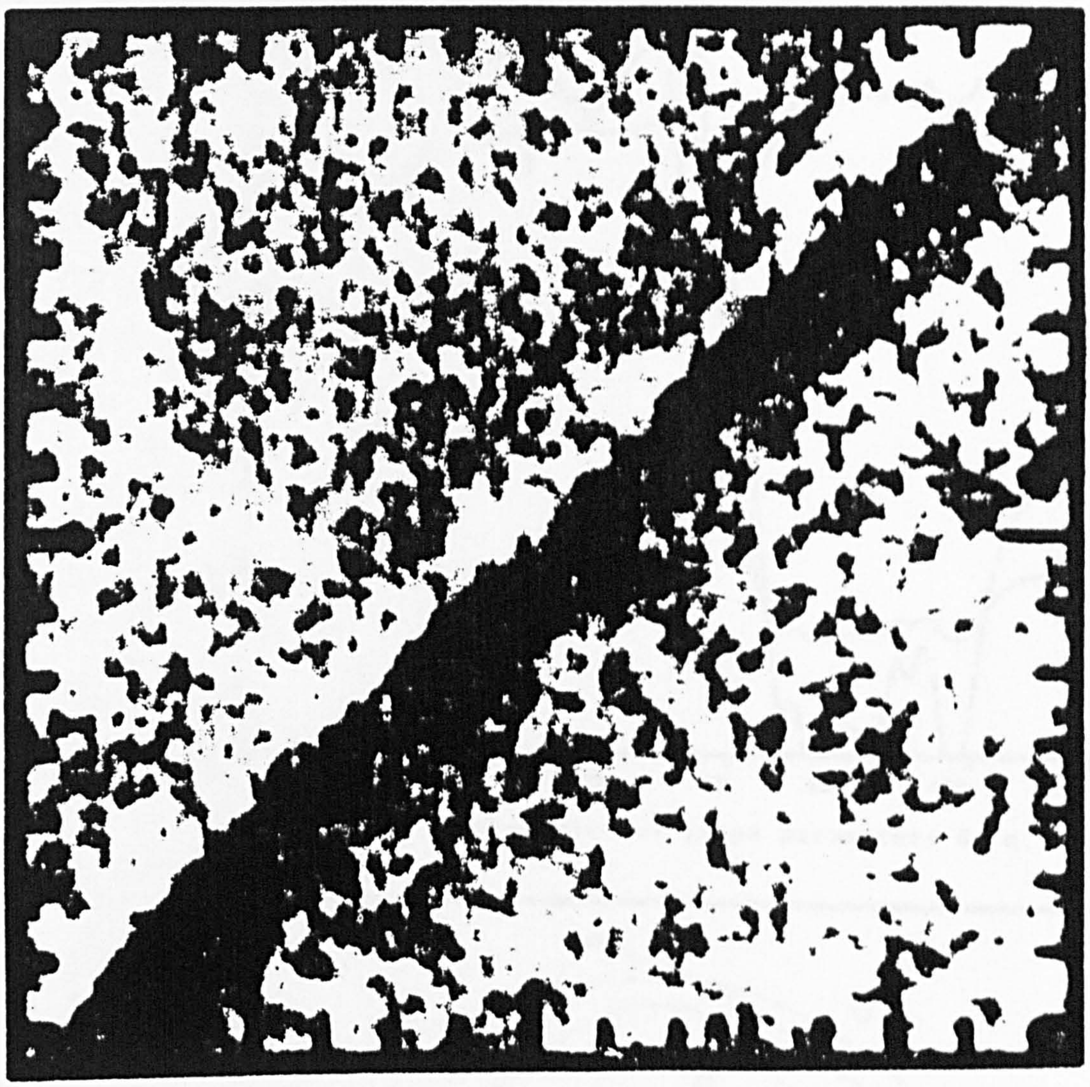

Fig.IV.3 Southern Bight — Image: Submatrix 2, extracted from submatrix 1, is centred on station SF on the bank top (Fig.I.5), located where a dark wake trails towards the bank from the feature to the east.

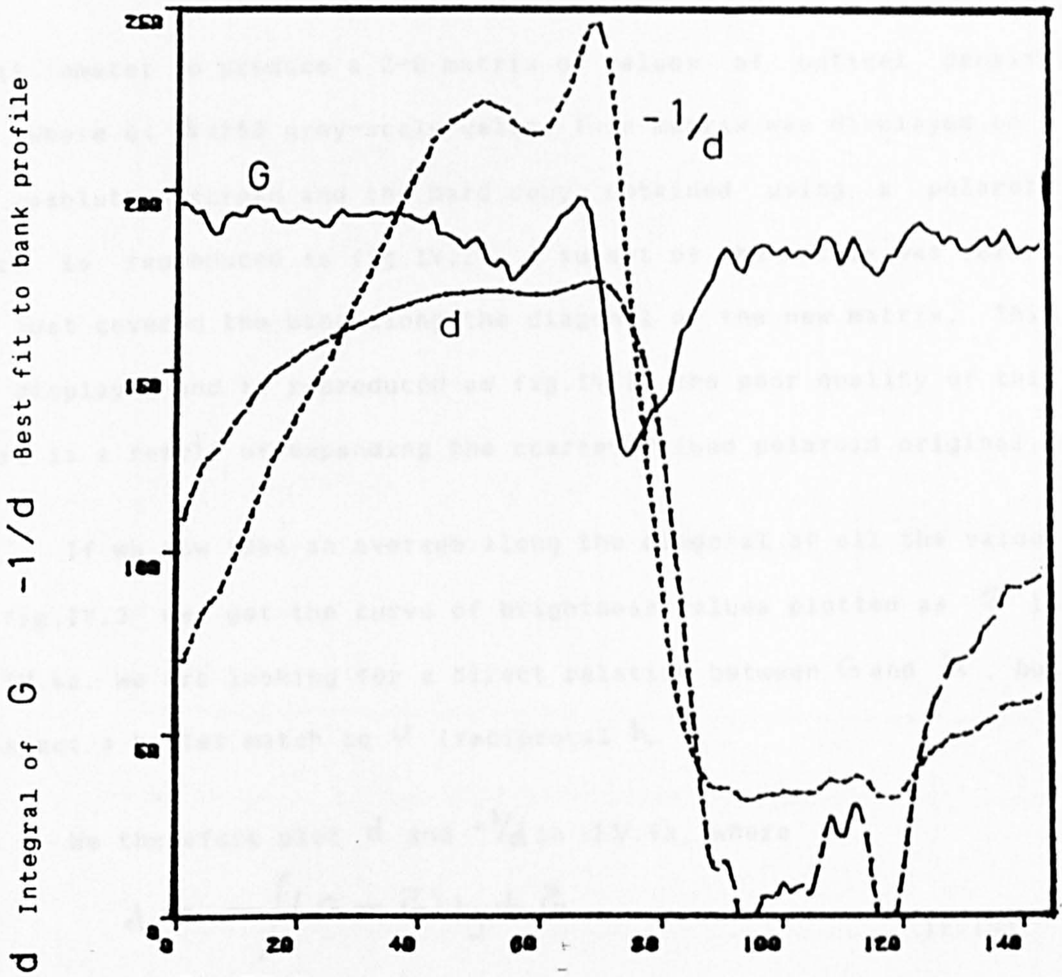

Fig.IV.4a Global plot of image parameters G, d, −1/d

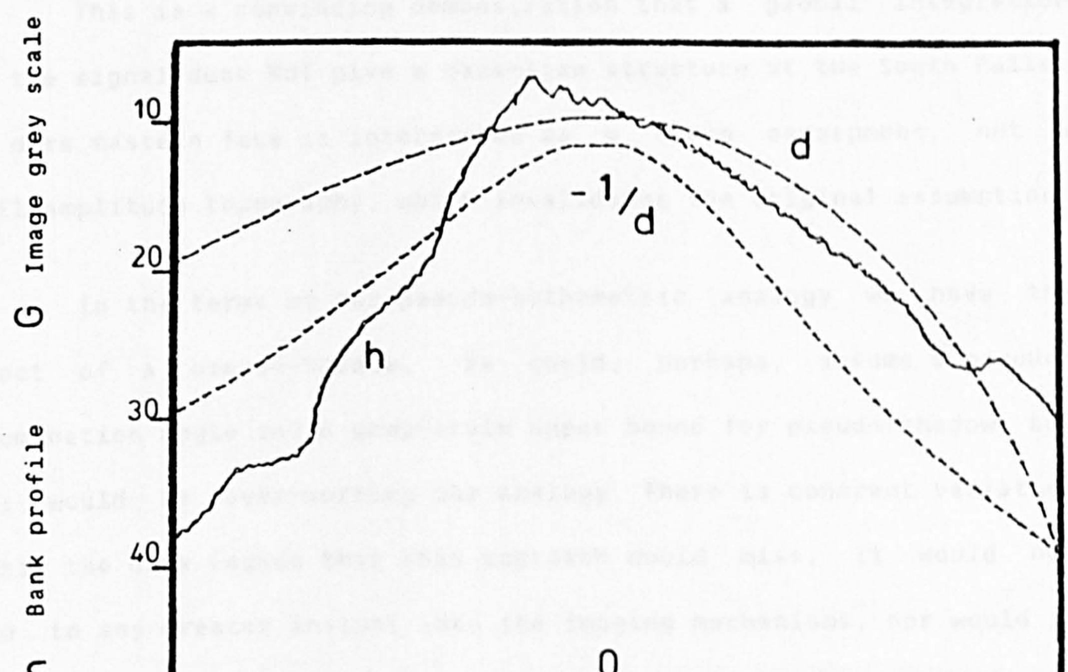

Fig.IV.4b Local fit to image parameters G, d, −1/d densitometer to produce a 2-D matrix of values of optical density G, where $0 < G < 250$ grey-scale value. This matrix was displayed on a high resolution screen and the hard copy obtained using a polaroid camera is reproduced as fig.IV.2 . A subset of the matrix was formed that just covered the bank along the diagonal of the new matrix. This was displayed and is reproduced as fig.IV.3, the poor quality of this figure is a result of expanding the coarse-grained polaroid original.

If we now take an average along the diagonal of all the values of fig.IV.3 we get the curve of brightness values plotted as G in fig.IV.4a. We are looking for a direct relation between G and h, but we expect a better match to v (reciprocal h).

We therefore plot d and $-1/d$ in IV.4a, where

$$d = -\int (G - \bar{G})\, dy + \bar{G} \qquad \text{IV.(01)}$$

This is a convincing demonstration that a global integration of the signal does NOT give a bank-like structure at the South Falls. The dark eastern face is interpreted as a steep escarpment, not a small amplitude topography, which invalidates the original assumption.

In the terms of our pseudo-bathemetric analogy we have the effect of a pseudo-shadow. We could, perhaps, assume a pseudo-illumination angle and a grey-scale upper bound for pseudo-shadow, but this would be over-working the analogy. There is coherent variation within the dark region that this approach would miss. It would not lead to any greater insight into the imaging mechanisms, nor would it help to find the bank related modulation of the surface wave field.

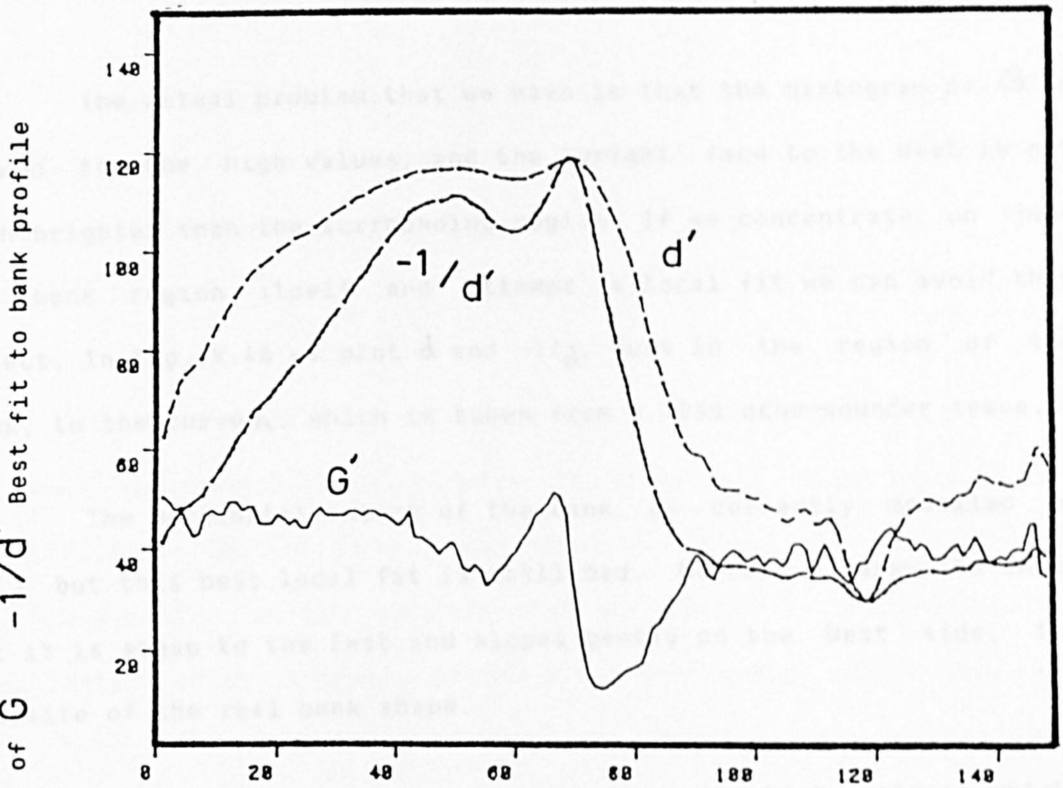

Fig.IV.5a Global plot of biassed parameters G', d', -1/d'

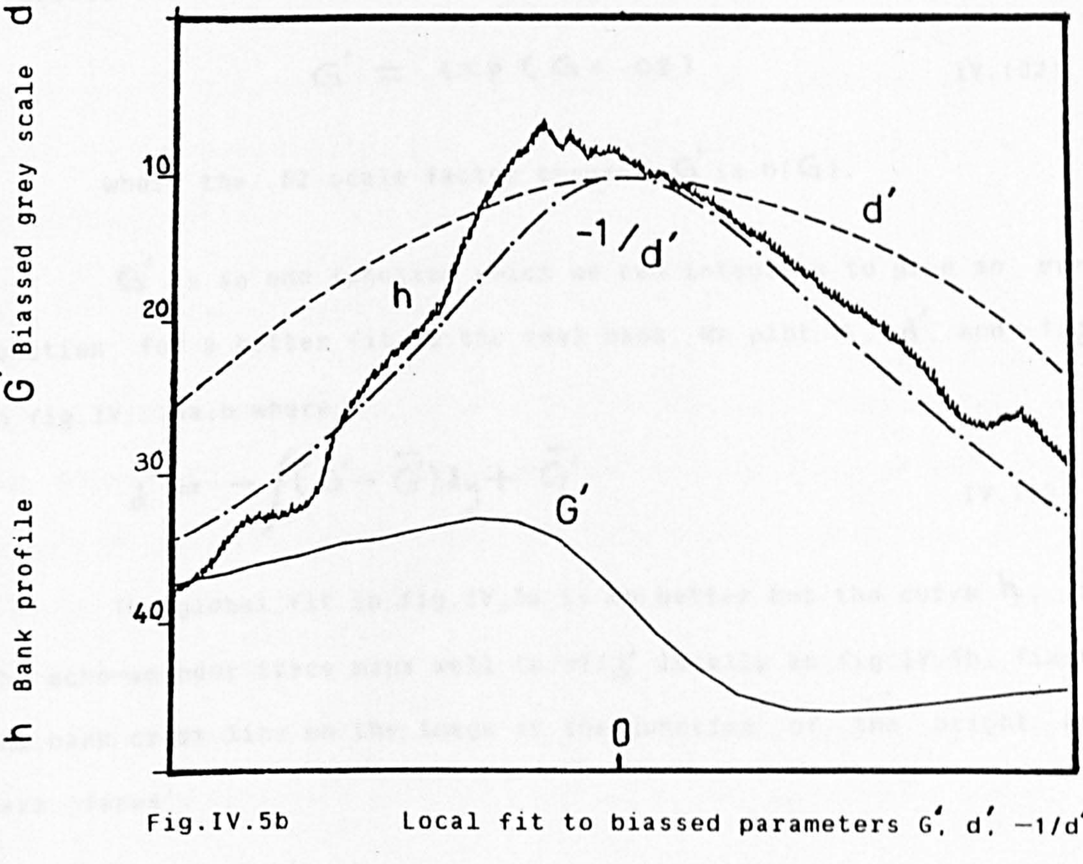

Fig.IV.5b Local fit to biassed parameters G', d', -1/d'

The actual problem that we have is that the histogram of G is skewed to the high values, and the 'bright' face to the West is not much brighter than the surrounding region. If we concentrate on just the bank region itself and attempt a local fit we can avoid this effect. In fig.IV.4b we plot d and $-1/d$, just in the region of the bank, to the curve h, which is taken from a 1980 echo-sounder trace.

The horizontal extent of the bank is correctly modelled by $-1/d$ but this best local fit is still bad. We have a bank-like shape but it is steep to the East and slopes gently on the West side, the opposite of the real bank shape.

This is the result of a local skew to high values which, unlike the global problem, can be removed. We stretch the coordinate to create the new variable G', by the transformation,

$$G' = \exp(G \times .02) \qquad \text{IV.(02)}$$

where the .02 scale factor ensures G' is $O(G)$.

G' is an odd function which we can integrate to give an even function for a better fit to the real bank. We plot h, d', and $-1/d'$ in fig.IV .5a,b where,

$$d' = -\int (G' - \bar{G}')\,dy + \bar{G}' \qquad \text{IV.(03)}$$

The global fit in fig.IV.5a is no better but the curve h, of the echo-sounder trace maps well to $-1/d'$ locally in fig.IV.5b, fixing the bank crest line on the image at the junction of the bright and dark 'faces'.

A good fit of δ to the bank would have implied that $G = \partial h / \partial y$, and so the better fit of $-1/\delta'$ does suggest that $G = \partial v / \partial y$, and hence, from equation III.(11)

$$G \sim g\left(-\frac{c}{h^2}\frac{\partial h}{\partial y}\right) \qquad \text{IV.(04)}$$

We have arrived at this relation by a comparison of real and apparent bathymetries. A similar relation has been derived in a parallel investigation (Alpers and Hennings, in press). This was from a consideration of the full Hydrodynamic Modulation Function for the modification of the response of the Bragg scattering wave components over the bank. The HMF includes the effect of the modulation of gravity waves by the bank considered below in section IV.5.

In this section we have successfully identifed the position of the bank crest line on the image but the fact that we must transform G to G' for a proper fit to the bank profile suggests that this model lacks credibility and that we must take a closer look at the mechanisms involved.

IV.3 Surface velocity field

We have shown that we need the surface water velocities over the South Falls bank in order to model the variation of the surface waves. At present, shore-based HF ground-wave radar can measure surface currents to 1cm/s accuracy, up to 30km from the coast with a 1.2km range resolution, and up to 250km from the coast with a 15km range resolution. Furthermore, a surface following buoy is under developement to measure vertical profiles in the uppermost 2 metres.

However, in general, the provision of accurate oceanic and coastal sea surface water velocities is beyond the capacity of present day instrumentation. Certainly, no such instrumentation was deployed during the flight time of the Seasat satellite. Because of this, we take the approach here of estimating surface velocities by extrapolation from the sea-bed measurements previously used to estimate depth-averaged flow.

Equation III.(01) can be used as a first approximation for an analytical model. This has been done by Alpers and Hennings(in press), where the equations are utilised for the HMF. We are interested in a particular surface velocity field at South falls for the time of the Seasat overpass, 0646 GMT 19 August 1978.

Fortuitously, the pattern of tides at this time was very nearly duplicated by those of 25 October 1980, and this can be seen in table A below.

TABLE IV.A

DOVER TIDAL PREDICTIONS

DATE		GMT	METRES
1978	AUG 18	23.03	6.9
	AUG 19	06.40	0.6
	AUG 19	11.27	7.1
1980	OCT 24	23.05	7.1
	OCT 25	06.50	0.6
	OCT 25	11.26	7.2

NOTE: The heights are above Chart Datum which is LAT for Dover. Extracted from: vol-I ADMIRALTY TIDE TABLES NP200-78,80

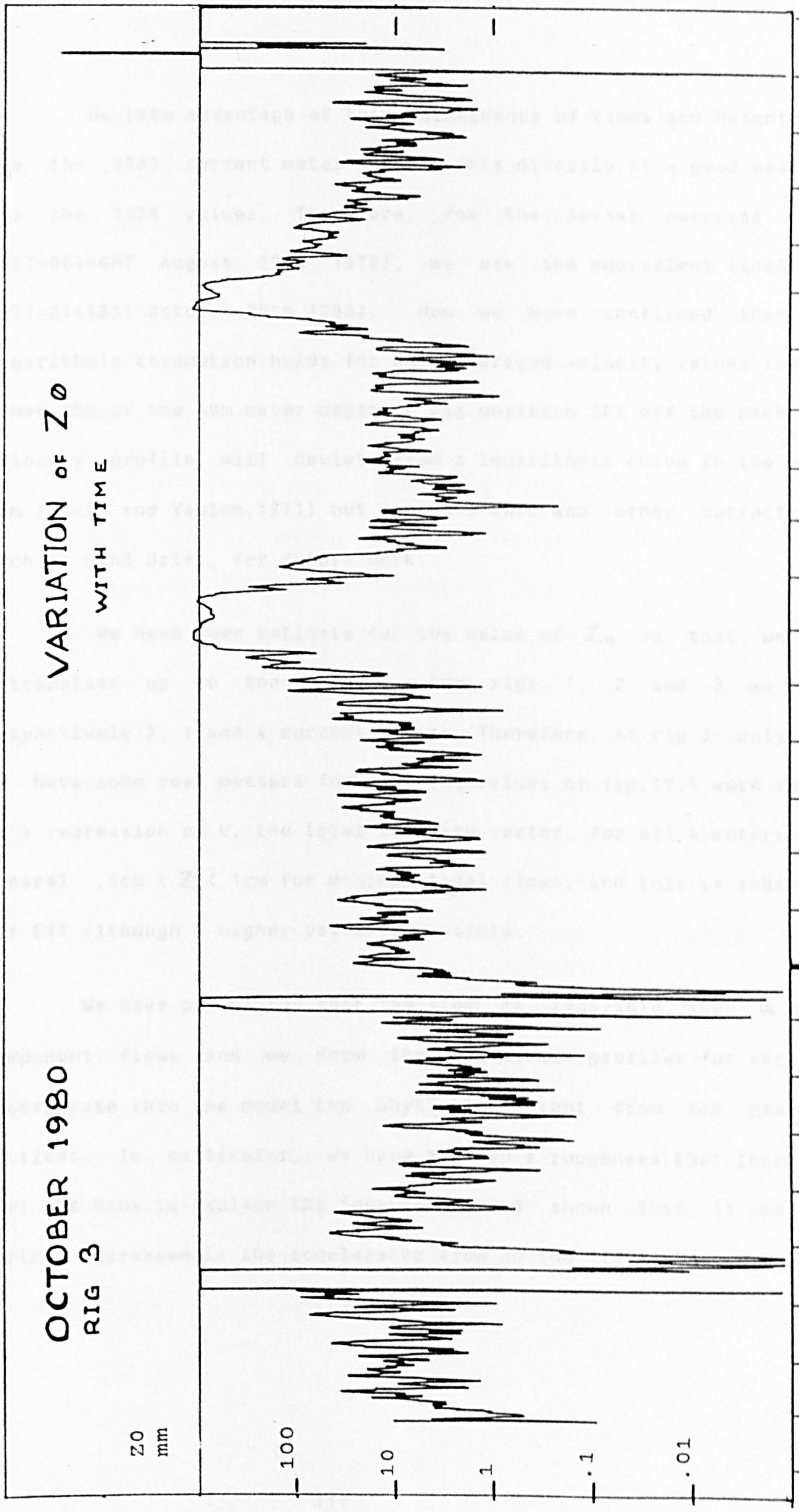

Fig.IV.6 Z_0 variation with time 116

We take advantage of this coincidence of times and heights to use the 1980 current meter measurements directly as a good estimate for the 1978 values. Therefore, for the Seasat overpass time (SST=0646GMT August 19th 1978), we use the equivalent tidal time (ETT=0746BST October 25th 1980). Now we have confirmed that the logarithmic assumption holds for 5min—averaged velocity values for the lower 20m of the 40m water depth at rig position SF3 off the bank. The velocity profile will deviate from a logarithmic curve in the upper 20m (Monin and Yaglom,1971) but we leave this and other corrections, such as wind drift, for future work.

We need some estimate for the value of z_0 so that we can extrapolate up to the surface. For rigs 1, 2 and 3 we have respectively 2, 1 and 4 current meters. Therefore, at rig 3 only, we do have some real measure for z_0. The values of fig.IV.6 were formed by a regression on U, the total velocity vector, for all 4 meters. In general $.1\text{cm} < z_0 < 1\text{cm}$ for maximum tidal flows, and this is indicated for ETT although a higher value is possible.

We have postulated that the flow is separable into u and v component flows and we form the logarithmic profiles for each. We incorporate into the model the physical insight from the previous sections. In particular, we have assumed a roughness that increases over the bank to explain the invarient u and shown that it may be further increased in the accelerated flow on the flank.

The rig 3 component flow values for ETT from fig.III.8,9 are plotted in fig.IV.7. The curve for u indicates a z_0 value compatible with the fig.IV.6 z_0 value. The 10cm value for $v = 0$, although well supported, is a surprise. It may indicate an unusual roughness feature or a bottom jet and weakens, but does not invalidate, the separable flow assumption over the bank. Surface values at SF3 follow directly by extrapolation up to 40m height above the sea bed.

At rig 1 the 1m values indicate a sharp direction change with height that creates widely differing z_0 values. We expect similar values, since sandwaves should be aligned normal to the flow and this is ~45deg to the bank here, from the 2m flow direction value 245deg. Whether real or due to compass error this flow would invalidate the separable flow assumption and cannot be included in the model. It can be removed by taking the SF1–1m velocity amplitude with the SF1–2m value for direction to give new values u = .40 and v = .48m/s. These give u = 0 at 10.4cm i.e. 4 x 2.6cm (the value at SF3), which is the correct ratio, and the same value for the v curve, as required.

We really have problems at rig 2. There is only the one meter reading and the roughness value will be affected by the accelerated flow. We take double the rig 3 values. This gives an acceptable curve for v but that for u gives an abrupt variation in surface values and a poor approximation to invariant u. Although the different roughness values contradict this also, it is not important for the mass flux if the upper layer values are correct.

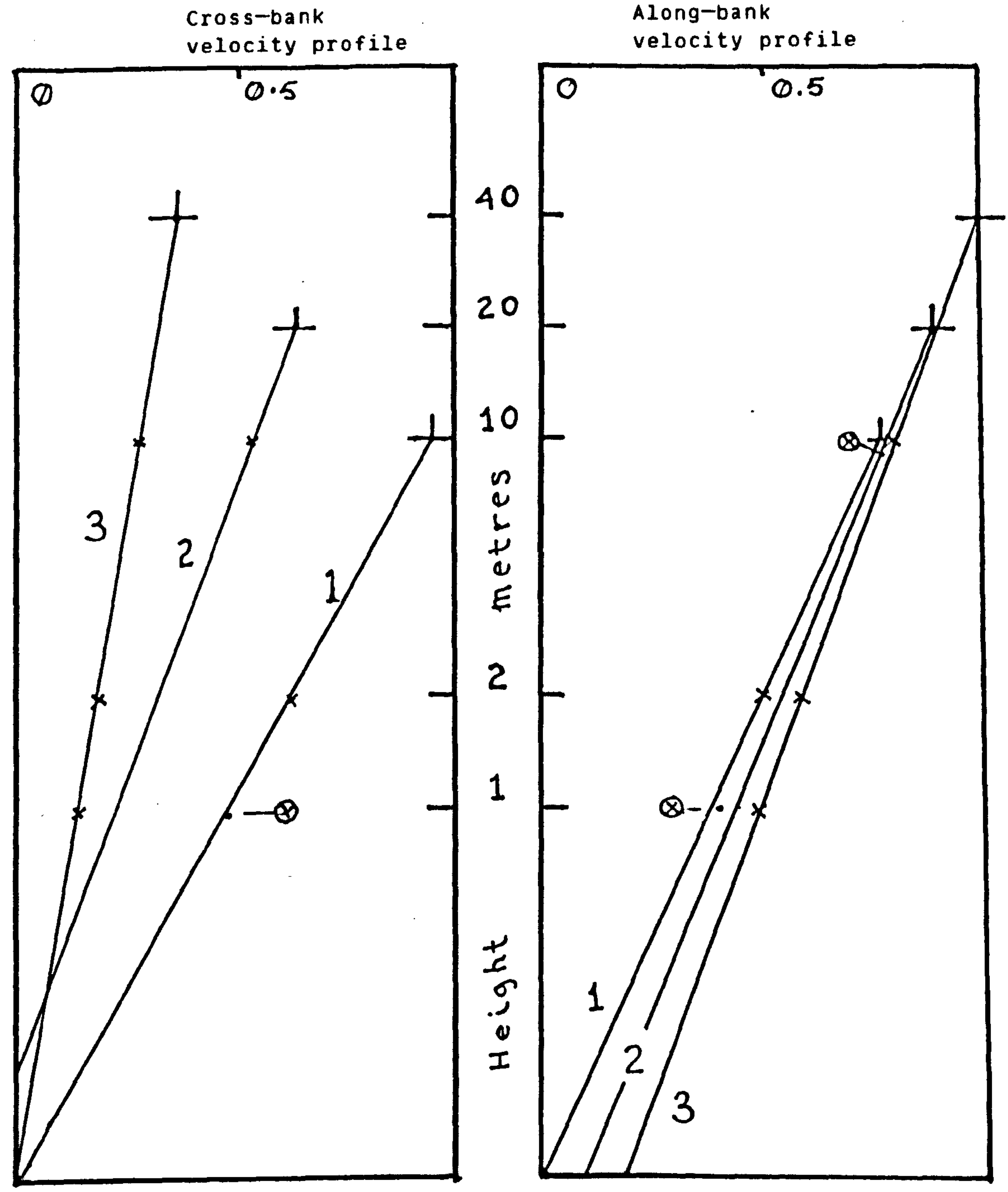

Water speed in metres/sec.
Height above sea-bed in metres.

⊥ Derived surface velocity value

× Measured u, v values

⊗ Rejected measured values

1, 2, 3 rig numbers

Fig.IV.7 South Falls .... ETT velocity profiles

Inspection of fig.III.8 reveals that the SF2 value exceeded the SF3 value only minutes before ETT. It is unfortunate that we reject the only data point we have for this curve, but we do so in order that we can better understand the dynamics of the model. We therefore take the u curve for rig 2 from the 5.2 value for z_0 to the intersection point of the other two u curves. This gives a u value at 10m of 0.78m/s, which is plausible, and a smoother model which is summarised below.

TABLE IV.B

Water velocities South Falls bank			0646 GMT on 25th Oct 1980			Derived Surface values	
rig	h	Z0 cm	u v at height Z 1m	2m	10m	u v	Speed /angle
SF1	10	10.4	0.29	0.50	–	0.77	1.23
		10.4	0.59	0.59	–	0.96	/248
SF2	20	5.2	–	–	0.70	0.89	1.09
		20.8	–	–	0.53	0.63	/232
SF3	40	2.6	0.49	0.58	0.80	0.99	1.06
		10.4	0.14	0.19	0.28	0.37	/217

NOTE: The velocity plots – fig.IV.8,9 exhibit temporal fluctuations, local to each rig, and the velocities above are smoothed estimates typical for the whole bank length.
NOTE: At SF1, the 1m component values are reworked, using the angle at the 2m level, to give new values that are in agreement with a separable model for the flow.

IV.4 Wave blocking

When wave propagation is in the opposite sense to that of a current we must consider the possibility that some of the high frequency waves will be 'blocked'. A blocked wave component is one for which the phase velocity is insufficient for its propagation against the adverse current. The mechanisms considered are critical flow and the related but more important effect of radiation stress.

Shallow water critical flow occurs when a long wave can reach, but not pass, a point. This occurs when the local adverse current v is equal to c_s the phase velocity of the long (shallow-water) waves

$$c_s = \sqrt{gh} \qquad \text{IV.(05)}$$

A wave of length $L > 20\,h$ is defined as shallow; therefore

off the bank, in 40m water depth $L > 800$m, $c_s > 20$m/s ($T > 40$s),

on the bank, in 10m water depth $L > 200$m, $c_s > 10$m/s ($T > 20$s).

Thus no shallow water waves are blocked by this mechanism as the maximum adverse current we need consider is 1.5m/s.

Waves short enough to be considered as deep water waves have length $L < 2h$, and the phase velocity is

$$c_d = \sqrt{g/k} \qquad k = 2\pi/L \qquad \text{IV.(06)}$$

so that short wave Froude number will vary with wave frequency.

Off the bank, in 40m depth $L < 80$m, $c_d < 11$m/s ($T < 7$s),

on the bank, in 10m depth $L < 20$m, $c_d < 5.6$m/s ($T < 3.6$s), so not all deep water waves are blocked by this mechanism.

However, although the profile of the wave may pass over the bank we must consider the amplitude that it may have. While long wave energy travels with the phase speed, for short waves the energy and hence the amplitude, travels at the group velocity C_g, which is half the phase velocity. Thus for the 3.6s waves (L < 20m) C_g = 2.8m/s and we lose most of the short wave energy.

There is however an even more stringent criterion for wave blocking whereby the current does work on the waves through the radiation stress term of the energy balence equation. This is discussed in detail in the next section, but we note that fig.IV.8 indicates that when σ is just one quarter of the phase velocity in an adverse current the amplitude amplification is such that wave breaking will occur. Thus the wave energy will be dissipated and no short wave energy passes the bank when opposed by the maximum tidal velocity.

We can see that the criterion for blocking is that the wavelength L < 20m, and thus all intermediate and shallow water waves will pass over the bank while short wave energy accumulates downstream of the bank crest.

IV.5 Wave modulation

We follow (Longuet-Higgins and Stewart,1960/1961), hereinafter referred to as LHS0/LHS1, which demonstrated that the equation for the variation of wave energy must include a radiation stress term through which the current can do work upon the waves and vice versa.

For the local variation of surface tidal current found, we assume that the change of topography will have an effect that is similar to the upwelling condition of case(1)-LHS1. The case(2)-LHS1, with a side inflow condition, verified that a constant current normal to the wave direction does not affect the equation for energy balance.

We therefore write down the argument, as given in case(1)-LHS1, with the x and y coordinates transposed.

The equation for the balance of wave energy, as modified by currents of arbitrary form, is given by

$$\nabla \cdot \left[E \left(C_g + V \right) \right] + \tfrac{1}{2} S_{ij} \left(\frac{\partial V_i}{\partial x_j} + \frac{\partial V_j}{\partial x_i} \right) = 0 \qquad \text{IV.(07)}$$

here the radiation stress tensor is

$$S_{ij} \equiv S \equiv \begin{Bmatrix} S_x & 0 \\ 0 & S_y \end{Bmatrix}$$

where for a current (u, v) and a wave in direction y

$$S_x = E \left[C_g/C - \tfrac{1}{2} \right] \qquad S_y = E \left[2 C_g/C - \tfrac{1}{2} \right]$$

The energy balance equation IV.(07) may therefore be written

$$\frac{\partial}{\partial y} \left[E \left(C_g + v \right) \right] + S_x \frac{\partial u}{\partial x} + S_y \frac{\partial v}{\partial y} = 0 \qquad \text{IV.(08)}$$

For short waves, $C_g = C/2$ and IV.(08) becomes

$$\frac{\partial}{\partial y} \left[E \left(C/2 + v \right] + E/2 \frac{\partial v}{\partial y} = 0 \qquad \text{IV.(09)}$$

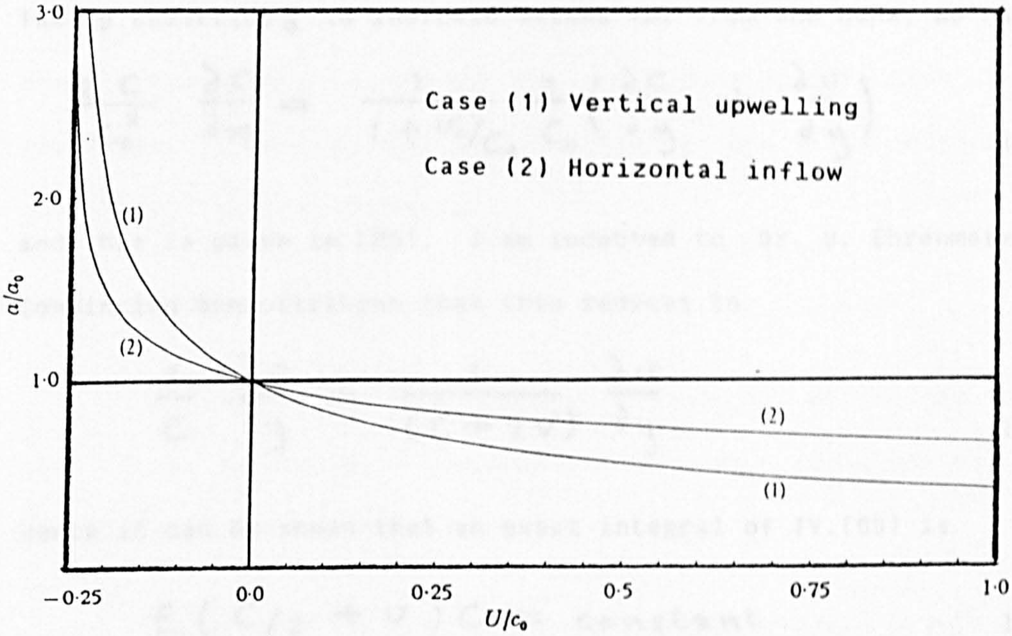

Current U is normalized by deep-water wave phase speed c_o
Wave amplitude a is normalized by deep-water amplitude a_o

Fig.IV.8 Wave/current interaction (after LHSØ)

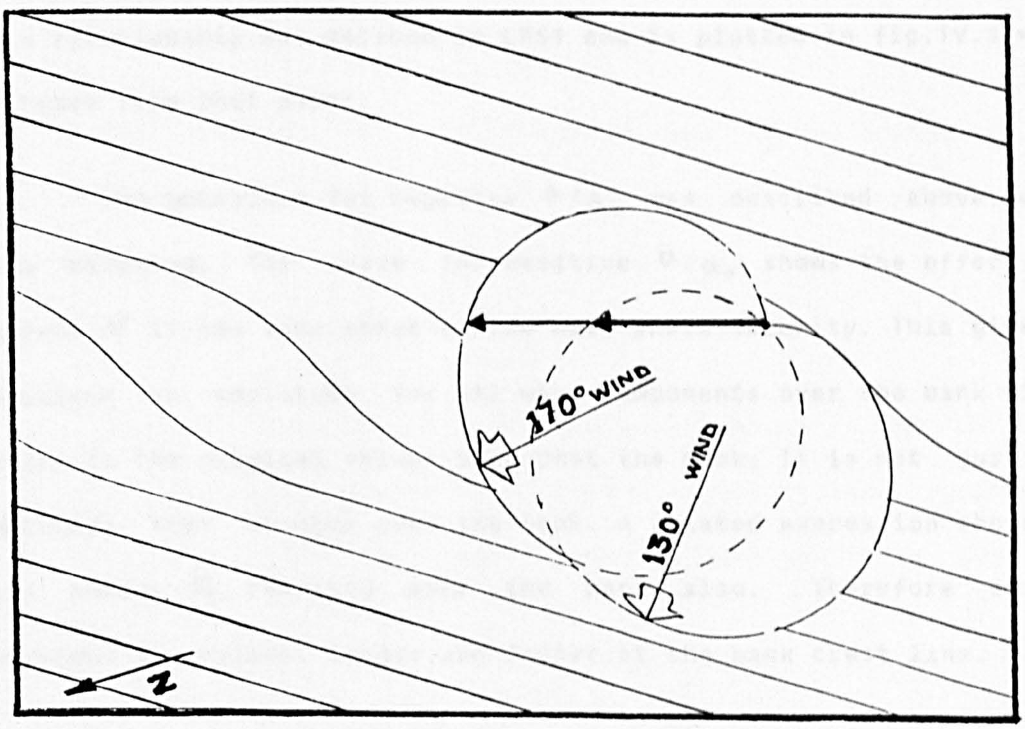

Arrows show 2 possible along-bank wind components

Fig.IV.9 South Falls : ETT surface velocity streamlines & superimposed cardiod directional wave spectrum.

Taking subscript $_o$ to indicate values far from the bank, we have

$$\frac{2c}{c_o^2}\frac{\partial c}{\partial x} = \frac{1}{1+v_o/c_o}\frac{1}{c_o}\left(\frac{\partial c}{\partial y} + \frac{\partial v}{\partial y}\right) \qquad \text{IV.(10)}$$

and this is given in LHS1. I am indebted to Dr. U. Ehrenmark for a convincing demonstration that this reduces to

$$\frac{1}{c}\frac{\partial c}{\partial y} = \frac{1}{(c+2v)}\frac{\partial v}{\partial y} \qquad \text{IV.(11)}$$

Hence it can be shown that an exact integral of IV.(09) is

$$E\,(c/2 + v)\,c = \text{constant} \qquad \text{IV.(12)}$$

and it follows that

$$\frac{a}{a_o} = \left[\frac{c_o(c_o+2v_o)}{c(c+2v)}\right] \qquad \text{IV.(13)}$$

This relationship was derived in LHS1 and is plotted in fig.IV.8 which is taken from that paper.

The behaviour for negative a/a_o was described above under wave blocking. The curve for positive a/a_o shows the effect of a current v in the same sense as the wave phase velocity. This gives a reduction in amplitude for all wave components over the bank with a return to the original values once past the bank. It is not just the amplitude that changes over the bank. A related expression shows the wave number k reducing over the bank also. Therefore a wave component is smaller, longer and faster at the bank crest line.

We can take at least one component in each direction to model the image intensity change of fig.IV.1 as a variation in surface roughness. However we must consider that a wave field consists of wave components from all directions.

IV.6 Surface wave field

We now include wave components from all directions and show that this extension is compatible with a wave amplitude minimum over the flank of the South Falls.

We need not do a detailed wind analysis since a full hindcast for SST is not required. We use available information to describe, in a general sense, the varying wind wave field over the bank. The SST surface velocity is taken as that for ETT above. The reports from coastal stations gave winds 6–12knots from 130–170deg.
This spans the space craft azimuth direction of 155deg.

The spectrum of a wind–driven sea must include large amplitudes in some of the higher frequencies. For a wind speed of 10knots (Pierson et al,1955) gives wave periods 1–6s between which this occurs, with the maximum amplitude at 1.8s.

For each frequency, the maximum amplitude is in the direction with the wind and there is a minimum ε, possibly zero, against the wind. A model for the variation between these extremes has been proposed (Tyler et al,1974)

$$G(\theta) = \varepsilon + (1 - \varepsilon) \cos^{S(\omega)}(\theta/2) \qquad \text{IV.(14)}$$

$$-\pi < \theta < \pi$$

For the above equation $S(\omega)$, the power of the cosine, is even integer and varies inversely with frequency.

The plot of $G(\theta)$ in fig.IV.9 is for the S value of 4, appropriate for high frequencies, and is superposed upon a plot of the surface velocity field for ETT. Directional behaviour will vary between that for cross-bank and for along-bank orthogonals. Cross-bank wave components have been well described above and we now consider an along-bank component. From the diagram we can see that, although South going waves will have been negligible, the North going along-bank wave components could have had a considerable amplitude.

We therefore take a ray-path, or wave orthogonal, along the South Falls eastern flank at $\partial v/\partial y$ = max. Shallow water refraction will divert intermediate and long waves from this path and they will not have contributed to the roughness. Now deep water waves can be refracted by a shearing current (LHS1), but here

$$\frac{\partial v}{\partial x} + \frac{\partial u}{\partial y} = 0$$

This rate of strain tensor will be invariant under coordinate rotation so that no shear can exist.

We now introduce the idea that wave energy may be transported along the bank crest line by a process related to wave diffraction. The eastern flank is an area of fluid velocity divergence at ETT and the water particles are therefore subject to dilatation. To demonstrate this we extend the LHS0/LHS1 analyses to consider a wave propagating normal to the case1—LHS1 flow.

We have then a constant current against the wave which causes group velocity wave blocking for wave periods $T < 1$s. For the SST configuration, this passes a 1s–2s period band of slow moving wave energy.

We have a varying transverse current and we assume

$$V \equiv (u, v) \qquad C_g \equiv (C_g, 0)$$

this gives $S_x = E\left[2C_g/C - 1/2\right] \quad S_y = E\left[C_g/C - 1/2\right]$

and from IV.(08) the energy balance becomes

$$\frac{\partial}{\partial x}\left[E(C_g + u)\right] + \frac{\partial}{\partial y}(Ev) + E\left\{\frac{2C_g}{C} - \frac{1}{2}\right\}\frac{\partial u}{\partial x} + E\left\{\frac{C_g}{C} - \frac{1}{2}\right\}\frac{\partial v}{\partial y} = 0 \qquad \text{IV.(15)}$$

Now u is constant and for deep water $2C_g = C$ so that

$$S_x = E/2 \qquad S_y = 0$$

giving

$$\frac{\partial}{\partial x}\left[E(C/2 + u)\right] + \frac{\partial}{\partial y}\left[Ev\right] = 0 \qquad \text{IV.(16)}$$

Now for South Falls $\Delta x = 20\,\Delta y$ and we can take

$$\frac{\partial}{\partial y}\left[Ev\right] = 0 \qquad \text{IV.(17)}$$

Therefore the amplitude reduces with the increase in current over the bank and we have shown that the image of fig.IV.1 is compatible with what information we have for the surface roughness variation at SST.

The general wave field must include the effect of current reversal and the different fetch conditions for other wind directions. However, we have demonstrated here the main effects of spatial variation of wave amplitude at South Falls bank.

V DISCUSSION

The hydrodynamics of a linear sand ridge have been investigated. The tidal flow over a sand ridge has been measured and compared with dynamical models. The effect of waves has been modelled and compared with a SAR image. The implications of this work are considered below.

In chapters III and IV we described the present day regimes of wave and tide over the South Falls. We now consider the effects of past regimes of wave and tide upon the bank, in the light of the model results that indicate that the bank has a neutral roughness.

V.1. GENESIS AND STABILITY

The bank forming mechanism proposed by Houbolt(1968) was twin helical secondary vortices, aligned with the main flow. Little evidence has been found for this effect, and it is suggested in the next section that secondary vorticity generates a friction driven bottom flow that acts everywhere in a shallow sea. The way that this would be modified by the presence of a sand ridge is not clear, but it should be related to the cross-bank water slope.

The measured ebb/flood imbalance around a bank of Smith(1969) and Caston and Stride(1970) was explained in hydrodynamical terms by Huthnance(1973). This flow regime was used in Huthnance(1982a,b) with small perturbations of the sea-bed to demonstrate bank growth up to an equilibrium profile for many wave-numbers.

The Southern Bight sea area was created by an increase in mean sea levels after the Flandrian transgression. It has been suggested (Jelgersma, 1979) and (D'Olier, personal communication) that the sand banks were created at that time. The suggested mechanism is wave action on beaches which would be concentrated on high ground as the sea level rose. These same beach processes would tend to destroy the bank and disperse bank material as water level topped the bank. However, it is suggested that the material accumulation was sufficient to offset this. The residual material not dissipated would modify the local fluid dynamic regime to create the conditions required for bank accumulation, and the material may still exist as a bank core.

Are linear sand ridges relic beaches modified by wave action during the initial transgression? Are they growing or moving, either of which could cause significant navigational problems? Such questions of the stability, both of size and position, relate to mechanisms for bank growth. Any mechanisms that can cause bank growth may also have created the linear sand ridges. We first consider the mechanisms that may exist within the present day flow regime.

We consider here the possibility of a bank forming mechanism that is related to differential roughness of the sea-bed. Within a region of constant depth, the flow could be modified by variations in roughness. Now McLean(1981) gave a model for smooth sand ribbons over a rough bed that generate a helical flow that sustains their existence. The initial growth mechanism suggested was the result of wake flow on individual point sources of roughness.

Variation of the turbulence between different areas could be generated by different roughness values that exist over a sufficiently large area of the sea-bed to affect the main body of the tidal flow. Higher turbulence levels mean larger turbulent viscosity values, so that the roughness element should act to slow the flow.

The model of section III.2.4 is again applied to a constant depth region of a channel flow. We take depth H as constant and equation III.(10) becomes

$$X = uK - f\upsilon$$
$$\frac{\partial}{\partial y}\left[\left(H + {}^{p}/_{g} \right) \upsilon \right] = 0$$
$$\frac{\partial p}{\partial y} = -K\upsilon - fu \qquad \text{V.(01)}$$

We can use the function h' as a modifier for K as before. However, since h' is no longer water depth the dynamics are very different. The velocities no longer link back through the continuity relationship and we have no horizontal viscosity for a link either. The results should be interpreted with caution.

Now continuity gives υ = constant always, so that u will decrease over a rough area and increase over a smooth area for any relation of K and f. The numerical solutions of fig.V.1 show the associated surface slopes.

It is instructive to relate this equation for flow over an element of roughness (with $K = k / h'$) with that for the flow over a neutral bank (with $K = k$). If we compare at the level of the mass flux we can see, in fig.V.1d, that the cross bank mass flux is very nearly

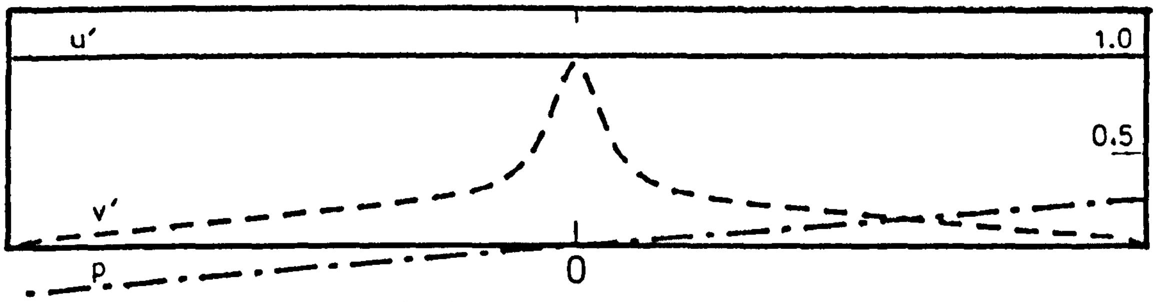

(a) Neutral bank

$u' = u / U$ $\qquad$ $v' = v / V$

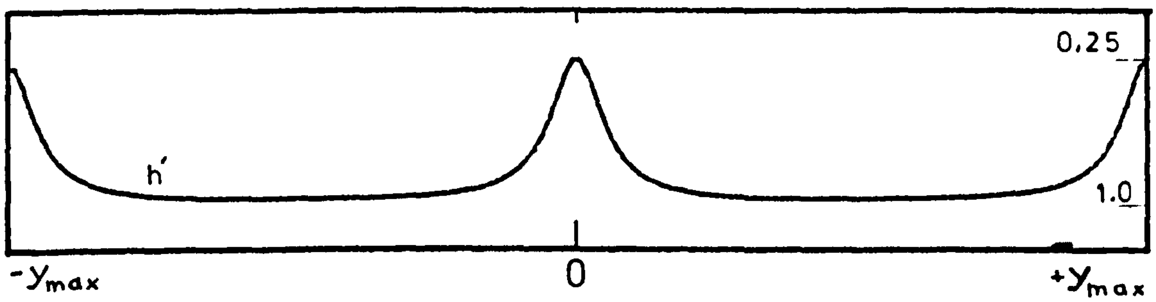

(b) Viscosity variation for constant depth model

$h' = A\zeta_{max} / A\zeta$

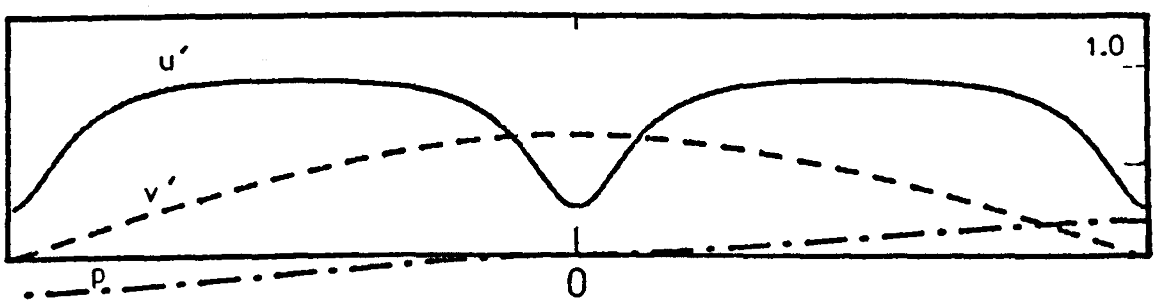

(c) Rough element

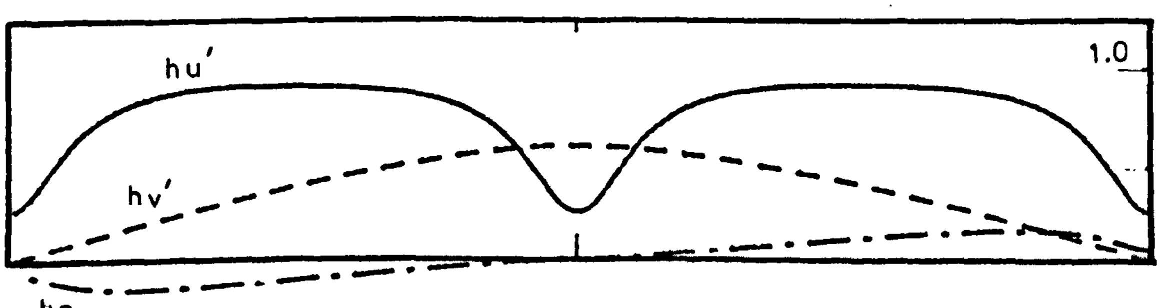

(d) Mass flux — neutral bank and rough element

Fig.V.1 Model, Steady-state - Mass flux comparison constant over the bank region for both models as required by continuity. The along bank mass flux is the same also, being proportional to h' in both cases. However, for the constant depth model the reduced mass flux means a reduced velocity vector so that deposition will occur.

We consider then that, assuming a sufficient supply of sand, a long thin roughness element will accumulate sediment that will modify the flow. First the original roughness will be covered by sand. If this forms a smooth sheet then velocities will increase to scour the rough area. This suggests that the covering sand will not accumulate as a sheet but as a sand wave field such as Cutler Bank, off the east coast. Here the bed between sand waves is swept clear by the cross-bank flow giving a constant depth. The flow may be represented by that for a small rough bank with similar reduced mass flux and velocity to the original rough element.

Once this stage has been reached bank growth will occur in a manner similar to that for a bank that is formed from a core of beach material. The mechanisms for bank growth at this stage may well be those investigated in Huthnance(1982a).

We assume that sand accumulation will cease when the flow approaches that of a neutral bank. At this stage the velocity vector off and on the bank have the same value and any increase of bank size would create conditions for erosion. We can therefore assume that a neutral bank is an equilibrium profile and hence a stable feature.

We postulate that a loose boundary flow with varying roughness sufficient to affect the turbulent viscosity will adjust by erosion and deposition so as to create a uniform mass flux for the water flow. This is not related to the helical flow erosion and deposition of Mclean(1981), since sand ribbons contain only a small mass of sand relative to the depth of the flow.

For small interruptions to the flow such as South Falls a uniform mass flux of water over the bank is possible, but interruptions such as Sandettie and the Goodwins should be able to sustain some permanent reduction to the mass flux and are exceptions to the above theory.

The indications are, from the mechanisms considered, that banks could have formed quite rapidly. However, they give no definite evidence for the time of the commencement of bank building activity.

Some banks may have formed at the initial transgression and be located by old high ground positions. Other banks may have formed at any time around areas of roughness, as discussed above. The bed instability considered in Huthnance(1982a) may be sufficient to initiate bank growth. We do not have evidence that rules out any mechanism discussed, and each mechanism may play its part at some time during the period of bank growth, requiring only a sufficient supply of sand. Notwithstanding this, the most opportune supply of sand may well have occured during the initial transgression.

The model result suggests that a narrow smooth element of less than the surrounding roughness would be swept clear of sediment by slightly increased velocity and remain unmodified by deposition. A sand wave field might accumulate at the edge of a broad smooth region and hence form a bank. The South Falls lies on the eastern edge of the Chalk outcrop and only on its northern end is it on rougher Tertiary Sands.

The destructive effect of wind waves may be countered by some of the mechanisms within the tidal flow that are considered above. We now show that lower frequency wind waves and swell waves may have a constructive effect upon a sandbank that has attained a certain size. In chapter IV we showed that many high frequency waves could be blocked by such a bank. For some intermediate frequencies the wave itself may pass over the bank but most wave energy cannot. We can expect that, in general, a sink for the wave energy will coincide with a source of sand accretion, since the sand entrained by a swell wave off the bank may be deposited at the bank from any direction.

However, we should expect that if the swell waves predominantly arrive from one direction then that side of the bank would increase more. For a stable bank this might give an erroneous impression of a sand transport direction that opposes the swell direction, since transport direction is often inferred from sandwave or bank shape. The cross-section of the South Falls, in fig.I.6, does indicate transport in the westerly direction, towards the prevailing direction for swell waves from the Dover Straits.

V.2 VORTICITY

In the work so far we have assumed that the velocity profile is approximately logarithmic so that, for the purpose of modelling spatial variation, we represent this profile by a bulk value u, v which is used with the equations for a depth-averaged region with 2 dimensions in the horizontal.

The water velocity measurements of fig.III.6 confirm that the flow west of the South Falls bank, when smoothed over a 10min period, does increase with height above the sea-bed to approximate a logarithmic profile. This effect occurs both on the ebb and flood tide with no noticable wake effects on the downstream side of the bank. These measured values show no veering of the current between 1m and 20m above the sea bed. Therefore any deviation from a simple 2-D flow must occur in the upper 20m of the water column, which is affected by waves, or in a layer only a few centimetres thick at the sea bed.

The measured values on top of the bank do indicate some variation of flow direction with depth although the exact nature of this variation is not clear. Study of fig.III.3b suggests that this variation may be a result of problems with the rig.

V.2.1 Friction driven bottom flow

We now consider whether we must directly model secondary vorticity effects in order to fully specify the flow over a bank. We should expect secondary vorticity to be vertically asymmetric and concentrated at the bed, where $\partial u/\partial z$ is a maximum.

What balance of forces could generate the flow that we have measured? That is, a generally 2-D logarithmic profile with, at most, a small spiral effect close to the bed. For river meandering a bottom flow mechanism has been demonstrated (Scorer,1978).

The meander curvature induces a centrifugal force that displaces water to the outer bank until the effect is balanced by the pressure force that is associated with the surface slope. Now the pressure must be uniform with depth, since it is a perturbation from the static pressure.

However, the centrifugal acceleration that it balances varies with depth as

u^2/r ,where r is flow curvature, since

$$u(z) = \frac{u_*}{K} \ln\left(\frac{z}{z_0}\right) \qquad \text{V.(02)}$$

from the mainstream logarithmic profile. As u decreases rapidly to zero close to the bed, the centrifugal acceleration must reduce faster, being proportional to u^2. The excess pressure produces a bottom flow, a very thin layer at the bed with a strong flow across that of the mainstream. This bottom flow scours the outer bend to deposit sediment at the inner bend and enhance the original meander path. The laboratory investigation of a flow of this nature is described in sub-section II.3.1.

We seek an analogous balance between the Coriolis force and some parameter that is constant over water depth. The difference could generate an oceanic and shallow-sea bottom flow that would be an important sediment transport mechanism. The effect must be much weaker than that for river meandering since, not only is it proportional to u rather than u^2, but we have shown that the Coriolis balance is only a second order effect for flow at the South Falls.

However, there is some hope since river meandering is very rapid when considered on geological timescales and the continued existence of linear sand ridges in a strong tidal regime is an aspect of the phenomenon that we seek to explain.

If we consider a new coordinate system x', y' aligned with the mainstream flow V in the x'-direction, since we have deliberately not included a transverse Reynolds stress term, the equations III.(10) become

$$V = \frac{1}{K}\frac{\partial p}{\partial x'} .$$

$$\frac{\partial p}{\partial y'} = -fV \qquad \text{V.(03)}$$

where in the x'-direction the pressure driven flow is balanced by friction, but in the y'-direction the flow is balanced by the Coriolis force. This is the balance we seek and it suggests that, subject to the assumptions we have made such as the rejection of the horizontal Reynolds stress terms, a bottom flow normal to the the mainstream flow does exist.

The Ekman equations for current veering describe a balance of the Coriolis force and the turbulent friction term by ignoring the pressure term (Gill, 1982). Within an ocean or sea with any considerable current the surface slopes would not be negligible.

In general, therefore, we prefer this solution to Ekmans for shallow seas and other regions of strong bottom current. For sea and ocean surface flows $\partial u/\partial z$ will only be large instantaneously within an increasing wind field. For oceanic flows, that are forced by an integrated wind stress, the Ekman solutions apply.

The numerical solutions fig.III.14 show that $\partial p/\partial y$ for channel flow away from the bank top does generate a bottom flow that acts alternately towards each coastline. The sense of this flow is opposite to that of the Coriolis force and so to the left of the mainstream in the Northern hemisphere.

It is of interest that this effect is independent of the choice for the parameterization of friction. Away from the high friction regime of the South Falls the thickness of the bottom flow may increase to approach the form of an inverted Ekman flow.

V.3 HYDRODYNAMIC MODELLING IN TWO-DIMENSIONS

We now consider the reduction of the number of dimensions that relate to a problem. This technique is used extensively for the model equations in chapter III. All fluid motion is of spatial dimension 3, yet most hydrodynamic modelling uses 2-D, or even 1-D models. A thorough justification for this practice seems to be lacking in the basic texts.

V.3.1 Weak and strong dimensions

We suggest here a formal structure within which the use of such modelling can be discussed. The practice suggests that a physical process can be described as n-dimensional if n continuous real parameters are sufficient to describe it. This is discussed in Mandelbrot(1982) where the 'fractal' or fractional dimension of Hausdorff is covered in some detail. Here some fractal measures for turbulence are suggested, but this is essentially a geometry of objects and not a description of processes, although a physical process can be regarded as a four-dimensional object.

We find it useful here to follow the laymans practice and separate time and the spatial dimensions. Thus, hereinafter the term dimension will refer solely to spatial coordinates that measure a space or a physical process. In order to discuss the parameterization of friction we define a fractional dimension for a physical process. This is done to avoid causing confusion by any misuse of the relatively well-defined mathematical concepts of topological dimension and Hausdorff dimension.

Therefore, without reference to previous usage by any other authors, we introduce the concepts of the weak and strong dimensionality of a physical process. By a weak dimension we mean one for which all internal parameter variations are small and/or one for which physical processes may be neglected without large errors. The converse applies to a strong dimension. This must then imply that each dimension is a variable that has some value less than 1.

We do not attempt to quantify this value, but merely assert that a strong dimension is not close to zero and that a weak dimension is not close to one. We may consider, as an example, a spherical wave as being weakly 3-D and strongly 1-D. This suggests that the weak dimensionality of a process describes the Euclidean space that contains it while its strong dimensionality describes an important aspect of the nature of the process itself. We will therefore speak of a process as being only weakly 3-D to imply that it can be modelled using less than the 3 dimensions of the space that it occupies.

V.3.2 Parameterization of friction

When we consider the full 3-D equations of motion, the effects of bottom friction are entrained up into the body of the flow by a vertical turbulent diffusion of momentum. It is assumed for the purposes of modelling linear sand ridge hydronamics, that the flow is strongly 2-D and only weakly 3-D. When we make this assumption, and average over depth, we impose constraints upon the model that must reflect the physical reality.

In order to model the tides in the Irish Sea Taylor(1919) found that a 2-D model needed a friction term that varied with depth. This reflected the physical fact of differing friction between the deep and shallow flows for the region considered. Similarly, Proudman and Doodson(1924) used the same friction term to produce numerical models of the amplitude and phase of the tides in the North Sea as reproduced in fig. I.1b.

It is not certain that this effect will translate to the hydrodynamics of a linear sand ridge. For the Irish Sea and North Sea scales of flow, velocity profiles will differ between deep and shallow regions, since both deep and shallow flows are deeper than the boundary layer. This may not be the case for linear sand ridge flow. Here both deep and shallow water flow may be dominated by boundary layer effects and may be adequately represented by a logarithmic law right up to the surface. In such a case the deep and shallow flows will have a depth-averaged value that is essentially the same, and the friction term that we use for the model should not be depth-dependent.

V.4 TIDAL FRICTION

We now consolidate the description of the tidal flow over a narrow bank and its relation to the flow of a shallow continental shelf sea. We also consider the effect of the sand banks upon the flow, the other side of the tidal friction problem.

The choice in section III.2.4 of a neutral, rather than a rough, bank implies that, within the South Falls region, friction does not change with change of depth from 40m to 10m. For this condition, both mechanisms discussed in Huthnance(1973) will not be significant, and the flood/ebb imbalance (Smith,1969) (Caston and Stride,1970) may not be present. The unsuccessful 1981 current meter deployment was intended to answer this question.

How shallow are the regions that provide the friction to dissipate tidal energy? Our model implies that for a neutral bank, with $K = k$ the South Falls does not contribute to friction in the Southern Bight. It is as if the flow adapts to the bank presence by modifying the bank so that friction is minimised.

We cannot presume that shallow regions do not contribute to tidal friction. The above argument only applies to linear sand ridges, not large banks such as the Sandettie that are of sufficient breadth to ensure that the reduced mass flux across the bank cannot be compensated for by an increased velocity. There must be cross bank friction for a broad bank, although it may not contribute greatly to tidal friction if the main flow is elsewhere.

The average friction for the Irish Sea has been calculated (Taylor,1921) using the formula

$$F = \cdot 00013 \left(1 + {}^{1}/_{h}\right)^2 \rho u^2 \qquad \text{V.(04)}$$

This value varies very little for values of $H = 40$m and $H = 10$m which is in accordance with the notion that friction on and off the bank should have the same value. While it may be that other linear sand ridges such as the Norfolk banks do not contribute to friction we have not shown this. If the Norfolk banks are rough banks, in the sense that along bank velocities are lower on the bank than off the bank, then they will contribute to the tidal friction.

The concept that friction does not change greatly with change of depth in shallow sea regions where the friction is high may help to explain the success of many of the large-scale numerical models of shallow seas. The exact parameterization of friction through the Reynold stresses and accurate representation of bottom roughness elements is not possible because of the limited spatial resolution. In spite of this the models (Proudman and Doodson, 1924) give values for tidal heights and tidal streams that match well with measured values. This concept cannot be applied to very shallow regions of near critical flow, such as the Goodwin Sands, where numerical models are known to give a poor representation of reality.

V.5 SUMMARY

The first chapter contains introductory information to define the physical region and the problem. It includes a review of work by previous authors on the flow over tidal current ridges.

Chapter II contains the preliminary work which included field trips for the assessment of the viability of available oceanographic measuring equipment. The velocity profile section gives discussion of rough and smooth turbulent flows, the laminar sublayer, parting lineations and Magnus force and also considers sediment settling velocity and entrainment. A computational sub-section includes a low R_e model that uses a vorticity-stream function solution for laminar channel flow. A turbulent flow computer model was implemented that used a simplified Nikuradse curve to generate smooth and rough flow solutions with a linear sublayer.

A sea-bottom rig was designed and constructed to measure water velocity, sediment concentration, salinity and temperature. In fact, salinity and temperature did not vary significantly, and water velocity was the only parameter that could be measured satisfactorily. Field work with this new equipment demonstrated successful measurement of water velocity vectors at two sites within the Thames Estuary.

Next was an introduction to the powerful effects of secondary vorticity. Laboratory work was undertaken with Professor Scorer at Imperial College on fixed bed flow visualization and loose bed adaptation. Clear evidence was found for the existence of the centrifugally driven bottom boundary flow.

Some water velocity measurement data was obtained from HRS Wallingford. Analysis of the raw data was inconclusive. Some ready analysed data was plotted as a mainstream logarithmic profile and plots of the cross-stream flow were made. These seemed to show a secondary vorticity effect but in fact this was a result of the aliasing of turbulent fluctuations that arose from the method of profiling with a single current meter.

Chapter III contains the major investigation that was undertaken into the hydrodynamics of the South falls bank.

Tidal flow measurement

The field work involved the deployment of a current meter rig designed with help and advice from RVS Barry. This used Aanderaa current meters supported on a wire rope between a bottom weight and a sub-surface buoyancy buoy. This type of rig was used for all future field work. A sand bank top free from sand waves was identified after a side-scan survey of the majority of the Southern Bight sand ridges. No data resulted since the rig was not recovered.

A rig re-design gave on bank, flank and off bank rigs to be deployed in a straight line across the bank. Field work results were exceptional with a data return of 100%. This data was processed to give 24hour length plots of along-bank and cross-bank velocity vectors. As expected the cross-bank velocity was dominated by continuity. Unexpectedly, the along-bank velocity at each height showed little variation on and off the bank. An attempt was made in 1981 to collect data to confirm this but the data return was poor.

Tidal flow modelling

The first simple theory assumed for flow over a linear sand ridge used cross-bank continuity and the logarithmic profile derived from constant depth channel flow. Fluid accelerations and horizontal turbulent viscosity effects were ignored.

For the 1980 theoretical work a full dynamical model of an infinite length sand bank was implemented. This finite width model was similar to the infinite width model of Huthnance(1973). The vertical viscosity was approximated by a linear friction term, but the non-linear advective and horizontal viscosity terms were ignored. A numerical model with sinusoidal forcing in time gave unacceptably high values for cross-bank surface slope when run until repeatable values were achieved. This is because the bank width and length are not large by comparison with the tidal wavelength.

For the third year some synthesis of the 1980 measured values and the dynamic model was sought. Steady-state equations were formed from a consideration of the different timescales for the tidal and spatial variations of velocity. If we take the measured velocity values as given, then the only free parameter for the equation is the value of K for linearized friction.

Two possible solutions were identified. The solution that seemed most likely was that the bank retarded the flow. This gave a balance between Coriolis and friction and from the Ekman solutions we should expect that this would cause a veering of the velocity vector within the water column. The measured off-bank flow refutes this, there is no measurable veering of the flow. We must choose the solution for a neutral bank that is effectively frictionless and does not retard the bank flow. This requires a balance of surface slope amd friction so that this frictionless bank must exist within a region of high friction.

Chapter IV contains an investigation of the wave field variation over South Falls bank. A Synthetic Aperture Radar image from SEASAT shows a very strong variation in brightness over the South Falls. The measured velocity values, from chapter III, were used to model the surface velocity field over the bank for the time of the satellite over-pass. The effects of wave blocking due to critical flow and of wave modulation by radiation stress were both considered. An approximate hindcast for the region showed that the variable roughness due to wave-current interaction was directly proportional to this brightness.

In chapter V the effects of waves and tide upon the bank were considered in the light of the model results that indicated that the bank had a neutral roughness.

Section V.1 gave consideration to the extrapolation of the present day flow regime to investigate the tide and wave regimes of previous time. This might help to explain the origin and continued existence of linear sand ridges.

From the work in chapter III it was argued that a sand ridge could form around any abrupt change of roughness of the sea bed. The only pre-requisite is a sufficient supply of sand for the bank to grow. Neutral banks like South Falls are no longer growing and are stable features of the flow.

We have no evidence to distinguish between the different mechanisms that exist within a tidal flow for bank genesis and growth. Indeed, a bank may even rely upon the bank building properties of swell waves for its final stability.

In section V.2 the laboratory work on secondary flow was assessed. It lead directly to the idea of the friction driven bottom flow from a balance of pressure and Coriolis force.

Some three-dimensional aspects of bank and channel flow were considered for an analogous mechanism to the river meander bottom flow from a balance of Coriolis force and cross-channel surface slope. For a rough bank this Coriolis driven secondary vorticity would be moderately strong.

However, for a neutral bank, the preferred solution above, Coriolis is a second order effect, so that a friction driven bottom boundary flow will be weak and act only within a thin layer. Since it acts at the loose boundary we can assume that the effect will still be significant.

In section V.3 we considered the effect of the reduction of model dimensions upon the parameterization of friction.

In section V.4 the implications of the assumption of a frictionless neutral bank were considered. This suggests that linear sand ridges may not contribute to the dissipation of tidal energy in shallow seas.

V.6 CONCLUSIONS AND FUTURE WORK

The construction and operation of the bottom mounted rig for velocity measurement was very successful and lead into the main thesis topic of flow over a linear sand ridge.

The 1980 data set on velocity over the South Falls is the keystone for the whole thesis. The experience gained from previous fieldwork gave me confidence in the quality of the data obtained. While this confidence means that I have been able to use the information for quite far—reaching assumptions about the dynamics of bank flow, these are only speculation without confirming measurement. It must be borne in mind that that the data collection was only possible because an anomalous bank top region was found that was free from sandwaves. An assumption has been made that the character of the flow is not different within this region.

We should not expect the turbulence characteristics to be the same for this smooth bank top region and if the turbulence levels are analysed they should not be used to describe the frictional characteristics of the bank top in general. A consideration of the SAR image of fig.IV.1,2, suggests that the turbulent wake from a wreck could provide an explanation for the existence of this smooth region.

It has not been shown that the rejection of all non-linear terms from the dynamic model is valid. Even so this has led to a greater insight into the basic mechanisms of bank flow. The most useful contribution has been the synthesis of the dynamic model results and the measured velocity values.

Work on this numerical model was commenced at a late stage of the investigations presented here and has not yet been brought to a successful conclusion. The most promising results have been obtained by using equations that have been normalised by k. This ensures that individual terms are close to 1 and thus avoids numerical instabilities. It appears that the relation of the timestep to the value of k must be constrained for successful operation.

Work should continue on the numerical model, but satisfactory results have not been obtained with the present form. There were interesting and adventurous aspects to this model. One was the semi-implicit centered difference scheme which allows naturally implemented diffusive terms by a Dufort-Frankel form of differencing (Venn,1977). However, since we have avoided diffusive terms, meaningful results might be rapidly achieved by the use of a simple explicit numerical scheme.

Another good aspect of the model was the linear form with no horizontal viscosity, and this should be retained. For future work the model should include a $v \partial v / \partial y$ term.

The work with the SAR image gave a clear picture of wave variation due to the velocity field over a bank. The sediment transport implications of such a wave field need more study, but swell wave blocking may have a bank building effect.

The analysis of satellite images may become an important source of oceanographic information, but although new techniques may show promise we must be aware of the limitations. The ground based HF ground-wave radar systems use signal-processing techniques to obtain accurate quantitative measurements. However, here the space based micro-wave radar has been used in an imaging mode that is essentially qualitative. The extraction of quantitative information from such an image is a subject for further research, and it may be that the radar altimeter will prove to be of greater scientific use than SAR.

The friction-driven bottom flow was first investigated as a potential bank-building mechanism. In fact, the curves for cross-bank surface slope III.14 clearly show that this $\partial p / \partial y$ generated mechanism operates everywhere else within the channel flow, but that it is not clear how it operates over the bank. The $\partial p / \partial y = 0$ lines each side of the bank should suppress transport.

This still gives a method for sand accumulation at the bank edges but the actual mechanisms over the bank need to be modelled in more detail.

Any such modelling must include the vertical dimension, and this may best be achieved by the rejection of the u, v, p modelling technique. The solution of the vorticity and stream function equations, the method used in section II.2.2, may be the best approach to take for future work.

We have not managed to provide evidence that would help to distinguish between different theories for bank genesis and stability. The helical flow of Off(1963) and McLean(1981) may have had important effects on some scales at certain times. The well-confirmed hydrodynamic flow of Huthnance(1973), and the effect upon the tidal flow of the differing roughness values of large sea-bed patches, that is argued above, may each play some part in the growth of sand ridges. The destructive effects of wind waves may even be offset by sand deposition that is a result of swell waves.

—o—

APPENDIX A

EQUIPMENT USED

The practical work involved laboratory studies, field work in the Thames Estuary and Southern Bight and the processing and analysis of a synthetic aperture radar image from the Seasat satellite.

A.1 Flow tank

Laboratory studies were conducted using the Armfield flow tank in the Theoretical Mechanics laboratory of Imperial College. This can be used with a white or dark plastic bottom layer or with a fine sand mobile bed. Sand is trapped by a downstream stilling tank and the recirculated water is pumped to an upstream stilling tank. Here the pump-induced turbulence dissipates as the fluid rises to the upstream free-surface level of the flume.

Passive tracers can be used for a direct flow measurement. The pump speed is related to the water mass flux and this can also be used as a measure of relative water velocity. There is a problem associated with the minimum flow required for the pump lubrication so that laminar flow conditions cannot be achieved.

A.2 Water velocity measurement

Much of the field work has involved the measurement of water velocity. Any such values should be treated with caution, since water velocity meters of different type often give readings that are not compatible.

Any sampling equipment acts as a filter and the recorded data values are subject to the space-time resolution threshold for the instrument which is the grid-scale below which we cannot measure. The measured parameter that is achieved will be an averaged value, related to the size and response time of the sensor. Now for any model we construct from the readings the grid-scale is a function of the sampling period Δt, which is the time between consecutive readings. As an example, $u\Delta t$, the product of the velocity and sampling period gives a lower bound for the length scale of the eddies that we can measure or model.

A.2.1 Braystoke

This is a direct reading current meter with a digital wire link to the on-board recorder. The speed sensor is a lightweight plastic impellor kept pointed into the flow by a thin stainless steel vane. Response times for both speed and direction changes are good.

An instantaneous reading is taken for direction but the velocity is measured as a count of impellor revolutions and is usually integrated over a sample time of 30s. In this case the minimum sampling period is then 60s. The count can be taken as a reading in metres per second. The counters of the recorder need to be manually zeroed before each velocity and direction reading. No digital data logger was available for use with this equipment.

A.2.2 Aanderaa RCM4

This recording current meter was fitted with pressure transducer suitable for shallow water deployment. The temperature, salinity, pressure and current direction are instantaneous readings while current speed is integrated over a sample time equal to the sampling period. The current speed register can be scaled to avoid overflow. The readings are stored on magnetic tape that must be translated for the data processing. Tape size and battery life both limit the instrument to a maximum of 10,000 samples. Thus the total time is 2yr for deployment with the maximum sampling period Δt of 2hr, and with the minimum sampling period of 30s the total time is 3.4days.

The current speed sensor is a lightweight Savonius rotor that records speed from any direction. Speed response time is good but the sensor can over-read when the speed values oscillate at a frequency greater than $1/\Delta t$. The current direction sensor is a 1m wide by 37cm deep weighted plastic vane. The rotational inertia is large so that directional response is slow.

A.2.3 ECM

The electromagnetic current meter works by recording the change of magnetic flux resulting from the flow past the 10cm diameter, lozenge-shaped sensor. It is suitable for turbulence measurements since the sample rate > 1Hz. These instruments require careful calibration and those used for the data analysed in section II.3 suffered from drift.

A.3 Radar

There are many analogies that can be drawn between the familiar sonar remote sensing equipment that uses acoustic waves and the equivalent electro-magnetic instrumentation. However, the difference is that whereas, with the right waveguide, low frequency sound can travel kilometres without significant attenuation, radio waves in water attenuate within centimetres. This limits radio instruments to measurements of the sea surface by propagation through the atmosphere.

At high angles of the incident ray, the return from radar signals may be by specular reflection but at grazing angles the backscattered return is by the coherent addition from many wave crests of a sinusoid with wavelength half that of the radio wave. This is referred to as Bragg resonant backscatter by analogy with the diffraction phenomenon.

Microwave radar range is limited by the line of sight propagation mode of the GHz frequencies used. Range can be improved by the use of a high platform. Side looking airborne radar (SLAR) can record sea surface images. The operating principles are very similar to those of a sidescan sonar (Dyer, 1979).

Synthetic aperture radar (SAR) must be deployed from a moving instrument platform such as an automobile, train, aircraft or spacecraft. Unlike the SLAR and sidescan sonar SAR has a small real aperature antenna that gives a broad azimuthal beamwidth. Thus any target remains within the beam for several pulse returns which are all analysed. Since each of these pulses was emitted from a different vehicle position, when they are analysed together, they synthesise a long effective antenna length and give a high resolution in azimuth. Thus this resolution is related only to real antenna size.

The synthetic aperture system does have its faults. The main difficulty encountered is that of moving targets. Azimuthal position of the target relative to the vehicle is calculated from the Doppler frequency of its speed relative to the vehicle. This calculation assumes that the target is stationary. A moving target such as a train or ship will be displaced relative to its surroundings in the SAR image. To a smaller degree this will affect surface waves. The Seasat satellite was operational for a few weeks in 1978. It contained an altimeter and scatterometer that both produced valuable oceanographic data. It also contained the SAR that was used to produce the Southern Bight image of fig.IV.1.

APPENDIX B

Venn, J.F. and D'Olier, B., 1983. Preliminary observations for a model of sand bank dynamics, In: Sundermann, J. and Lenz, W. (Editors), NORTH SEA DYNAMICS, springer-verlag: 472-485.

Preliminary Observations for a Model of Sand Bank Dynamics

J. F. Venn and B. D'Oliver[1]

Introduction

We report here on some field observations of bedforms, of the internal structure of sandbanks and on some current meter readings at a narrow linear sand ridge, the South Falls bank. Some preliminary studies of the hydrodynamic velocity field are also presented. The modelling suggests that the extreme narrowness of the bank is an important factor determining the results obtained from the field studies. These results cannot therefore be extrapolated to broader banks such as the Sandettie. We suggest that local sea surface slope could be one of the factors affecting the genesis and maintainance of the South Falls bank.

Oscillatory tidal flow over parallel topography was considered by Huthnance (1973) to determine the time-mean currents. We consider the time-varying flow within the tidal cycle for similar topographies and apply the results to the South Falls Bank (Fig. 1).

The sediment transport implications for this flow show that "bank-building" mechanisms may exist in the flow immediately above the sea bed. We suggest that a friction-driven bottom boundary flow fulfils this requirement. The resulting picture agrees with that suggested by an analysis of bedforms.

Modelling the Water Circulation

We consider a free surface flow in a rotating channel, a region bounded by coastlines at $y = \pm Y$ max. Variations in x are slow compared to the local variation such that all parameters may be considered invarient in x, except P which is linear in x. The free surface is $\zeta = \zeta(y)$ above the mean sea level $z = 0$ with the sea bed $h = h(y)$ below.

1 Polytechnic, City of London, London, Great Britain

North Sea Dynamics, ed. by Sündermann/Lenz

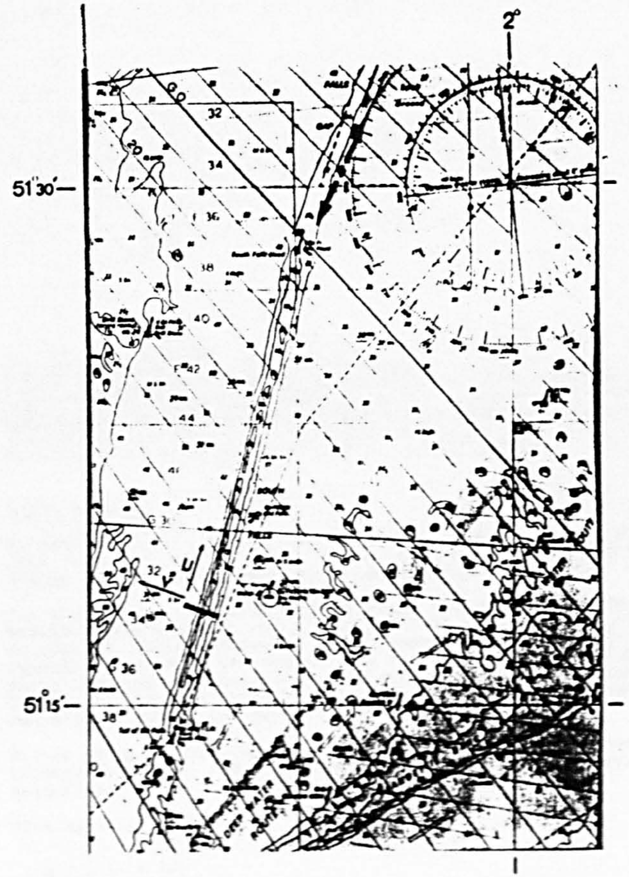

a)

Fig. 1. South Falls Bank.
(a) Position of velocity measurements and bank cross-section shown in Fig. 2b

(Fig. 1b see page 474)

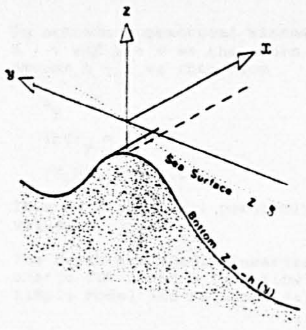

<u>Fig. 1b.</u> Definition of axes and topography

The depth-averaged equations of motion and continuity reduce to:

$$u_t + vu_y - fv = -\frac{1}{\rho} P_x - Ku + Au_{yy}$$

$$v_t + vv_y + fu = -\frac{1}{\rho} P_y - Kv + Av_{yy}$$

$$\zeta_t + [(h + \zeta)v]_y = 0 \qquad (1)$$

where u and v are velocities in the directions x and y and subscripted variables indicate the partial derivative with respect to the subscript.

Here $K = K(y)$ is a linearized eddy viscosity term also known as the Guldberg-Mohn coefficient of virtual internal friction. This assumption is rarely used now, particularly where friction is important since it is known to be inaccurate.

The flow we are modelling is a strong tidal stream with $u > 1\ ms^{-1}$ maximum stream value in charted depths of $-7\frac{1}{2}m < z < -37\frac{1}{2}m$ with tidal range 5 m. Friction will therefore be very important and our choice of a value for K and its spatial variation will dominate the solution. We have little to guide us in this choice except for the oceanic K values of $10^{-6}\ s^{-1}$ used in Neumann and Pierson (1966) for flows very obviously not friction-dominated.

We will assume $K \sim f$. Thus for $f \sim 10^{-4}\ s^{-1}$ we take a general value $K = 10^{-2}\ s^{-1}$ for a shallow sea. We will ignore the *underlined* non-linear terms in Eq. (1) so that we retain the ability to superpose independent solutions. The advection terms vu_y and vv_y were shown by Huthnance (1973) to generate an important tidal residual flow and the horizontal viscosity terms Au_{yy} and Av_{yy} may also be important. However, these might be included when the full model is considered.

We redefine pressure as $(1/\rho)P(x,y) = p(y) - Yy - Xy$. This is the pressure anomaly from the hydrostatic balance where water height $\zeta = p/g$ metres.

We utilize the X and Y imposed slope as a sinusoidal variation in time to generate a u, v field for the channel. The South Falls is a type A bank as defined by Kenyon et al. (1981), that is, the axial offset α is anticlockwise with respect to the regional direction of peak tidal flow. We can therefore take $Y = 0$ since v can be generated to the correct order of magnitude from X alone.

Subject to these conditions Eqs. (1) become

$$u_t - fv = X - Ku$$

$$v_t + fu = -p_y - kv$$

$$\zeta_t + [(h + \zeta)v]_y = 0 \quad . \qquad (2)$$

Numerical modelling of the equations in this form was not rewarding. The shallow regions go out of phase with the deeper regions by the end of one tidal cycle. A numerical model which may have to include some of the non-linear terms will be the subject of a further paper. However, some simple modelling can be achieved if we consider a separation of timescales.

<u>Depth Variation</u>

We consider now the effect upon a channel flow of a long ridge with crest at $y = 0$ as shown in Fig. 1b. This parallel topography is similar to that considered by Huthnance (1973).

For the spatial variation of K we might expect that for the smaller depth scale on top of the bank the eddy viscosity would be reduced. Indeed Hüthnance (1973) used $K = k/h$ with k constant. However, apart from the region used for the current meter observations the bank top is covered with sandwaves. This should locally increase the turbulence, so we will assume that these two effects cancel and take $K(y) = K$ constant.

For an angle $\alpha > 10^{\circ}$, spatial variation will be on a faster timescale than the tidal variation which can thus be considered invarient.

Thus Eqs. (2) become

$$u = \frac{1}{K}(x + fv)$$

$$[(h + \zeta)v]_y = 0$$

$$p_y = -Kv - fu \qquad (3)$$

for the local variation of the velocity field over a narrow sand ridge.

To achieve a practical kinematic model we consider that since $K > f$ and $u > v$ we therefore have $Ku \gg fv$. If we further can assume $h >$; we then have

$$u_y = 0$$

$$(hv)_y = 0$$

$$(P_y h)_y = 0 \quad . \tag{4}$$

This is a practical predictive tool given the external flow value.

The depth-averaged, linearized flow described with no spatial change for u and a '2-D flow' change for v is a surprisingly simple model and requires validation.

South Falls Bank Field Studies

We were fortunate to discover on the South Falls bank a region not covered with sand-waves, and thus suitable for fieldwork connected with an investigation into bank dynamics.

Equations (3) and (4) are utilized for a prediction of the local flow variation for this region (Fig. 1).

Flow prediction:

given that off the bank in 40 m water depth

$u = 1$ m/s and $\alpha = 17^\circ$ i.e. $v = 0.25$ m/s ,

then on the bank in 10 M water depth

$u = 1$ m/s and $v = 1$ m/s i.e. $\alpha = 45^\circ$,

i.e. the velocity vector on the bank is greater than the tidal stream vector off the bank, and its angle to the bank increases by 28°.

Water flow measurements obtained during 1980 and 1981 are used to test the accuracy of these predicted velocity vectors (Fig. 2a).

Current Meter Data Analysis

Aanderaa current meters were deployed on South Falls bank (Fig. 1). The meter positions relative to the bank are marked on an echo sounder trace of the bank cross-section (Fig. 2b). Velocities off the bank are compared with the velocity on the flank and on the bank crest, at the same height above the bottom. The assumption is that the vertical variation in velocity is logarithmic. The velocities plotted in Figs. 3 and 4 have been averaged over 4½ min (i.e. 9½ min sampling intervals).

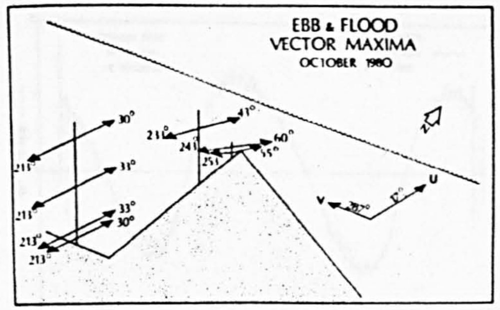

Fig. 2a. Summary of tidal current vector information. Measured angles quoted are from true north. Length of arrow equals approximate amplitude

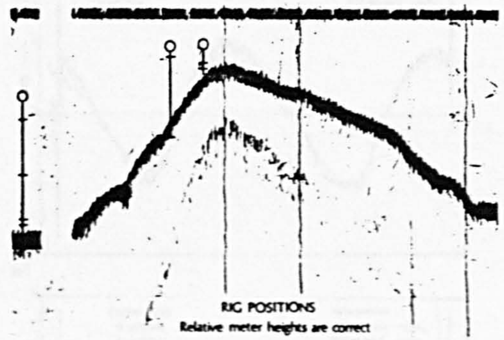

Fig. 2b. Tidal current measuring positions on the bank cross-section. Rig positions to the west of bank crest

The v values are plotted as Fig. 3.

In Fig. 3a, the variation between the 40 m off bank flow and the 20 M flank flow is compared at 10 m above the bottom. The factor of 2 between the measured flows is predicted by the relation Hv = constant.

In Fig. 3b, the plot of v variation off and on the bank at 2 m, we expect a factor of 4 from the 40 m/10 m depth ratio. The measured factor is closer to 3.

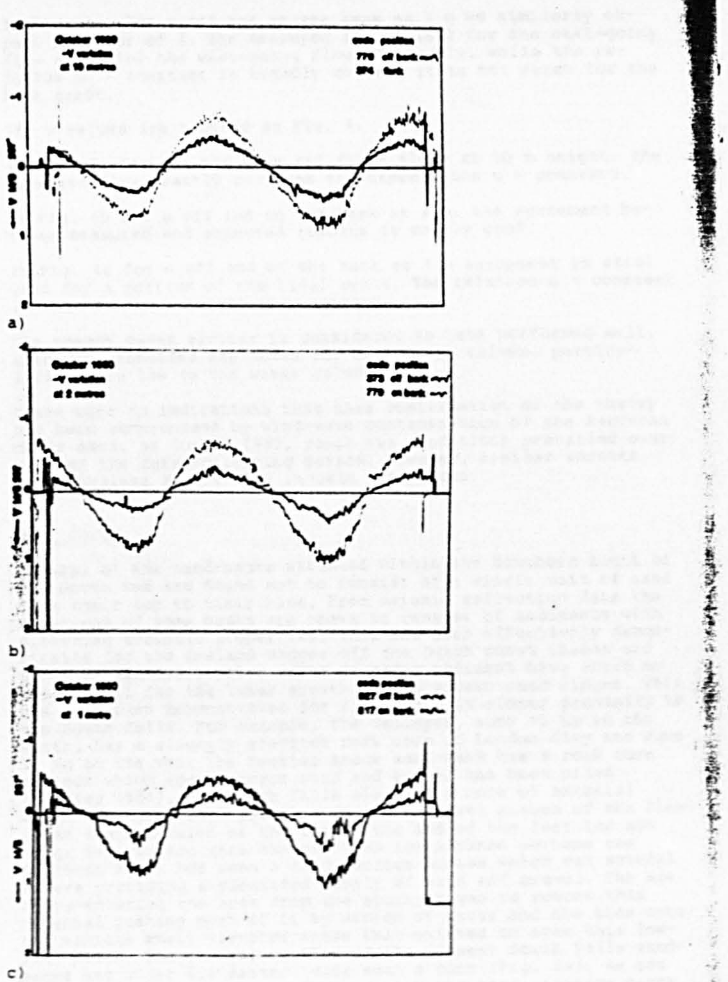

Fig. 3a-c. Velocity (v), normal to the bank at measured heights above the sea bed of a) 10 m, b) 2 m, c) 1 m

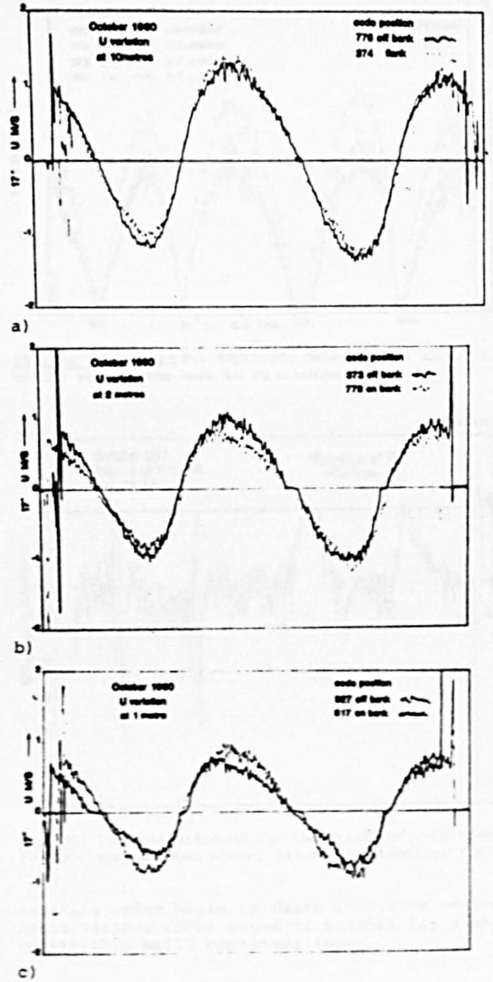

Fig. 4a-c. Velocity (u) parallel to the bank at measured heights above the sea bed of a) 10 m, b) 3 m, c) 1 m

In Fig. 3c, for v off and on the bank at 1 m we similarly expect a factor of 4. The measured factor is 2 for the east-going flow and 3 for the west-going flow. Obviously, while the relation Hv = constant is broadly correct it is not exact for the bank crest.

The u values are plotted as Fig. 4.

In Fig. 4a for the off bank and flank flows at 10 m height, the measured flow exactly confirms the expectation u = constant.

In Fig. 4b for u off and on the bank at 2 m, the agreement between measured and expected results is mostly good.

In Fig. 4c for u off and on the bank at 1 m agreement is still good for a portion of the tidal cycle. The relation u = constant is shown to be substantially correct.

The theory given earlier is considered to have performed well, although anomalies are noted for bank crest values, particularly those low in the water column.

There were no indications that this confirmation of the theory had been compromised by wind-wave contamination of the Aanderaa meter data, as during 1980, rough sea conditions prevailed over much of the data collecting period. However, similar results were obtained during 1981 in calm conditions.

Bank Cores

Several of the sand-banks situated within the Southern Bight of the North Sea are found not to consist of a single unit of sand from their top to their base. From seismic reflection data the interiors of some banks are shown to consist of sediments with differing acoustic properties. This has been effectively demonstrated for the Zeeland Ridges off the Dutch coast (Laban and Schuttenhelm 1981) where cores of older sediment have acted as the nucleii for the later growth of the modern sand ridges. This has also been demonstrated for sand-banks in closer proximity to the South Falls. For example, the Galloper, some 15 km to the north, has a slightly elevated rock core of London Clay and some 15 km to the west the Kentish Knock sand-bank has a rock core against which some coarser sand and gravel has been piled (D'Olier 1981). The South Falls also has a core of material which was swept into position in the earliest stages of the Flandrian transgression of the sea at the end of the last ice age (Fig. 5a). During this and previous ice advance perhaps the Southern Bight had been a land surface across which can several rivers providing a plentiful supply of sand and gravel. The sea, on re-entering the area from the south, began to rework this material pushing much of it by action of waves and the tide onto the various small elevated areas that existed on even this lowland plain. The central section of the present South Falls sandbanks has under its eastern side such a core (Fig. 5a). As sea level rose connection was effected with the more northern parts of the North Sea basin and a strong tidal system much like that

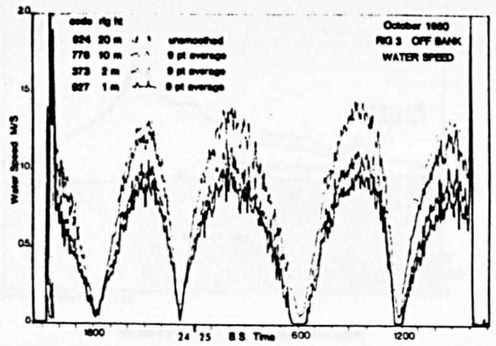

Fig. 5a. Tidal current amplitude data for the off-bank position. This is to the west of the bank in 40 m water depth

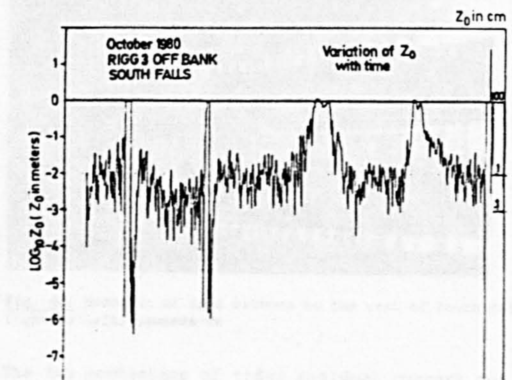

Fig. 5b. Time variation of z_0, the height of zero speed. This is calculated from the speeds shown above, (a), and is undefined for low speed levels

existing today began to cause extensive regional sand transport. These various cores acted as nucleii for a phase of sand-bank growth that still continues today.

Bedform Analysis

The sand ribbons shown in Fig. 5b are situated on the upstream side of the sand-bank in respect to the regional direction of peak tidal flow. They are aligned parallel to the tidal streams and as such should curve in increasingly towards the crestline of the bank as they approach it. This is as predicted and can be seen quite clearly on this sonogram (Fig. 5b).

Sediment Transport

The reduction of water speed with decreasing height above the bed is well demonstrated by the plot of readings for the off bank rig (Fig. 6a). Inspection of the plots indicates that the consistently higher water speeds are from the meters further from the seabed. It is often assumed that this increase of velocity with height increase is logarithmic.

Logarithmic Profile

To check the validity of the assumption a regression of speed on ln z was performed for all of the 4 -min averaged speed values (Fig. 6b). The height at which the speed profile cuts the zero speed line was given by $0.1 < z_0 < 1.0$ cm. This allows the calculation of the shear velocity U_* and shear stress τ. Using the Shields relation it is found that this stress is sufficient to entrain sand grains up to 2 mm diameter for >60% of the tidal cycle.

Bank Mobility

The measured on-bank flow exceeds the off-bank flow and if logarithmic should entrain sand grains up to 2 mm diam. Paradoxically, the bank material is fine sand 0.2 mm diameter. If the on-bank flow has the same excess tractive force as that measured at the off-bank position then sediment could be transported 10 km from the bank on each tide. Horizontal diffusion would spread this material, rapidly destroying the bank unless there was some strong bank-building mechanism not present in our simple model. Furthermore, the mechanism must act equally for each tidal direction or the bank would change position as well as shape whereas we believe that the bank has been in existence since an earlier phase of the Flandrian transgression.

We have confirmed a locally increased roughness on the bank top everywhere except the current meter rig position. We have assumed that this counters the turbulence damping effect of reduced depth such that eddy viscosity does not vary over the bank. The effect that this could have on local sediment critical shear stress values is not clear.

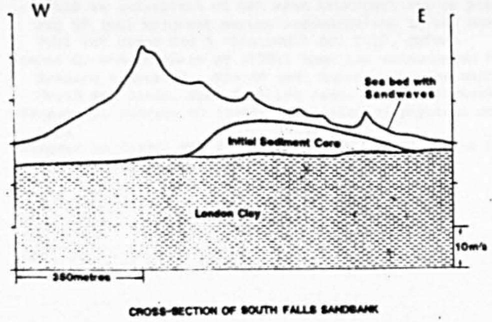

Fig. 6a. Cross-section of South Falls sand-bank showing initial core

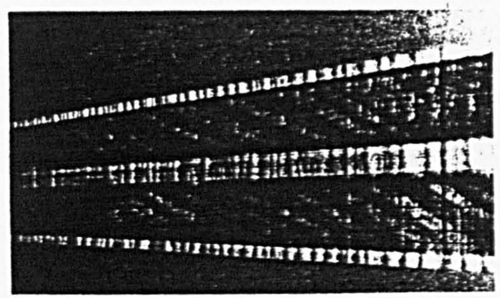

Fig. 6b. Sonogram of sand ribbons to the east of South Falls. Ships track, right to left, towards SW

The two mechanisms of tidal residual current due to Huthnance (1973) have been proposed as a possible bank building mechanism.

Spiral currents were suggested by Houbolt (1968), generated by a difference in on- and off-bank surface velocity. We have not investigated the upper 20 m of the off-bank flow and cannot therefore rule out this effect. However the fieldwork suggests that any difference is, at the very least, not large on the South Falls bank. The concept of a secondary flow might still be useful if we could consider some intensification of the bottom boundary flow where the bed-load transportation occurs.

Results

The lack of spatial variation in the measured water velocity along a narrow bank does suggest that the superposition of separate solutions may yield a good model for the velocity field.

Although the kinematic Eqs. (4) quite successfully modelled the measured velocity field, we must interpret this with caution. The model rejects much of the dynamics in order to focus on a particular aspect - the bank-related sea surface slope. The rejected terms will have an effect and may dominate for some bank configurations. We must definitely restrict the use of this model to very narrow banks.

It has to be borne in mind in considering the fieldwork that the RCM4 Savonius rotor can be contaminated by wave action. In addition the current metering position was chosen since it was the only part of any bank of those in the Southern Bight that we investigated that had no sand-waves. While this did make it possible to measure bank flow velocities with no fear of contamination from local sand wave effects, it is an anomalous region.

Future Work

The trapped wave associated with a narrow sand-bank described by $(P_y h)_y = 0$ is to be further investigated. We intend to explore the possibility that this effect could be a factor ensuring the stability of linear sand ridges and also a possible mechanism for bank genesis through flow over a roughness element or bank core.

A weak coupling between some sand-waves and surface waves has been suggested by Hammond and Heathershaw (1981). This coupling effect between surface waves and sea bed features, whether sand-waves or sand-banks is given support by a Synthetic Aperture Radar Scan of the Dover Straits region from Seasat (Kenyon 1981).

References

D'Olier B (1981) Sedimentary events during Flandrian sea-level rise in the south-west corner of the North Sea. In: Nio SD (ed) Holocene marine sedimentation in the North Sea Basin. Spec Publ Int Assoc Sed 5. Blackwell Sci Pub, Oxford

Hammond FDC, Heathershaw AD (1981) A wave theory for sand-waves in shelf-seas. Nature 293:208-210

Houbolt JJHC (1968) Recent sediments in the southern bight of the North Sea. Geol Mijnbouw 47 (9):245-273

Huthnance JM (1973) Tidal current asymmetrics over the Norfolk sand-banks. Estuarine Coast Mar Sci 1:89-99

Kenyon NH, Belderson RH, Stride AH, Johnson MA (1981) Offshore tidal sand-banks as indicators of net sand transport and as potential deposits. In: Nio SD (ed) Holocene marine sedimentation in the North Sea Basin. Spec Publ Int Assoc Sed 5. Blackwell Sci Publ, Oxford

Laban C, Schuttenhelm RT (1981) Some new evidence on the origin of the Zeeland Ridges. In: Nio SD (ed) Holocene marine sedimentation in the North Sea Basin. Spec Publ Int Assoc Sed 5. Blackwell Sci Publ, Oxford

Neumann G, Pierson WJ (1966) Principles of physical oceanography. Prentice-Hall

Pingree RD (1978) The formation of the Shambles Bank by tidal stirring of the seas. J Mar Biol Assoc UK 58:211-226

REFERENCES

Within this list the author and journal are capitalised, books are in upper-case, with parenthesised original publication date where this is applicable and with the name of the publisher not capitalised.

Admiralty tidal stream atlas,
NP 233 Dover Strait,
NP 249 Thames Estuary,
NP 251 North Sea, Southern portion.

Admiralty tide tables, NP 200,
Vol-1, European Waters – 1978,1980.

Allen, J.R.L.: CURRENT RIPPLES,
north-holland,1968.

Allen, T.D., 1983. A review of Seasat.
In: T.D. Allen (Editor),
SATELLITE MICROWAVE REMOTE SENSING,
ellis horwood : 15-44.

Alpers, W.R. and Hennings, I., A theory of the imaging mechanism of underwater bottom topography by real and synthetic aperture radar, (in press).

Alpers, W.R. and Rufenach, C.L., 1979.
The effect of orbital motions on synthetic-aperture radar imagery of ocean waves,
IEEE Trans. Ant. Prop., AP-27: 685-690.

Alpers, W.R., Ross, D.B. and Rufenach, C.L., 1981.
On the detectability of ocean surface waves by real and synthetic aperture radar,
J. Geophys. Res. 86, C7: 6481-6498.

Bagnold, R.A., THE PHYSICS OF BLOWN SAND AND DESERT DUNES,
methuen and co, 1941.

Bagnold, R.A., 1947. Sand movements by waves: some small scale experiments with sand of very low density,
J. Inst. Civil Engrs., 27, 447-469.

Batchelor, G.K., AN INTRODUCTION TO FLUID DYNAMICS,
cambridge university press, 1967.

Bird, R.B., Stewart, W.E. and Lightfoot, E.N.,
TRANSPORT PHENOMENA, john wiley, 1960.

Blackman, R.B. and Tukey, J.W.: THE MEASUREMENT OF POWER SPECTRA, dover, 1958.

Brigham, E.O., THE FAST FOURIER TRANSFORM,
prentice-hall, 1974.

Brown, T., 1978. Tidal Models with applications to the North Sea, Ph. D. Thesis, City of London Polytechnic.

Caston, G.F., 1981. Potential gain and loss of sand by some sand banks in the Southern Bight of the North Sea, Mar. Geol., 41: 239-250.

Caston, V.N.D., 1972. Linear sand banks in the Southern North Sea, Sedimentology, 18: 63-78.

Caston, V.N.D. and Stride, A.H., 1970. Tidal sand movements between some linear sand banks in the North Sea off Northeast Norfolk, Mar. Geol., 9: M38-M42.

Cloet, R.L., 1954. Sand waves in the Southern North Sea and in the Persian Gulf, J. Inst. Navigation, 7:272-29.

Davies, A.G., 1974, Tidal and sedimentation studies in the Outer Thames Estuary, Ph. D. Thesis, City of London Polytechnic.

Defant, A., PHYSICAL OCEANOGRAPHY, pergamon press, 1960.

D'Olier, B., 1981. Sedimentary events during Flandrian sea-level rise in the south-west corner of the North Sea. In: Nio, S.D. et al (Editors), HOLOCENE MARINE SEDIMENTATION IN THE NORTH SEA BASIN, Int. Associ. Sed. Spec. Publ. 5: 221-227.

Dyer, K.R., ESTUARINE HYDROGRAPHY AND SEDIMENTATION, cambridge university press, 1979.

Dyer, K.R., COASTAL AND ESTUARINE SEDIMENT DYNAMICS, wiley-interscience, 1986.

Fredsoe, J., 1974. On the development of dunes in erodible channels, J. Fluid Mech., 64-1: 1-16.

Gadd, P.E., Lavelle, J.W., Swift, D.P.J., 1978. Estimates of sand transport on the New York shelf using near-bottom current meter observations, J. Sediment. Pet., 48, no. 1: 239-252.

Gill A.E., ATMOSPHERE-OCEAN DYNAMICS, academic press, 1982.

Gordon, C., Greenwalt, D. and Witting, J., 1983.
Asia rip: Surface wave expression of bathymetry,
NRL Memorandum Report 5027,
Naval Research Laboratory, Washington DC, 40 pp.

Halpern, D., 1980. Moored current measurements in
the upper ocean. In: Dobson, F., Hasse, L.,
and Davis, R. (Editors), AIR-SEA INTERACTION,
plenum pub. corp.: 127-140.

Halpern, D., Weller, R.A., Briscoe, M.G., Davis, R.E.
and McCullough, J.R., 1981. Intercomparison tests
of moored current measurements in the upper ocean,
J. Geophys. Res., 86, C1: 419-428.

Hinze, J.O., TURBULENCE: An introduction to its
mechanism and theory, mcgraw-hill, 1959.

Houbolt, J.J., 1968. Recent sediments in the
Southern Bight of the North Sea,
Geol. Mijnbouw 47, 9: 245-273.

Howarth, M.J. and Huthnance, J.M., 1984. Tidal and
residual currents around a norfolk sand bank,
Estuarine Coast. Shelf Sci., 19: 105-117.

Huthnance, J.M., 1973. Tidal current asymmetries
over the Norfolk sand banks,
Estuarine Coast. Mar. Sci., 1: 89-99.

Huthnance, J.M., 1982a. On one mechanism forming
linear sand banks,
Estuarine Coast. Shelf Sci., 14: 79-99.

Huthnance, J.M., 1982b. On the formation of
sand banks of finite extent,
Estuarine Coast. Shelf Sci., 15: 277-299.

Jelgersma, S., 1979. Sea-level changes in the N Sea basin.
In: Oele, E., Schuttenhelm, R.T.E., Wiggers, A.J.
(Editors), THE QUATERNATY HISTORY OF THE N SEA,
almquist and wiksell, Stockholm: 233-248.

Kennedy, J.F., 1969. The formation of
sediment ripples, dunes and anti-dunes,
Ann. Rev. Fluid Mech., 1: 147-169.

Kenyon, N.H., Belderson, R.H., Stride, A.H., and
Johnson, M.A., 1981. Offshore tidal sandbanks as
indicators of net sand transport and as potential
deposits. In: Nio, S.D. et al (Editors), HOLOCENE
MARINE SEDIMENTATION IN THE NORTH SEA BASIN,
Int. Associ. Sed. Spec. Publ. 5.

Kenyon, N.H., 1983. Tidal bedforms investigated by
Seasat, In: T.D. Allen (Editor),
SATELLITE MICROWAVE REMOTE SENSING,
ellis horwood: 261-270.

Kinsman, B., WIND WAVES: their generation and
propagation on the ocean surface,
prentice-hall, 1965.

Lamb, H., HYDRODYNAMICS, 6th ed.,
cambridge university press, (1879) 1932.

LHS0 .. short form for following reference.
Longuet-Higgins, M.S. and Stewart, R.W., 1960.
Changes in the form of short gravity waves on
long waves and tidal currents,
J. Fluid Mechanics 8: 565-583.
LHS1 .. short form for following reference.
Longuet-Higgins, M.S. and Stewart, R.W., 1961.
The changes in amplitude of short gravity
waves on steady non-uniform currents,
J. Fluid Mechanics 10: 529-549.

McCave, I.N. and Langhorne, D.N., 1982.
Sand waves and sediment transport around
the end of a tidal sand bank,
Sedimentology, 29: 95-110.

McLean, S.R., 1981. The role of non-uniform
roughness in the formation of sand ribbons,
Mar. Geol., 42: 49-74.

Mandelbrot, B.B., THE FRACTAL GEOMETRY OF NATURE,
freeman and co, San Francisco, 1982.

Monin, A.S., and Yaglom, A.M.,
STATISTICAL FLUID MECHANICS:
Mechanics of turbulence,
vol. 1 & 2, mit press, 1971.

Off, T., 1963. Rythmic linear sand bodies
caused by tidal currents,
Bull. Am. Ass. Pet. Geol., 47: 324-341.

Pierson, W.J., Neumann,G., and James, R.W., 1955.
Practical methods for observing and forecasting
ocean waves by means of wave spectra & statistics.
U.S. Navy Hydrographic Office pub. no. 603.

Pingree, R.D., 1978. The formation of the Shambles and
other banks by tidal stirring of the seas,
J. Mar. Biol. Ass. U.K., 58: 211-226.

Phillips, O.M., THE DYNAMICS OF THE UPPER OCEAN,
cambridge university press, 1966.

Pond, S. and Pickard, G.L.,
INTRODUCTORY DYNAMIC OCEANOGRAPHY,
pergamon press, 1978.

Prandtl, L. and Tietjens, O.G., FUNDAMENTALS OF HYDRO-
AND AEROMECHANICS, dover, (1934) 1957.

Proudman, J. and Doodson, A.T., 1924. The principal
constituent of the tides of the North Sea.,
Phil. Trans. Roy. Soc. Lond., A, 224: 185-219.

Raudkivi, A.J., LOOSE BOUNDARY HYDRAULICS,
pergamon press, 1967.

Riley, K.F., MATHEMATICAL METHODS FOR THE PHYSICAL
SCIENCES, cambridge university press, 1974.

Rouse, H., ELEMENTARY MECHANICS OF FLUIDS,
dover, (1946) 1978.

Scorer, R.S., ENVIRONMENTAL AERODYNAMICS,
ellis horwood, 1978.

Schlichting, BOUNDARY LAYER THEORY,
mcgraw-hill, 1960.

Smith, J.D., 1969. Geomorphology of a sand ridge,
J. Geol., 77: 39-55.

Soulsby, R.L. and Dyer, K.R., 1981.
The form of the near-bed velocity profile in
a tidally accelerating flow,
J. Geophys. Res., v86, C9: 8067-8074.

Stroomatlas, NOORDZEE, zuidelijk deel,
Hydrografisch Bureau, 's-Gravenhage, Netherlands.

Sverdrup, H.U., et al, THE OCEANS: THEIR PHYSICS,
CHEMISTRY, AND GENERAL BIOLOGY,
prentice-hall inc, 1942.

Taylor, G.I., 1919. Tidal friction in the Irish Sea.
Phil. Trans. Roy. Soc. Lond., A, 220: .

Taylor, G.I., 1921. Tidal oscillations in
gulfs and rectangular basins,
Proc. Lond. Math. Soc., 2, 20:148-181.

Tyler, G.L., Teague, C.C., Stewart, R.H., Peterson, A.M.,
Munk, W.H., and Joy, J.W., 1974. Wave directional
spectra from synthetic aperture observations of
radio scatter, Deep-Sea Research, 21: 989-1016.

Teichmann, H., PHYSICAL APPLICATIONS OF VECTORS AND
TENSORS, george g. harrap and co, 1969.

Venn, J.F., 1977. Irish Sea Salinity Modelling, M. Sc., University College of North Wales at Bangor.

Venn, J.F. and D'Olier, B., 1983. Preliminary observations for a model of sand bank dynamics, In: Sundermann, J. and Lenz, W. (Editors), NORTH SEA DYNAMICS, springer-verlag: 472-485. (bound in this volume as Appendix - B)

Yalin, M.S., MECHANICS OF SEDIMENT TRANSPORT, 2nd ed., pergamon press, (1972) 1977.

Zimmerman, J.T.F., 1981. Dynamics, diffusion and geomorphological significance of tidal residual eddies, Nature, 16th April, 290: 549-555.